

EVALUATION OF SITE EFFECTS BASED ON THE 1999 KOCAELI AND
DÜZCE EARTHQUAKE EVENTS AND SEISMIC MICROZONATION OF
GÖLYAKA, DÜZCE, TURKEY

A THESIS SUBMITTED TO
THE GRADUATE SCHOOL OF NATURAL AND APPLIED SCIENCES
OF
MIDDLE EAST TECHNICAL UNIVERSITY

BY

KARIM YOUSEFI BAVIL

IN PARTIAL FULFILLMENT OF THE REQUIREMENTS
FOR
THE DEGREE OF DOCTOR OF PHILOSOPHY
IN
GEOLOGICAL ENGINEERING

FEBRUARY 2022

Approval of the thesis:

**EVALUATION OF SITE EFFECTS BASED ON THE 1999 KOCAELI AND
DÜZCE EARTHQUAKE EVENTS AND SEISMIC MICROZONATION OF
GÖLYAKA, DÜZCE, TURKEY**

submitted by **KARIM YOUSEFI BAVIL** in partial fulfillment of the requirements
for the degree of **Doctor of Philosophy in Geological Engineering, Middle East
Technical University** by,

Prof. Dr. Halil Kalıpçılar
Dean, Graduate School of **Natural and Applied Sciences**

Prof. Dr. Erdin Bozkurt
Head of the Department, **Geological Engineering**

Prof. Dr. Haluk Akgün
Supervisor, **Geological Engineering, METU**

Assoc. Prof. Dr. Mustafa Kerem Koçkar
Co-Supervisor, **Civil Engineering, Hacettepe University**

Examining Committee Members:

Prof. Dr. Asuman G. Türkmenoğlu
Geological Eng., METU

Prof. Dr. Haluk Akgün
Geological Eng., METU

Prof. Dr. Ayşegül Askan Gündoğan
Civil Eng., METU

Prof. Dr. Berna Unutmaz
Civil Eng., Hacettepe Uni.

Assoc. Prof. Dr. Elçin Gök
Geophysical Eng. Seismology, Dokuz Eylül Uni.

Date: 10.02.2022

I hereby declare that all information in this document has been obtained and presented in accordance with academic rules and ethical conduct. I also declare that, as required by these rules and conduct, I have fully cited and referenced all material and results that are not original to this work.

Name Lastname: Karim Yousefi Babil

Signature:

ABSTRACT

EVALUATION OF SITE EFFECTS BASED ON THE 1999 KOCAELI AND DÜZCE EARTHQUAKE EVENTS AND SEISMIC MICROZONATION OF GÖLYAKA, DÜZCE, TURKEY

Yousefi Babil, Karim

Doctor of Philosophy, Geological Engineering

Supervisor: Prof. Dr. Haluk Akgün

Co-Supervisor: Assoc. Prof. Dr. Mustafa Kerem Koçkar

February 2022, 151 pages

The high seismicity study area situated in a near-fault region in Gölyaka, Düzce, makes the determination of the bedrock geometry more complex, and hence, it makes this area very challenging in terms of a site response study that would aid a seismic hazard assessment. This study developed a basin model to evaluate the site effects in the tectonically controlled and formed Plio-Quaternary fluvial sediments of the Gölyaka region that uniquely falls within the bifurcated near-field fault section of the North Anatolian Fault System (NAFS). Surface seismic surveys and deep vertical electrical sounding (VES), coupled with boring studies, have been performed to determine the presence of the geological heterogeneities and the geometry of the basin over a vast area, and a 3-D basin geometry model was developed. 1D and 2D numerical analyses using an equivalent linear approach were performed to characterize the near-field dynamic soil behavior within the Gölyaka pull-apart basin in the presence of a probable ground motion. The results of the numerical analysis were compared and the performance of the used method was reviewed to ascertain the site effects in the study region. A shear wave velocity of 1100 m/s was accepted

as the bedrock depth limit in the region. Based on the VES results, the alluvial thickness in the center of the basin could be much thicker, i.e., almost 450 m. The results of 1D and 2D numerical calculations for soft/weak soils revealed 2D basin effects in spectral accelerations in a 1s period. A three-dimensional effect could also be noticed for the Seis-18 analysis point by comparing the acceleration and velocity spectra along the E-W and NW-SE cross-sections. Based on the recorded weak motion, it was observed that the spectral acceleration showed significant similarity to the results of 1D and 2D analyses. For this particular case, it was deemed that weak motion earthquake was a good indicator of the seismic site effects for the soft and thicker sediments of the study area.

Keywords: Seismic Characterization, 3D basin modeling, Near-field site effects, 1D and 2D site response, Gölyaka, Düzce

ÖZ

1999 KOCAELİ VE DÜZCE DEPREMLERİ TEMEL ALINARAK DÜZCE İLİ GÖLYAKA İLÇESİNİN SAHA ETKİLERİNİN DEĞERLENDİRİLMESİ VE SİSMİK MİKROBÖLGELEMESİ

Yousefi Babil, Karim
Doktora, Jeoloji Mühendisliği
Tez Yöneticisi: Prof. Dr. Haluk Akgün
Ortak Tez Yöneticisi: Doç. Dr. Mustafa Kerem Koçkar

Şubat 2022, 151 sayfa

Düzce, Gölyaka'da yer alan sismisitesi yüksek çalışma alanı, fayın yakınında bulunmasından dolayı anakaya geometrisinin belirlenmesini karmaşık bir hale getirmekte ve bu nedenle, sismik tehlike değerlendirmesine yardımcı olacak bir saha tepki çalışması yapılması açısından süreçleri zorlaştırmaktadır. Bu çalışmada, Kuzey Anadolu Fay Sisteminin (KAFS)'nin yakın alan etkisindeki özel bir havza bölümünde yer alan Gölyaka bölgesindeki tektonik-kontrollü oluşmuş Pliyo-Kuvaterner akarsu çökellerinin saha etkilerini değerlendirmek için bir havza modeli geliştirilmiştir. Bu geniş alandaki jeolojik heterojenliklerin ve havza geometrisinin belirlenmesi için yüzey sismik ölçümleri, derin düşey elektrik sondajı (DES) ile sondaj çalışmaları yapılmış ve 3 boyutlu bir havza geometri modeli geliştirilmiştir. Olası bir yer hareketinin gerçekleşmesi durumunda Gölyaka çek-ayır havzasındaki yakın alan dinamik zemin davranışını karakterize etmek için eşdeğer doğrusal yaklaşım kullanarak 1B ve 2B sayısal analizler yapılmıştır. Sayısal analiz bulguları birbiriyle karşılaştırılmış ve çalışma bölgesindeki saha etkilerini tespit etmek için kullanılan yöntemlerin performansı değerlendirilmiştir. Bölgede 1100 m/s'lik kayma

dalga hızı anakaya derinliği sınırı olarak kabul edilmiştir. DES sonuçları, havzanın merkezindeki alüvyon kalınlığının çok daha kalın; yaklaşık 450 m olabileceğini göstermektedir. Yumuşak/zayıf zeminler için 1B ve 2B sayısal hesaplamaların sonuçları, 1s periyodundaki spektral ivmelerde 2B havza etkilerini ortaya çıkarmıştır. Seis-18 analiz noktası için, D-B ve KB-GD kesitleri boyunca ivme ve hız spektrumlarının karşılaştırılması sonucu üç boyutlu bir etki fark edilebilir. Kaydedilen zayıf harekete dayalı olarak, spektral ivme, 1B ve 2B analiz sonuçlarıyla önemli benzerlik göstermektedir. Bu durumda, zayıf hareket sonuçları çalışma alanındaki yumuşak ve kalın sedimanlar için sismik saha etkilerinin iyi bir göstergesidir.

Anahtar Kelimeler: Sismik karakterizasyon, 3B basen modeli, Yakın-saha yer etkisi, 1B ve 2 B yer tepkisi, Gölyaka, Düzce

To my parents, brothers,
and my wife

ACKNOWLEDGMENTS

I would like to express my deepest gratitude to my supervisor Prof. Dr. Haluk Akgün and co-supervisor Assoc. Prof. Dr. Mustafa Kerem Koçkar for their guidance, advice, patience, encouragement, and insight throughout the research. Their insightful feedback pushed me to sharpen my thinking and brought my work to a higher level.

I would like to thank Prof. Dr. Asuman G. Türkemenoglu and Prof. Dr. Aysegül Askan Gündoğan for their support and innovative ideas during my thesis. Also, I have to give thanks to Prof. Dr. Berna Unutmaz and Assoc. Prof. Dr. Elçin Gök for giving me the opportunity to defend my Ph.D. thesis.

I would like to express my gratitude to my love, Seyedehnasim Seyedpour Esmaeilzad, who supported me in every step of my dissertation. I could not have completed this dissertation without the happy moments she has provided as pleasant distractions for resting my mind during my intense dissertation research and writing studies.

My parents and my brothers deserve special thanks because of their wise counsel and sympathetic ear. They were always there for me, and I could not have completed this dissertation without their support and inspiration.

My days in graduate school would not have been enjoyable without the company of my friends. I have experienced memorable moments with my dear friends. I would like to thank Dr. Arif Mert Eker, Selim Cambazoğlu, Arzu Arslan Kelam, Kadir Yertutanol, Aydın Çiçek, Gözde Pınar Yal, Gökalp Öner, Ecem Cansu Asan and Dr. Evrim Sopacı for their contribution and support.

I would like to express my appreciation to Mavi Girişim Engineering, Mining, Consulting, and Trading Co. Ltd. and Felek Group Engineering for assisting with and doing all of the field tests for this study.

I would also like to express my gratitude to several governmental organizations for their documentation assistance, particularly the General Directorate of Mineral Research and Exploration (MTA), the General Directorate of Highways (TCK), the Gölyaka Municipality, and the General Directorate of Provincial Bank (İlbank).

I would like to thank the Middle East Technical University (METU) Scientific Research Project (BAP-03-09-2012-002) for providing financial support for this study.

TABLE OF CONTENTS

ABSTRACT	v
ÖZ	vii
ACKNOWLEDGMENTS	x
TABLE OF CONTENTS	xii
LIST OF TABLES	xiv
LIST OF FIGURES	xv
CHAPTERS	
1 INTRODUCTION	1
1.1 Aims and motivations	1
1.2 Study area	3
1.3 Procedure	4
2 SEISMOTECTONICS AND REGIONAL GEOLOGY	7
2.1 Seismotectonics and seismicity	7
2.1.1 The Düzce earthquake	10
2.1.2 Geological setting	13
3 METHODOLOGIES FOR SITE CHARACTERIZATION AND SITE EFFECT STUDIES	17
3.1 Procedure performed for characterization studies	17
3.1.1 Field testing program and data analysis	19
3.1.2 Engineering geological and geotechnical boring study	20
3.1.3 Seismic surface wave methods	22
3.1.4 Vertical Electrical Sounding (VES) Method	29
3.1.5 H/V microtremor measurements	30

3.2	Procedure performed for 1D and 2D site response analysis	33
3.2.1	Procedure performed in numerical modeling	36
3.2.2	Development of a site-specific target spectrum.....	38
3.2.3	Selection and scaling of the input rock motions	40
3.2.4	Geometries of the 1D and 2D soil profiles	45
3.2.5	Characterization of non-linear soil properties.....	53
4	SITE CHARACTERIZATION AND BASIN MODELING.....	59
5	1D AND 2D NUMERICAL ASSESSMENTS OF SITE EFFECTS	73
6	RESULTS AND DISCUSSION	87
6.1	Comparison and evaluating 1D and 2D site response analysis	87
6.2	Validation of the weak motion records along with the site response analyses	92
7	CONCLUSIONS AND RECOMMENDATION	97
	REFERENCES	103
	APPENDICES	
A.	Geotechnical Boring Data and Deep Engineering Geological Boring Data 119	
B.	Surface Wave Method Analysis Results (MASW and MAM)	129
C.	Vertical Electrical Sounding (VES) Results	134
D.	H/V Spectral ratio Results.....	141
	CURRICULUM VITAE	149

LIST OF TABLES

TABLES

Table 1. A summary of the pulse-like ground motion records that were chosen (PEER Ground Motion Database, NGA- WEST 2).	42
Table 2. A summary of the seven earthquake records used to create the suit best matches the target spectrum.	45
Table 3. Variations in layer thickness along the E-W segment on a lateral and vertical scale.	46
Table 4. Variations in the unit weights of the layers along the E-W section.	46
Table 5. Variation in the shear wave velocity of the layers along the E-W section in lateral and vertical directions.....	47
Table 6. Variations in layer thickness along the NW-SE segment on a lateral and vertical scale.	47
Table 7. Variations in the unit weights of the layers along the NW-SE section.	48
Table 8. Variation in the shear wave velocity of the layers along the NW-SE section in the lateral and vertical directions.	48
Table 9. The maximum height (m) along the E-W section for the 1D soil response study.	49
Table 10. The maximum height (m) along the NW-SE section for the 1D soil response study.	50
Table 11. Summary of geometry and mesh characteristics	51

LIST OF FIGURES

FIGURES

Figure 1. The location of the study area.....	4
Figure 2. The western part of the North Anatolian Fault System (NAFS) is situated within the Eastern Marmara Region (Emre et al., 2011; Gürer et al., 2006) and the epicenter information of the major earthquakes (reproduced from KOERI, (2020). It should be noted that the rectangular area displays a close-up view of the bifurcated section of the NAFS in the Gölyaka basin and surface rupture of two major 1999 earthquake events.....	8
Figure 3. Acceleration time history of the 12.11.1999 earthquake records at the Düzce meteorological station.....	12
Figure 4. Shaking directions in Düzce and Bolu cities (Aydan et al., 2000).....	13
Figure 5. The generalized geological map of the Gölyaka basin (modified from MTA, A.U., 1999) and the western part of the North Anatolian Fault System (NAFS) that is situated within the Eastern Marmara Region (Emre et al., 2011; Gürer et al., 2006).	14
Figure 6. (a) A view of the Gölyaka basin and Efteni lake from the south looking at the N-NE direction; and a close-up view of the lithological units and Quaternary alluvium from the study area. Note: (b) Andesite of the Yigilca unit, (c) Sandstone outcrop of the Çaycuma formation at the margin of the basin, (d) sandy silty clay material, and (e) silty gravely sand material at the center of the basin.....	16
Figure 7. The geological reconnaissance map of the Gölyaka basin; Note that the dark striped dots display the MASW and MAM test locations, the light green dot displays the deep engineering geological boring data, the dark green triangles display the geotechnical boring data, and the blue striped dots display the vertical electrical sounding (VES) measurement points.	20
Figure 8. A view of three representative soil profiles concerning the boundary positions (a- deep engineering geological boring profile at the deepest part of the	

basin, b- and c- geotechnical boring profiles at the northern and southern margins of the basin, respectively).....	21
Figure 9. Plasticity Index (PI) variation with depth for available geotechnical boring data. The soil classes based on the Unified Soil Classification System (USCS) are CL and SM-SC.....	22
Figure 10. An example of the constructed experimental dispersion curve of a) Linear MASW and b) linear MAM records at Seis-15	26
Figure 11. Representative combined, processed dispersion curves from MAM and MASW measurements and the corresponding Vs profiles concerning the basin margin of the southern and northern parts along with the center of the basin	28
Figure 12. Examples presenting the processed 1-D profiles of Vertical Electrical Sounding (VES) measurements along with their inferred log profiles in the study area (from the measurement points of G7 and G9)	30
Figure 13. H/V spectral ratio curves that were selected to verify the given profile resulting from the measurements over the entire area.....	32
Figure 14. The cross-sections and measurement sites used in this study for a 1D and 2D site response analysis.	37
Figure 15. Site-specific target spectrum developed for the study area.....	40
Figure 16. The mean match spectrum is calculated by averaging the spectra of the seven earthquakes and the target spectrum.	43
Figure 17. Target spectrum of the original accelerograms of the seven earthquakes. The abbreviations for these records are listed in Table 2.....	44
Figure 18. Matched accelerograms of the seven earthquakes matched the target spectrum. The records are abbreviated in Table 2.....	44
Figure 19. 2D soil model of the E-W cross-section	46
Figure 20. 2D Soil model of the NW-SE cross-section.....	47
Figure 21. a) and c) Soil model of NW-SE and E-W sections, respectively. b) and d) a close view of these sections to show the lateral and vertical variations of the layers.....	52

Figure 22. The first layer's normalized modulus and damping curves utilized in the 1D site response assessment.	56
Figure 23. The second layer's normalized modulus and damping curves were utilized in the 1D site response assessment.	56
Figure 24. The third layer's normalized modulus and damping curves were utilized in the 1D site response assessment.	57
Figure 25. Material modulus reduction and damping curves for all layers were used in the 2D site response analysis	57
Figure 26. Material modulus reduction and damping curves for all layers were used in the 2D site response analysis	58
Figure 27. A 3-D basin model of the Vs results for the study area (Vertical Exaggeration: 5).....	62
Figure 28. A comparison of the three interpolated 2-D cross-sections of the Vs profiles along with the microtremor measurements that present the northern (a) and southern (b) margin along with the basin center (c) of the Gölyaka basin (Vs Profile Vertical Exaggeration: 10).....	65
Figure 29. Enlarged Fig. 2 shows the spatial distributions of the VES measurements and three parallel profile locations (i.e., A1, A2, A3). It should be noted that the apparent resistivity contrast in the A1, A2, A3 points of the profiles are due to the zone of faulting.....	67
Figure 30. A 3-D fence diagram of the VES model. It should be noted that the apparent resistivity results decrease due to the zone of faulting in the northeast section	68
Figure 31. Stability of the site responses by evaluating the variations of the acceleration spectrum after computing 1D and 2D analyses for seven earthquakes in a very dense/weathered rock site near the 1999 Kocaeli EQ earthquake fault rupture in the western part of the Gölyaka basin.	77
Figure 32. Stability of the site responses by evaluating the variations of the acceleration spectrum after computing 1D and 2D analyses for seven earthquakes located in the center of the basin at stiff soil sites.	78

Figure 33. Stability of the site responses by evaluating the variations of the acceleration spectrum after computing 1D and 2D analyses for seven earthquakes in the deepest part of the Gölyaka basin at the soft/weak soil site (Seis-18 located in the center of the Gölyaka county)	79
Figure 34. Stability of the site responses by evaluating the variations of the acceleration spectrum after computing 1D and 2D analyses for seven earthquakes in the northern and southern boundary of the basin at very dense/weathered rock (Seis-13) and stiff soil sites (Seis-29).....	80
Figure 35. The shapes of the velocity spectra for sites at the western part of the Gölyaka basin near the 1999 Kocaeli EQ fault rupture on very dense/weathered rock site after performing 1D and 2D numerical site response analyses	82
Figure 36. The shapes of the velocity spectra for sites at the basin center after performing 1D and 2D numerical site response analyses (Directivity effects).....	83
Figure 37. The shapes of the velocity spectra for sites at the deepest part of the basin after performing 1D and 2D numerical site response analyses (Directivity effects).	84
Figure 38. The shapes of the velocity spectra for sites at the northern and southern boundary of the basin at very dense/weathered rock (Seis-13) and stiff soil site (Seis-29) after performing 1D and 2D numerical site response analyses (Directivity effects).	85
Figure 39. 1D and 2D acceleration and velocity site response spectra in the western part of the basin with very dense/weathered rock soil profiles where the 2D and directivity effects are not observed.....	89
Figure 40. 1D and 2D acceleration and velocity site response spectra in the basin's center at stiff soil profiles where the 2D and directivity effects are evident, especially for Seis-10 and Seis-14.....	90
Figure 41. 1D and 2D acceleration and velocity site response spectra in the deepest part of the basin with soft/weak soil profiles where the 2D and directivity effects are evident	91

Figure 42. 1D and 2D acceleration and velocity site response spectra in the western part of the basin with very dense/weathered rock soil profiles show the 2D and directivity effects, especially for Seis-10 and Seis-14.	91
Figure 43. A view of the epicenter location and of the recorded weak motions (Kandili record_02.09.2016)-Mw= 3.7.....	94
Figure 44. 1D and 2D acceleration site response spectra compared to recorded weak motion and in the soft soil site where 2D and directivity effects were observed in the basin's center.....	95

CHAPTER 1

INTRODUCTION

1.1 Aims and motivations

The purpose of this dissertation is to compile a comprehensive database from the geotechnical field and laboratory experiments, geophysical in-situ testing utilizing surface wave techniques, vertical electrical sounding, Nakamura's method (H/V), and computational ground response analyses. These methodologies were employed to characterize the dynamic soil parameters and detect the nonlinear behavior of the local site effects. Field test results within soft and unconsolidated Upper Pliocene to Pleistocene fluvial and especially Quaternary alluvial sediments (henceforth referred to as Plio-Quaternary sediments in their entirety) deposited in the Gölyaka pull-apart basin that is situated southwest of the Düzce Province have been integrated. This research was conducted in Gölyaka, which is unique since it falls within the NAFS's near field portion (i.e., distances between ruptures range up to 8 km), that is one of the world's most significant transform fault systems capable of producing devastating earthquakes such as those that caused the Kocaeli (Mw=7.4) and Düzce (Mw 7.2) earthquakes in 1999.

The fundamental objective of this dissertation is to correlate, compare, and verify the different results obtained using in-situ characterization and site effect estimation techniques. The data was achieved using destructive and non-destructive (active and passive measurements of the surface wave) field survey and geotechnical survey (boring data and standard penetration tests). This research aims to compare and correlate the results of the geological surveys, field tests and laboratory experiments and their contribution to the vertical and lateral heterogeneity in the deep alluvial basin. The spatial variations of the results were explored within a GIS environment.

In the context of this study, non-destructive active (Multi-Spectral Analysis of Surface Wave) and passive (Microtremor Array Method) surface wave techniques were used to analyze local soil conditions. These two methods were combined with increasing the resolution throughout the shear velocity profile. The field configurations and parameters were employed for both approaches. A linear form and single mobile velocimeters were utilized to measure the local noise in the study area. These measures have been carried out in the defined area with the dominant soil periods and the soft soil spectral amplitudes. A systematic grid was used to gather the microtremor data records.

Various data sets have been used in this investigation, including geological, geotechnical, and geophysical data. This dissertation has examined the relationship between the geological units, the potential underlying geometry of the subsurface, vertical or lateral variations in the shear wave velocity data, vertical electrical sounding, fundamental periods, and spectral amplitudes. The findings of the destructive and non-destructive field studies were compared. The correlation results provided insight into the characterization of the stiffness of the soil that is present in the shallower regions (15 m depth) of the study area. The results of this analysis led to the idealization of the soil column, which represents an important step of the numerical analysis.

Another objective of this research was to analyze the site effects by comparing data from 1D and 2D site response computations. Strong ground motion records were used for numerical investigations related to the research area's seismotectonic characteristics. Additionally, this study compared and verified the recorded data for weak motion (small magnitude earthquake, $M_w=3.7$) during the field survey with numerical results. The final evaluation of the results was carried out in a Geographical Information Systems (GIS) environment by creating a database encompassing the entire region. As a result, a probable nonlinear behavior of the ground response in the presence of a potential excitation was hypothesized for several sites.

Motivations for initiating this study is that the study area uniquely falls within the near field portion of the NAFS (i.e., the distances vary next to the rupture up to 8 km), which is one of the most paramount transform fault systems globally that produce devastating earthquakes as witnessed during the 1999 Kocaeli ($M_w=7.4$) and Düzce (M_w 7.2) Earthquakes. The surface ruptures of the 1999 Kocaeli and Düzce Earthquakes bound the tectonically formed Gökyaka basin in the near-field from south to northwest, respectively, which makes this location unique and intriguing from a site effect point of view. In general, the westward propagating seismic activity along the NAFS starting from the 1939 Erzincan Earthquake ($M_s=7.9$), and lately, the 1999 Kocaeli and Düzce Earthquakes have triggered more than ten severe earthquakes during this century, which have led to more than 50,000 casualties (Barka, 1996; MTA, 2003). For this reason, the Gölyaka basin is a highly exclusive area for determining nonlinear behavior (i.e., velocity anomaly/contrast due to tectonic deformation) resulting from high seismicity in a near-fault region.

1.2 Study area

The study area is located in the Gölyaka basin that lies within the Eastern Marmara Region. It uniquely falls within the near field portion of the NAFS (i.e., the distances vary next to the rupture up to 8 km), which is one of the most paramount transform fault systems globally that produce devastating earthquakes, as witnessed during the 1999 Kocaeli ($M_w=7.4$) and Düzce (M_w 7.2) Earthquakes (Figure 1). The surface ruptures of the 1999 Kocaeli and Düzce Earthquakes bound the tectonically formed Gökyaka basin in the near-field from the south to the northwest, respectively, which makes this location unique and intriguing from a site effect point of view.

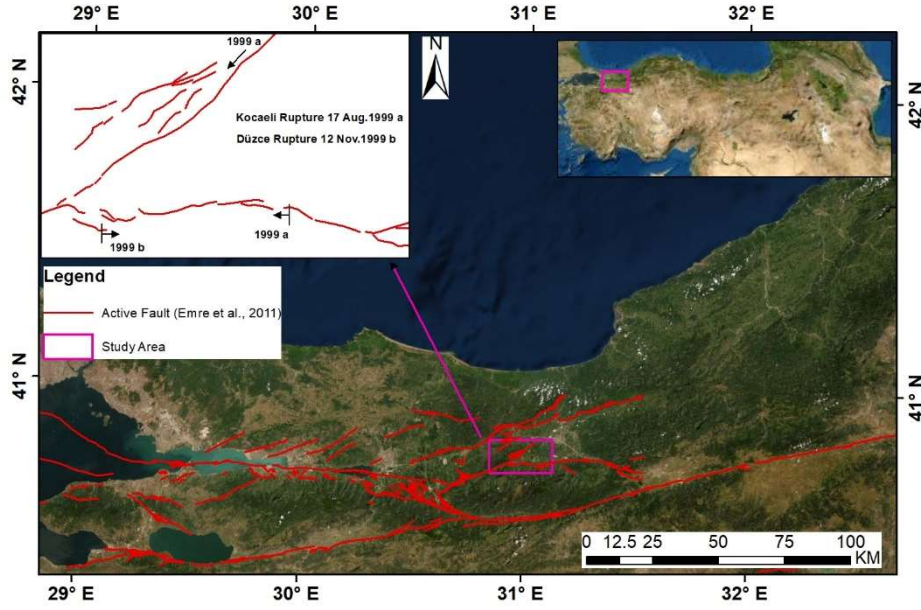


Figure 1. The location of the study area

1.3 Procedure

The procedure used in this study can be divided into five stages:

1. Collection of comprehensive data, including geological field data, deep and geotechnical borings, standard penetration tests, geotechnical laboratory tests, and pre-exploration geophysical surveys.
2. Performing additional field study encompassing Nakamura's method (H/V), surface wave methods (active and passive methods), vertical electrical sounding method (VES).
3. Studying the geological, geotechnical, and geophysical characterization of the region and identifying lateral and vertical changes in local soil conditions of the region. Developing a 2D and 3D basin model.
4. Analyzing 1D and 2D soil responses and determining the location's response period and spectral amplitudes.
5. Comparative analysis of site response studies.

This thesis includes seven chapters. Chapter 2 presents the regional geology and seismotectonics of the study area on a regional and local scale. A brief overview of the theoretical foundations for the approaches used in the characterization studies and the field application procedure has been provided in Chapter 3. The same chapter discusses site effect estimation and 1D and 2D numerical ground response evaluations. Site characterization and basin modeling are presented in Chapter 4. 1D and 2D numerical site response analysis are presented in Chapter 5. Chapter 6 includes a discussion section and the results of the site effect investigations. Recorded weak ground motion as compared with 1D and 2D dynamic analysis along with the results presented in the same chapter. Chapter 7 summarizes the results of this dissertation and highlights the most important conclusions.

CHAPTER 2

SEISMOTECTONICS AND REGIONAL GEOLOGY

2.1 Seismotectonics and seismicity

The study area is located in the Gölyaka basin in the Eastern Marmara Region and is uniquely situated within the bifurcated portion of the North Anatolian Fault System (NAFS). The unique feature of the Gölyaka basin is its location. The reason for this is that the eastern end of the surface rupture of the 1999 Kocaeli earthquake ($M_w=7.4$) has terminated in the eastern part of the Gölyaka basin (Figure 2, 1999 a), and the western end of the surface rupture of the 1999 Düzce earthquake ($M_w=7.2$) also initiated in the western part of the study area (Figure 2, 1999 b). These large destructive earthquakes have bound this tectonically formed basin in the near-field region (fault-controlled basin margin) from south to northwest, respectively (Figure 2).

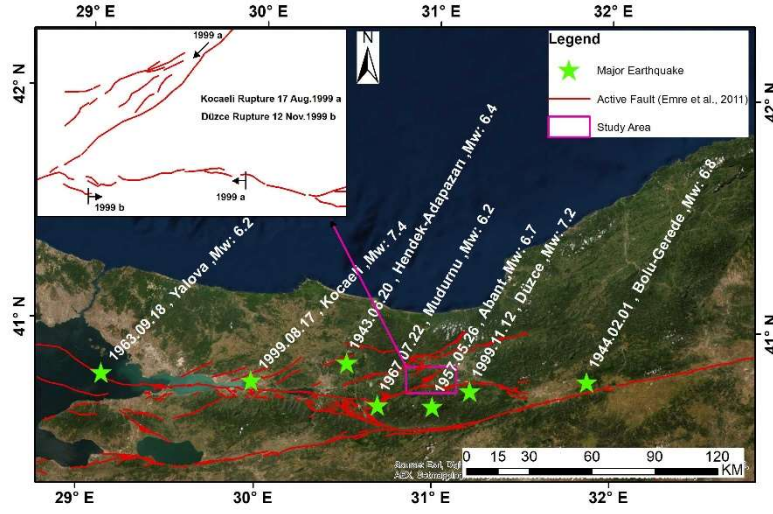


Figure 2. The western part of the North Anatolian Fault System (NAFS) is situated within the Eastern Marmara Region (Emre et al., 2011; Gürer et al., 2006) and the epicenter information of the major earthquakes (reproduced from KOERI, (2020)). It should be noted that the rectangular area displays a close-up view of the bifurcated section of the NAFS in the Gölyaka basin and surface rupture of two major 1999 earthquake events.

The first destructive event, namely, the August 18, 1999 Kocaeli earthquake, has caused surface ruptures ranging from 40 to 145 km in length, resulting in a 185 km of surface rupture in total (Akyüz et al., 2002; Barka et al., 2002). The horizontal displacement of the rupture surface was around 5 m in the vicinity of the epicenter of this earthquake in Gölcük and around 1.2 m in the east of the Gölyaka region (Cambazoğlu et al., 2016; Polat et al., 2002). The November 12, 1999 Düzce earthquake, which occurred three months later, is the second of the devastating 1999 Marmara earthquakes. This earthquake produced a horizontal and vertical displacement of 3.0 m and 5.0 m, respectively, and created a rupture surface of 45 km (Taymaz, 2000). The western end of the rupture line in the Gölyaka region is situated about 9 km to the eastern end of the 17 August Kocaeli earthquake rupture line (Barka, 1996). The NAFS, an active right-lateral strike-slip fault, is connected

to the Anatolian block extending northward to west. It usually represents a transformation margin following a region of pre-existing crustal weakness. Slip-rate of 20–30 mm/yr has been measured by the GPS networks (McClusky et al., 2000; Reilinger et al., 2006, 2000, 1997; Straub et al., 1997) in the northern side of the Anatolian block, with oriented vectors towards WNW in the eastern end, E–W in the center, and S–W in the Aegean region, respectively. The North Anatolian Fault System is divided into two main branches west of the Bolu district: the Düzce fault in the north and the Mudurnu fault in the south. The Düzce fault, situated north of these branches, passes through the study area. The Paleozoic–Eocene units of the Almacik block are separated from the Pliocene–Quaternary continental deposits of the Düzce pull-apart basin by the Düzce fault. This fault is in the proximity of the Karadere segment, which is the eastern part of the Kocaeli surface rupture. The Karadere segment and the Düzce fault constitute two diverging strike-slip strips connected by a no-step-over fault junction. This geometric sequence entails a releasing fault wedge, whose long-term morphological expression is represented by the wedge-shaped basin of the Gölyaka region (Figure 2; Pucci et al., 2007). The Düzce fault shows up in the east to join the single trace of the NAFS with a right-releasing step-over created by the Bakacak and Elmalık faults in the WNW–ESE direction. Contrarily, the western section of the fault extends from the WSW–ENE striking Karadere segment, which borders the İzmit fault. This western boundary of the Düzce fault section sets up a complex right-releasing step-over with the Karadere segment that supposedly has blocked the propagation of the Kocaeli earthquake fault rupture (Lettis et al., 2002). Consequently, this releasing zone controls the present-day Düzce basin depocentre Efteni Lake, situated in the study area (Pucci et al., 2007).

The rupture width of the Düzce earthquake has been determined to be 10 km according to the seismic data and between 14–24.5 km according to the literature (Bürgmann et al., 2002; Utkucu et al., 2003). The study area includes major seismic events that can be sorted from the most recent to the past as follows: the 17 August 1999 Kocaeli ($M_w=7.4$), the 12 November 1999 Düzce ($M_w=7.2$), the 22 July 1967

Mudurnu (Mw=6.2), the 18 September 1963 Yalova (Mw:6.2), the 26 May 1957 Bolu-Abant (Mw=6.7), the 1 February 1944 Bolu-Gerede (Mw=6.8) and the 20 June 1943 Hendek (Mw=6.4) (KOERI-RETMC, 2020) (Figure 2). These events have caused significant casualties and substantial economic losses (Akyüz et al., 2002; Ambraseys NN and Zatopek A, 1969; Barka et al., 2002; Barka and Kadinsky-Cade, 1988; Kondo et al., 2005; Palyvos et al., 2007).

2.1.1 The Düzce earthquake

On November 12, 1999, at 18:57 (16:57GMT), the primary shock occurred. Most severe damage to reinforced concrete structures occurred in Düzce and Kaynasli, built on alluvial deposits. The number of fatalities and injured were 1 and 68, respectively. A total of fourteen structures in Gölyaka have either collapsed or have been severe to moderately damaged.

The surface rupture of the Düzce earthquake was believed to be between 30 and 45 kilometers (Duman et al., 2000; Özden et al., 2000; Demirtaş et al., 2005). For approximately 9 kilometers, the surface rupture overlaps the eastern termination part of the 17 August 1999 event at the Karadere segment (Akyüz et al., 2002; Hartel et al., 2002). The Düzce rupture's faulting characteristics vary throughout the surface rupture area. While the primary rupture zone is dominated by a right-lateral strike-slip motion (Akyüz et al., 2002), normal (near Gökaya) and thrust (at the Düzce rupture zone) aspects are also present (Akyüz et al., 2002; Pucci et al., 2007). According to Duman et al. (2000), the earthquake's surface rupture is divided into three different segments by the Beyköy and Kaynaşlı restraining step-overs. The rupture's trend has been determined to be E-W (Duman et al., 2000; Çakır et al., 2003; Umutlu et al., 2004). For trends ranging from N80°E to N100°E, directional analysis of the extracted lineaments produced the same result. In this dissertation, the model was predominantly segmented according to the method described by

(Duman et al., 2000). Another segmentation model was also studied as an alternative rupture scenario, dividing the Düzce fault into western and eastern segments near the Cakırhacıbrahim village based on the coseismic fault trace (Pucci et al., 2007). At the Düzce portions, the slide rate is claimed to be 10mm/yr (Ayhan et al., 2001).

According to Kandilli Observatory's (KOERI) fault plane solutions, the earthquake began towards the western end of the seismic fault and moved eastward. The high acceleration values at Bolu station, which are even greater than those at the nearby Düzce station, could be due to the abrupt termination of faulting at the eastern end and some ground amplification. Bolu station's peak ground acceleration (0.805g) is likely to be the greatest ever recorded by Turkey's National Strong Motion Network, maintained by the Earthquake Research Department (ERD). The N-S, E-W, and UP-DOWN acceleration data at the Düzce Meteorological Station are depicted in Figure 3. According to the recorded station distributions, it appears that the northern side of the fault was subjected to more shaking than the southern side of the fault, owing to the area's location on the fault's overhanging side (Aydan et al., 2000).

Figure 4 depicts the horizontal plane traces of acceleration waves and combined displacement trajectories at the Düzce and Bolu stations near the epicenter. This image can be used to predict the various directions of structure toppling and shearing and slope and ground failures. The Düzce records suggest that the structures were subjected to cyclic torsional motion, whereas the Bolu records suggest an almost impulsive shaking in the NE-SW direction. In other words, the damage is far more likely in Düzce than in Bolu, although Bolu's peak acceleration is substantially greater than that measured at Düzce (Aydan et al., 2000).

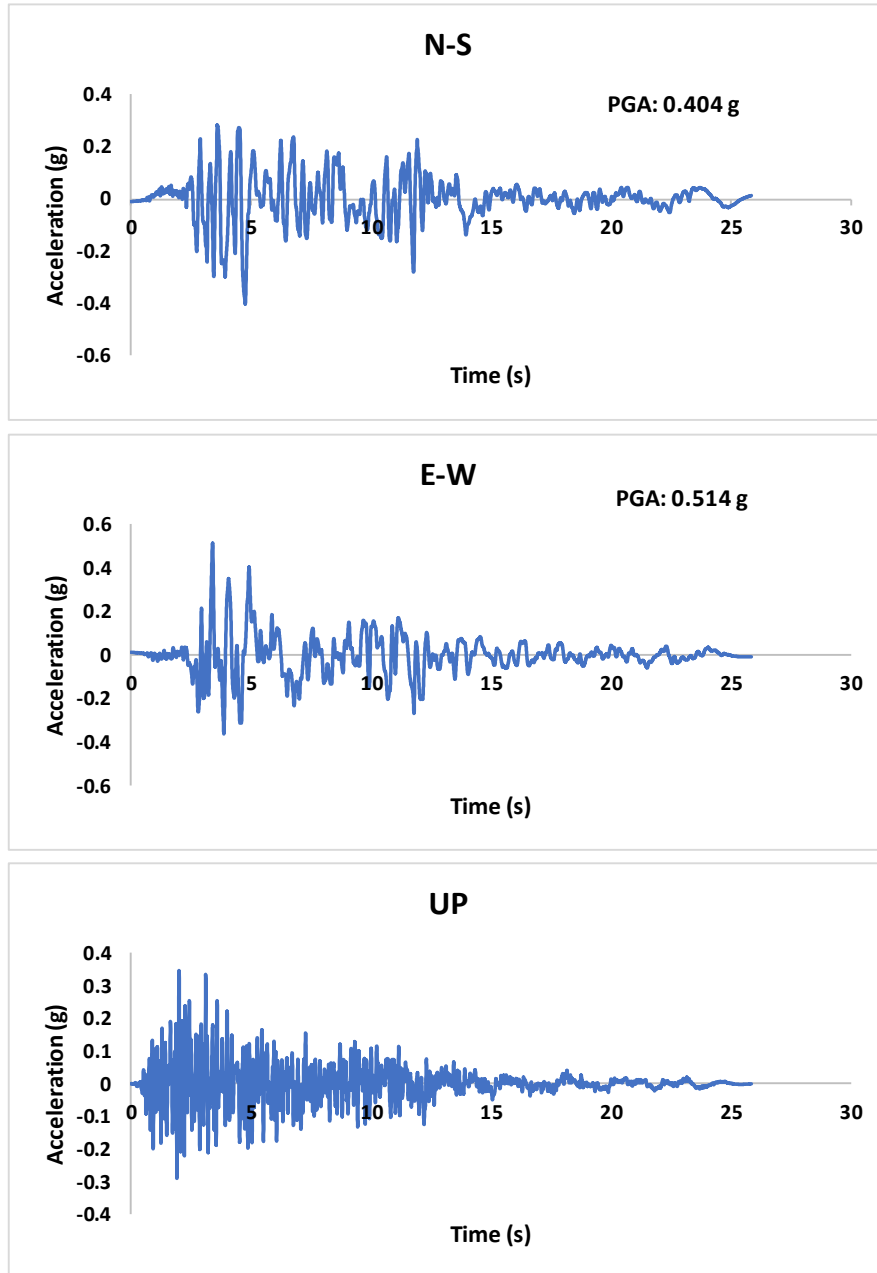


Figure 3. Acceleration time history of the 12.11.1999 earthquake records at the Düzce meteorological station

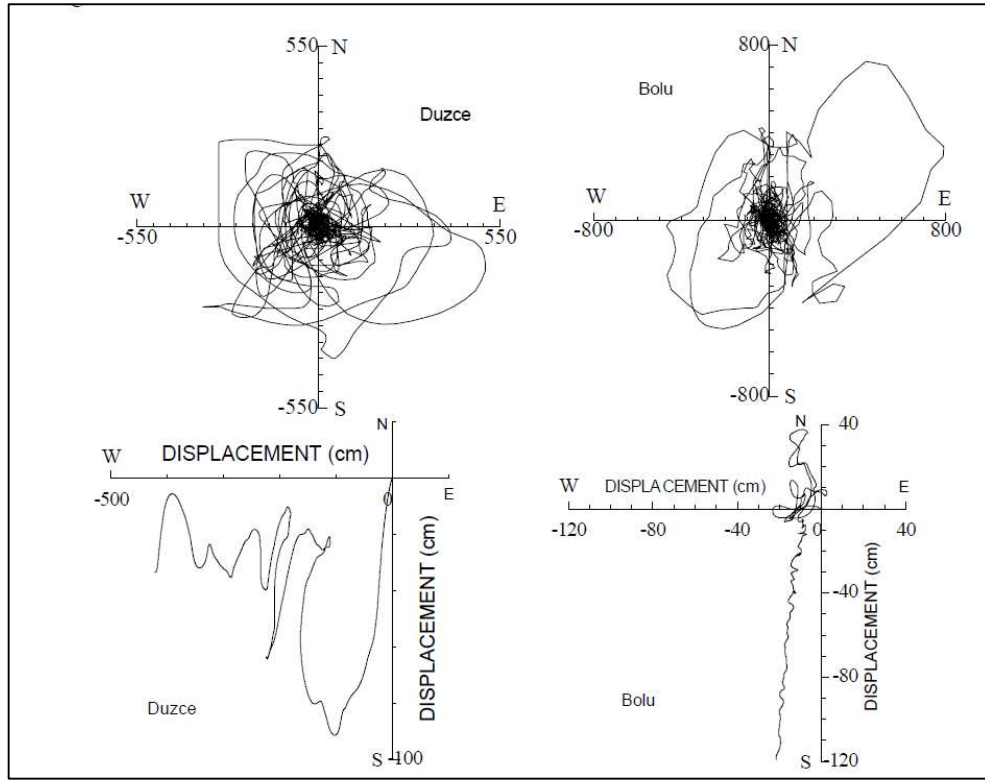


Figure 4. Shaking directions in Düzce and Bolu cities (Aydan et al., 2000)

2.1.2 Geological setting

The tectonically developed Gölyaka basin possesses unconsolidated Plio-Quaternary deposits intercalated with gravel, sand, silt, and clay that overlie older geological formations as a result of the fluvial activity (Figure 5). The Quaternary deposits are fluvial, lacustrine, and river delta sediments. The fluvial sediments primarily consist of gravel and sand material in the alluvial fans. However, the deposits of the Düzce basin are composed of thick layers of lacustrine and deltaic sediments, which primarily consist of silt and clay material (Figure 5). The thickness of the fluvial deposits (relatively coarser-grained material) becomes thicker towards the NE, whereas the lacustrine (fine-grained material) sediments become dominant towards the SW.

In the study area, the Cretaceous units are over-thrusted on the Eocene Yığılca Unit (Ty; andesites, basalts) and the Çaycuma formation (Tc; sandstones, mudstones, and limestones). The Quaternary alluvium and the unconsolidated Plio-Quaternary Karapürçek formation lie unconformably over the older units. The main geologic structure in the study region is the E–W striking northern section of the Düzce Fault in the North Anatolian Fault System. The Düzce fault has a fundamental importance in the region's structural deformation and geomorphological evolution. This dextral strike-slip fault and in some segments with its normal component forms the Düzce plain, which is an extensional Plio-Quaternary basin filled with sediments up to a thickness of 260 m (Şimşek and Dalgıç, 1997).

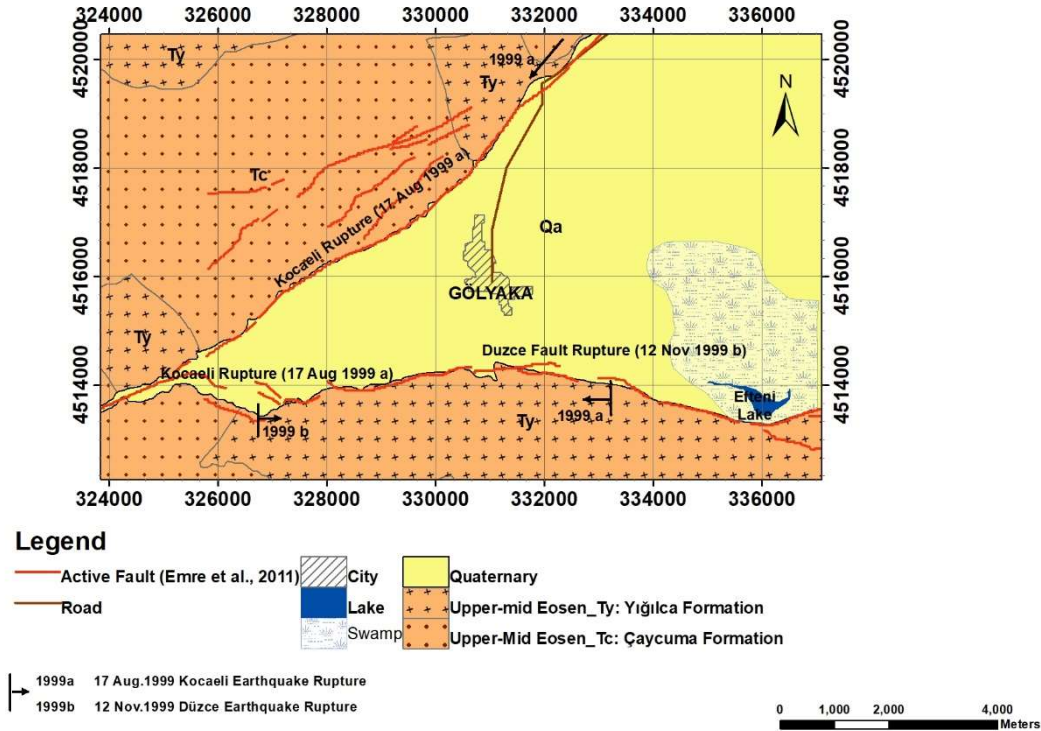


Figure 5. The generalized geological map of the Gölyaka basin (modified from MTA, A.U., 1999) and the western part of the North Anatolian Fault System (NAFS) that is situated within the Eastern Marmara Region (Emre et al., 2011; Gürer et al., 2006).

Figure 6 presents a general view of the study region located in the Gölyaka basin and Efteni Lake. As illustrated in this figure, a large part of the research site is situated within the lake's catchment area (i.e., marshy, reddish-colored area) towards the SE. In general, the area possesses heavy vegetation. The portions(Figure 6 that lack vegetation are located at the margins of the basin (Figure 6 (b) and (c)), and unconsolidated fluvial deposits exist near the main rivers (Figure 6 (d) and (e)).



Figure 6. (a) A view of the Gölyaka basin and Efteni lake from the south looking at the N-NE direction; and a close-up view of the lithological units and Quaternary alluvium from the study area. Note: (b) Andesite of the Yigilca unit, (c) Sandstone outcrop of the Çaycuma formation at the margin of the basin, (d) sandy silty clay material, and (e) silty gravely sand material at the center of the basin

CHAPTER 3

METHODOLOGIES FOR SITE CHARACTERIZATION AND SITE EFFECT STUDIES

3.1 Procedure performed for characterization studies

Seismic events in the last few decades have demonstrated that local site conditions, mainly those close to earthquake-prone areas, can generate substantial amplification and spatial variations of earthquake ground motion that considerably affect the level of ground shaking. Hence, the amplification of ground motion due to local site effects (i.e., basin geometry, topographical conditions, and ground motion resonance) plays a crucial role in enhancing seismic damage (Rodríguez-Marek et al., 2001; Koçkar and Akgün, 2012; Eker et al., 2015; Koçkar, 2016;). Almost all of the destructive earthquakes in the last decades (i.e., Kobe 1995; Chi-Chi 1999; Kocaeli and Düzce 1999; Sichuan 2008; New Zealand 2010; Van 2011 and Tohoku 2011) have brought particular attention to the significance of site effects.

Hence, it is essential to obtain detailed information on local site conditions to understand the regional variations of ground motion. In many circumstances, it is widely accepted that site characterization based on shear wave velocity is a critical factor in determining the intensity of ground shaking (Joyner et al., 1994; Dobry et al., 2000; Borchardt, 2002). Thus, it is a practical parameter to characterize local soil conditions for ground motion studies (Park and Elrick, 1998; Wills et al., 2000, 2015). In particular, a seismic surface wave is frequency-dependent and relies on the dispersive nature of Rayleigh-type surface waves in layered media (Seligson, 1970). This dispersive character of Vs can be efficiently utilized to form an underlying one-dimensional velocity model for a particular site (Rodríguez-Marek et al., 2001; Herak, 2008; Boaga et al., 2010; Pegah and Liu, 2016). Estimations have been performed by using data obtained through array applications. In some situations

where the topography and basin structure is complicated (i.e., near-fault regions, tectonically deformed areas), 2D and 3D shear wave velocity are required to account for the heterogeneities or the complex structures of basin models that may strongly affect the local hazard pattern (Piatti et al., 2013; Eker et al., 2015; Wang et al., 2016; Cushing et al., 2020; Mori et al., 2020).

High seismic activity in a near-fault region makes the determination of the topography and basin structure more complex, and hence, it is much more challenging to evaluate the site response characteristics as compared to areas situated at farther distances. Particularly in the near-source regions, rupture front and slip direction may have forward directional effects on the ground motion because they are aligned towards the area of interest (Bradley and Cubrinovski, 2011). Furthermore, due to the tectonic deformation, seismic velocity model complexity in the form of velocity contrast with lower velocity is sought to be significant in site-specific ground motions at regions near a fault or within the low-velocity fault zone (Dreger et al., 2007). Therefore, the crucial step in hazard estimation in sites situated near earthquake-prone areas is to reliably determine the basin geometry and define the alluvial and bedrock interface. In other words, without accurately defining the topography and basin structure, a well-developed basin model in an account for a site response study would be incomplete, no matter how robust the methodology is. Hence, for evaluating the seismic hazard associated with regional site conditions in the near-fault region, the basin geometry and well-defined topography based on the alluvial and bedrock interface are deemed critical factors.

This research has assessed the local site conditions and the dynamic sediment characteristics in the Gölyaka basin, then developed a 3-D basin model to characterize the sediment conditions based on the successfully obtained Vs profiles from different dimensions. In particular, it has focused on areas located at different positions concerning the basin margins, and more specifically, on areas at the northern and southern boundaries (fault-controlled basin margins) and in an area at the deepest part of the basin. The high-resolution Vs profile was obtained by conducting surface wave methods using a combination of active Multichannel

Analysis of Surface Wave (MASW) and passive Microtremor Array Method (MAM) measurements at a total of 29 locations. In other words, a combined utilization of these techniques was adapted to maintain the accuracy of the shear wave velocity results at shallow depths as well as at the deeper sections (Park et al., 2007; Gosar et al., 2008; Eker et al., 2012). At 14 locations, the Schlumberger Vertical Electrical Sounding (VES) technique has been applied to evaluate the depth of the basin bedrock. In addition, geotechnical data at 30 boring locations incorporating the results of a deep engineering geological boring with geological and basin topography data have been correlated with the Vs profile and the VES model.

Finally, microtremor data measured in the study site were used to verify the inferred basin depth. For this purpose, cross-correlation of the fundamental periods of the H/V microtremor measurements and the interpolated Vs profiles revealed a good agreement between the results. Comparison and verification of the two data sets showed strong concordance, especially in the center of the basin, but some nonlinear behavior was also encountered due to material deformation and basin edge effects next to the complex faulting. Due to the shallow bedrock, this nonlinear behavior may be interpreted as high periods at the basin edge. Finally, this comprehensive survey led to a well-developed 2-D and 3-D geometry of a basin model of the Gölyaka basin. The results have been used to characterize the basin's sediment characteristics and discuss the consequences of heterogeneity and basin effects on the seismic hazard.

3.1.1 Field testing program and data analysis

The field testing and data analysis were performed to assess the local site conditions and the dynamic sediment characteristics to develop a basin geometry model of the study area by conducting geophysical and geotechnical studies complemented by a thorough geological reconnaissance of the study site (Figure 7).

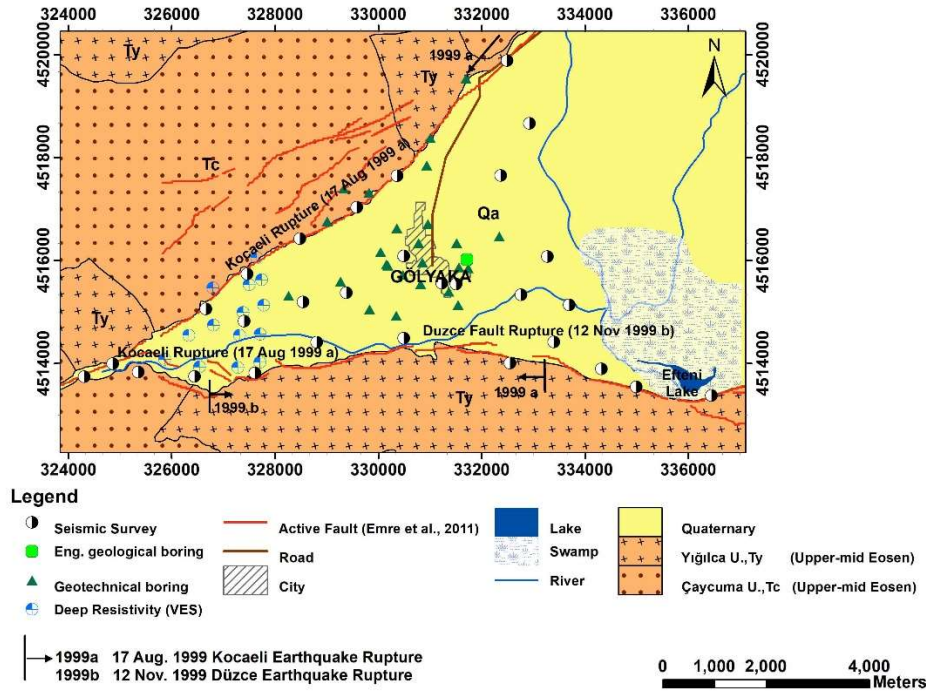


Figure 7. The geological reconnaissance map of the Gölyaka basin; Note that the dark striped dots display the MASW and MAM test locations, the light green dot displays the deep engineering geological boring data, the dark green triangles display the geotechnical boring data, and the blue striped dots display the vertical electrical sounding (VES) measurement points.

3.1.2 Engineering geological and geotechnical boring study

In order to investigate the subsurface sediments in the study area, a total of 30 geotechnical and deep engineering geological boring data have been utilized to investigate the Gölyaka basin-see appendix A for boreholes detail (Figure 8). The collected data was utilized to develop three profiles representing the basin margins of the northern and southern parts and the eastern section of the basin center (deepest part). According to the borehole data, groundwater was generally confronted at depths of 2.5 and 3.5 m from the surface. It was situated almost at the surface towards the southeastern part of the study area. The soil layers are an intermediate plasticity clay and sand, and non plasticity sand (PI=10-20 percent) (Figure 9).

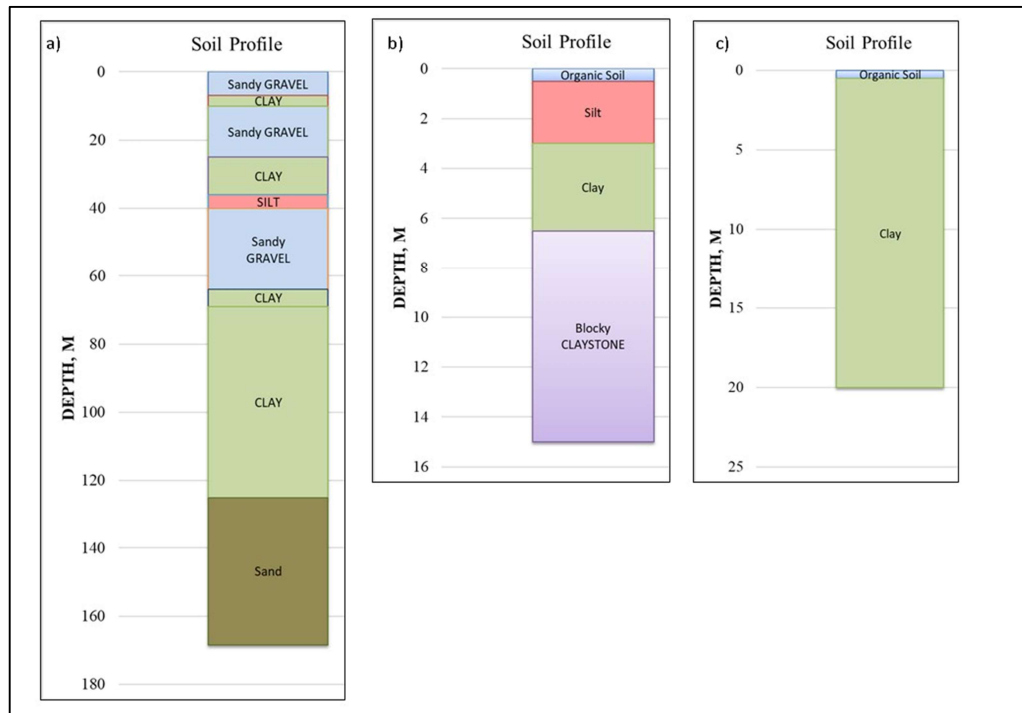


Figure 8. A view of three representative soil profiles concerning the boundary positions (a- deep engineering geological boring profile at the deepest part of the basin, b- and c- geotechnical boring profiles at the northern and southern margins of the basin, respectively)

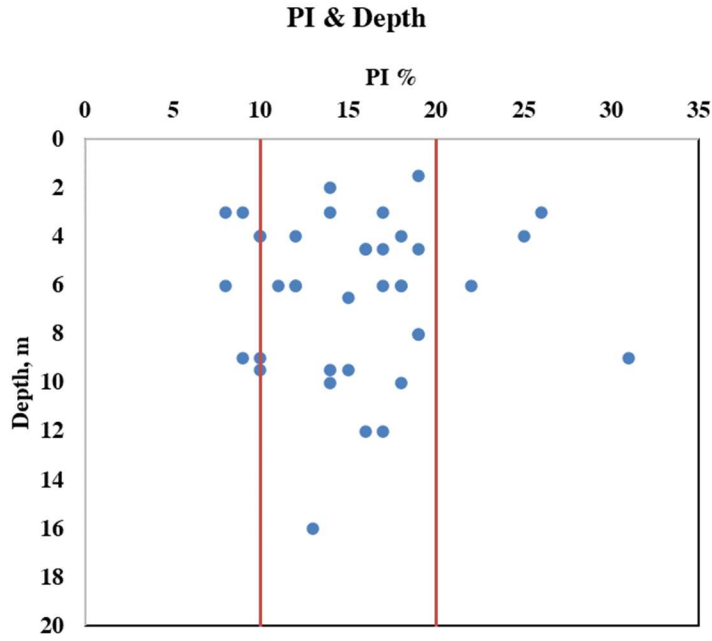


Figure 9. Plasticity Index (PI) variation with depth for available geotechnical boring data. The soil classes based on the Unified Soil Classification System (USCS) are CL and SM-SC.

3.1.3 Seismic surface wave methods

In situ characterization of the Vs profiles was performed in the Gölyaka basin utilizing non-invasive seismic testing methods that relied on the dispersive nature of the Rayleigh-type surface waves in layered media. In-situ seismic measurements of active and passive surface wave methods have been conducted in the study area to obtain the shear wave velocity results. These techniques have been used jointly to maintain reasonably high precision of shear wave velocity measurements not only at shallow depths but also at the deeper sections (Eker et al., 2012; Gosar et al., 2008; Gouveia et al., 2016; Koçkar, 2016; Koçkar et al., 2010; Koçkar and Akgün, 2012; Park et al., 2007). An active source implies that the seismic energy is created in purpose at a particular location relative to the geophone array, and the recording starts when the energy is conveyed into the ground (Park et al., 1999). On the other

hand, in passive surface wave techniques (Hayashi, 2008; Okada and Suto, 2003), there is no time break, and therefore motion from ambient energy is created by a series of artificial sources (i.e., cultural noise, traffic, machinery and so on) and natural phenomena (i.e., wind, wave motion) in different and often unknown locations according to the geophone array.

This study has mainly focused on high-resolution depths of 30 m or more, so the related configuration and instruments were selected accordingly. In order to obtain the subsurface Vs profile, Multichannel Analysis of Surface Wave (MASW) and Microtremor Array Method (MAM) have been preferred as active and passive surface wave methods, respectively. Active MASW and passive MAM surface wave measurements have been conducted to measure the shear wave velocity profiles to considerable depths. It should be noted that the acquisition patterns for both measured surface wave data need to be designed to optimize the complementarities of the collected frequency bands and to ensure an adequate overlap of the mutual frequency bands. As recommended in the literature, to measure the dispersion curve on the broadest possible frequency band, the concentric passive acquisitions have been applied from small to large spans (i.e., from 10 m up to 1 km or more depending on the targeted depth). As all dispersion curves were to be combined, active measurements were carried out near the center of the passive array, and finally, to prevent cross-contamination of the active and passive wave domains, the simultaneous acquisition was avoided, as suggested by Foti et al. (2018).

In the Quaternary alluvium and terrace sediments, a total of 29 surface wave measurements that entailed both passive (MAM) and active (MASW) methods have been performed to characterize the sediments based on their age and depositional settings. The spatial distribution of the measurement points is presented in Figure 7. In this part of the study, active MASW records with geophones spaced at 1.5 m with 5-10-15 m offset and a 16.5 m array length, and passive MAM records with geophones spaced at 5 m with 5 m offset and a 55 m length have been employed at each testing point. The field measurements were performed by adopting a grid system in which the seismic measurement points were placed approximately 700 m

apart. However, this grid system had to be modified slightly during the fieldwork due to environmental noise, dense vegetation, and accessibility problems throughout the lake site and the infrastructures. Since a combination of the distribution curves obtained by active and passive methods results in obtaining a high-resolution sediment profile for seismic characterization (Eker et al., 2012; Koçkar, 2016), a combined technique of the surface wave methods have been used to evaluate the underlying strata of the sediment profiles by using the Vs results in this study.

The primary difference between active and passive surface wave surveys in terms of outcomes is the different frequency ranges within which information can be gathered in such high-frequency components are usually relatively easy to generate and detect in active testing, whereas microtremors are frequently very active in the low-frequency range. Combining passive and active approaches has been proposed as a solution to overcome the constraints of each (Tokimatsu, 1995; Rix et al., 2002; Yoon and Rix, 2004). Combining two sets of data processed from passive and active field data, respectively, can be an extremely effective method for comprehending the overall modal nature over a wide variety of frequency and phase velocity ranges (Park et al., 2005).

A blind way technique was applied over the project site, and the primary purpose was to obtain the Vs profiles in the research site. To characterize the soil layers down to a depth of at least 30 m or more, the geophone type, offset length, and distance were selected accordingly, which allowed correlating the results of both testing methods according to diverse sources. Even though some active source (MASW) measurements were affected by the far-field effect, the results verified that the effort put forward during the study produced highly satisfactory results. This far-field effect was mitigated by comparing the results of reverse shot and MAM measurements. One of the fundamental assumptions of the surface wave methods is that the elastic characteristics of the materials underneath a seismic array are not lateral variables. To verify the validity of this assumption, the experimental dispersion curves created by forward and backward shots for the same seismic array can be compared in the MASW survey without changing any other data acquisition

parameters (Foti, 2005). The latest models were developed by the presumption that the fundamental mode of Rayleigh-type surface wave was recorded in the wave analyses.

All MASW and MAM data acquired were processed and analyzed using a SeisImager/SWTM V. 2.2 Surface Wave Analysis software. The same program was used to integrate active and passive SWMs at the same site. For the MASW and MAM records, the phase shift (Park et al., 1999) and spatial autocorrelation (SPAC) inversion (Okada, 2003) methods were used to obtain dispersion curves in the phase velocity frequency (v-f) domain. Figure 10 illustrates the MASW and MAM records that experientially produced v-f domain dispersion curves. Appendix A contains all the processed and analyzed surface seismic MASW and MAM data surveys.

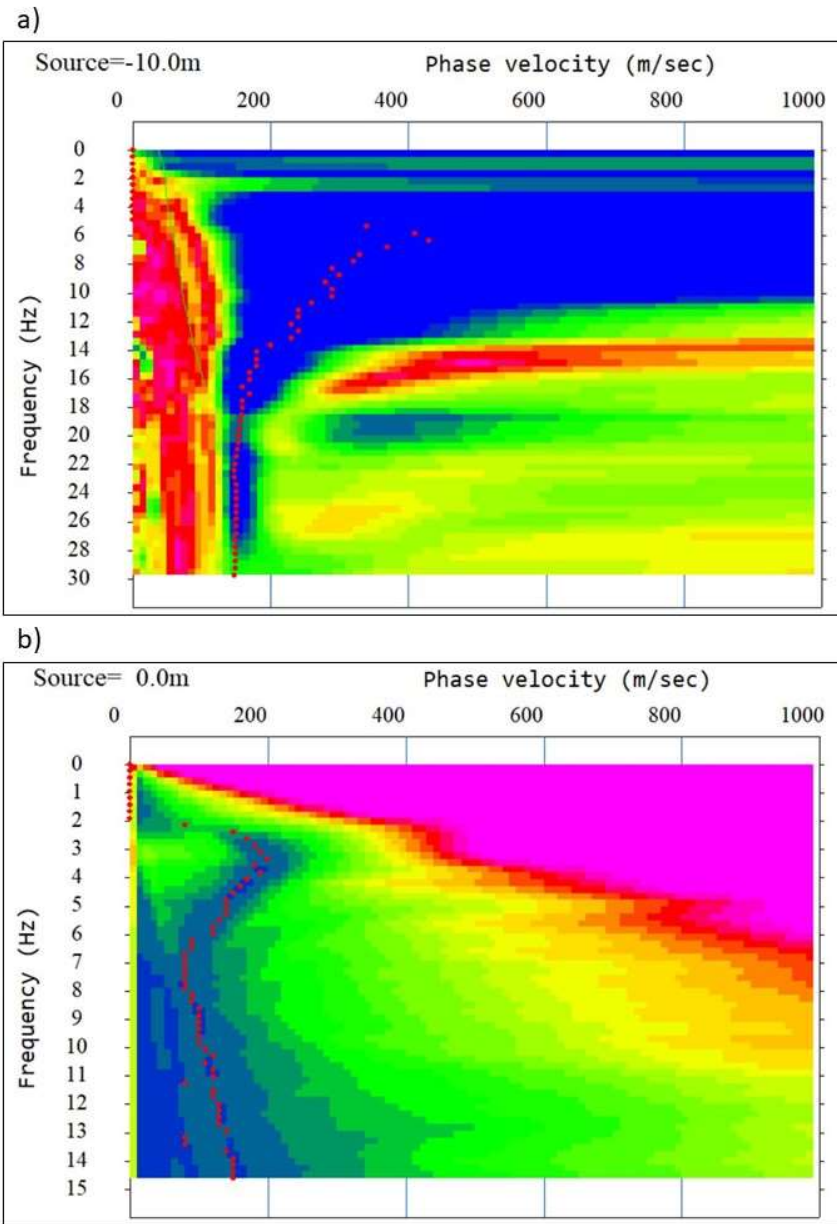


Figure 10. An example of the constructed experimental dispersion curve of a) Linear MASW and b) linear MAM records at Seis-15

Representative examples obtained from the processed dispersion curves were fit into the data, and the V_s profiles from the active and passive surface wave measurements were obtained, as presented in Figure 11. Similar to Figure 10, six profiles

representing the basin margin of the southern and northern parts along with the center of the basin are presented in Figure 11, where the consistency between these curves can be clearly seen. These results were also integrated and compared with the existing engineering geological and geotechnical boring data in the Gölyaka basin to confirm the validity of the conducted surface seismic testing results and thus aided in achieving more credible information on the subsurface sediments. With this procedure, the quality of the data collected from the surface wave measurements was assessed, validated, and later on, based on these results, the dimensional basin model of V_s was created.

Combining diverse data sets (surface wave measurements with different array spans) can supply an experimental dispersion curve over a wide frequency band. However, the branches of the dispersion curve in a variety of data sets must overlap with each other in the common frequency bands. A poor overlap might be related to various reasons (i.e., retrieval of different modes, lateral heterogeneity, lack of spectral resolution, difficulties in the processing step). An inadequate overlap confirms an analysis with poor reliability (Foti et al., 2018). In the Gölyaka basin, the combination of both methods has been thoroughly and accurately implemented, and representative examples extracted from different sections of the basin are given in Figure 11.

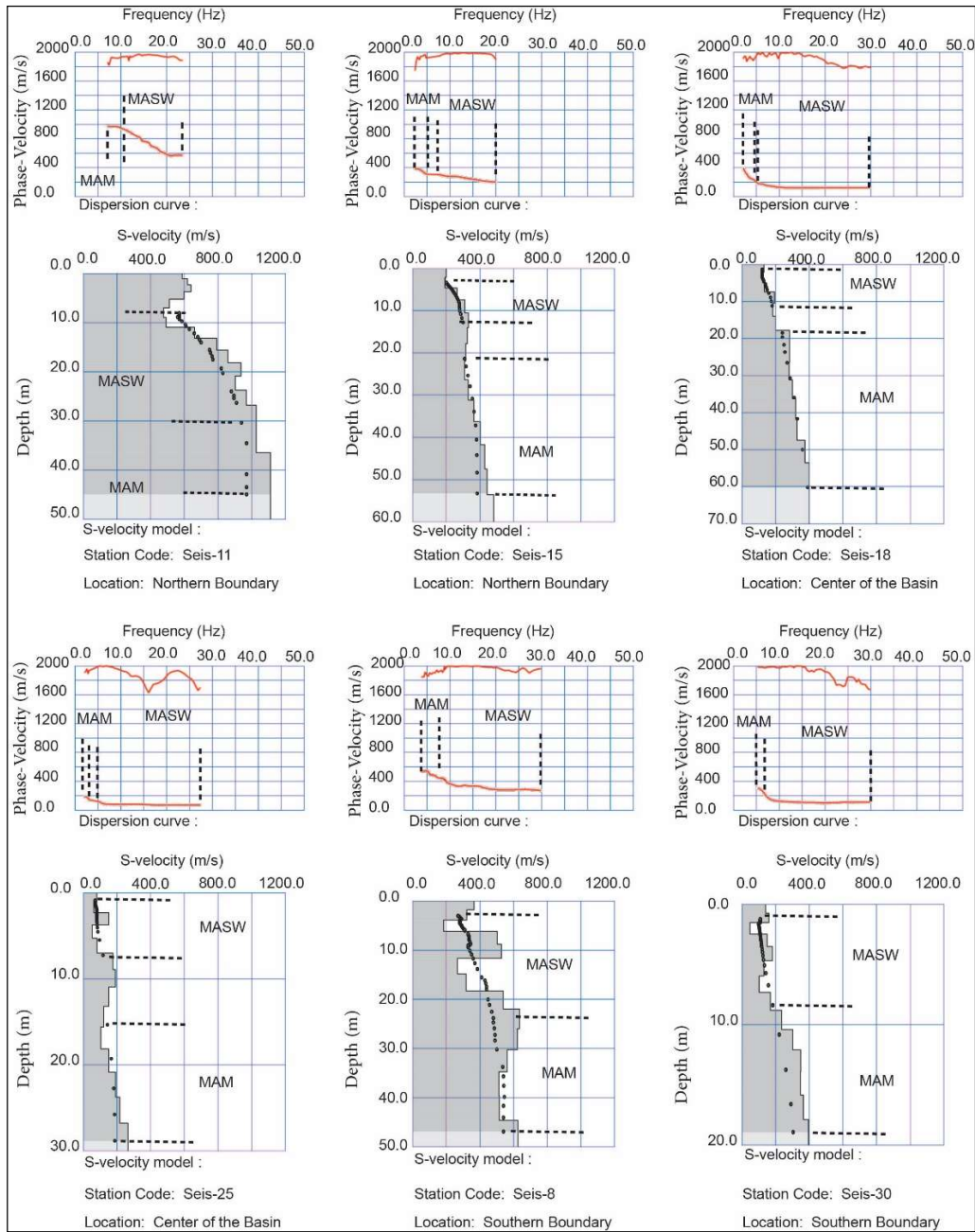


Figure 11. Representative combined, processed dispersion curves from MAM and MASW measurements and the corresponding Vs profiles concerning the basin margin of the southern and northern parts along with the center of the basin

3.1.4 Vertical Electrical Sounding (VES) Method

The Vertical Electrical Sounding (VES) method has become very popular in engineering investigations due to the simplicity of the technique. The VES method involves detecting the surface effects produced by the flow of the electric current inside the earth (Telford et al., 1976). Vertical Electrical Sounding (VES) was carried out using the Schlumberger array at 14 stations in the study area. Since the overburden thickness of the basin was significant, it required long current electrode spacing for greater penetration such that the largest current electrode spacing $AB/2$ used was between 600 and 1250 m. The field survey encompassed Vertical Electrical Sounding (VES) operations via the Schlumberger array (Takahashi, 2004).

All processed vertical electrical sounding (VES) data are supplied in Appendix B. Representative examples (from the measurement points G7 and G9) obtained from the processed 1-D profile of the VES measurements and the inferred log details are presented in Figure 12. According to Figure 12, the profile at point G7 illustrates a high resistivity value from the surface down to about 300 meters below the surface due to the interference of the electrical conductivity of the gravelly and blocky sediments in the Quaternary alluvium unit. There is an anomaly at a depth of about 300 m with low apparent resistivity. The decrease in resistivity beyond this depth is most likely due to the transition to marl, mudstone, and sandstone. It is inferred from this measurement that the thickness of the alluvium varies between 200 and 300 m. The profile of G9 at the northern edge of the boundary gave very different resistivity values as it progressed over the Quaternary alluvium units at shallower depths (i.e., at a depth of about 35 m). The high resistivity value beyond this depth suggests that it has interfingered with the Yıǵılca member (i.e., andesite-basalt member), which is accepted as bedrock. Hence, it most likely indicates a fault around this measurement point, which will be discussed in the latter sections.

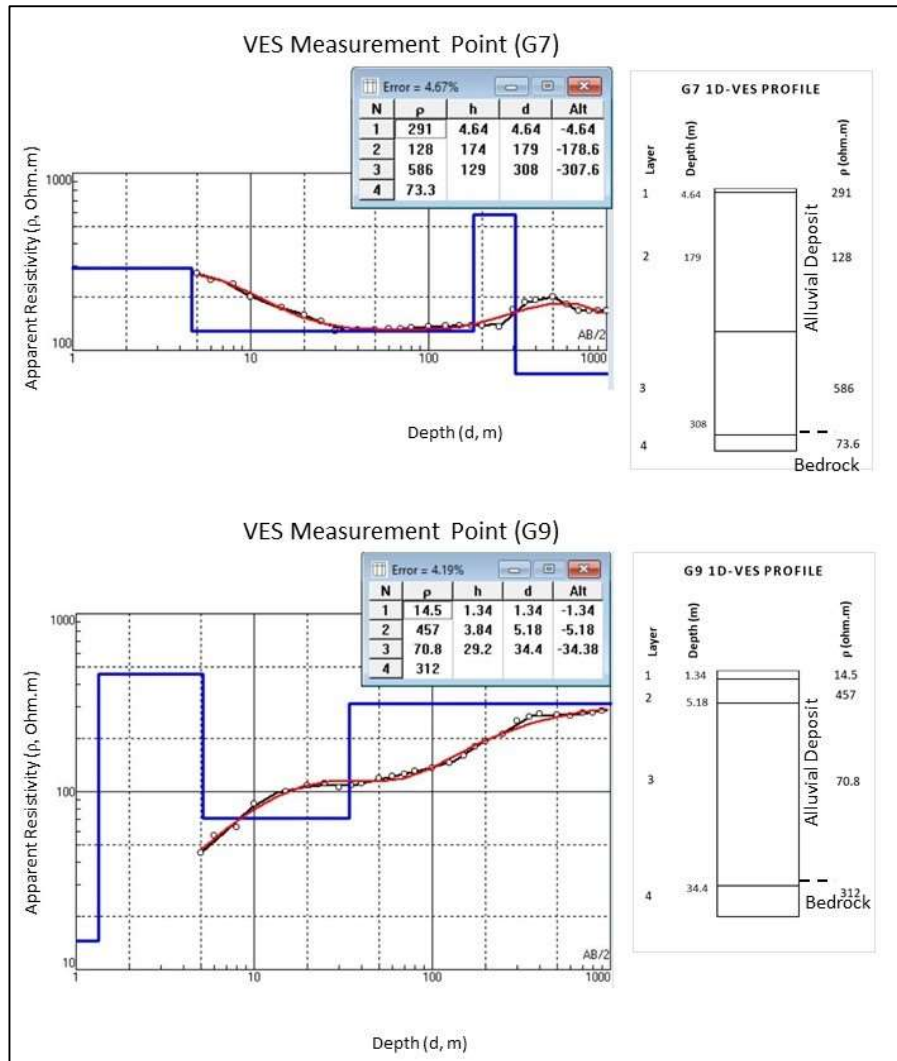


Figure 12. Examples presenting the processed 1-D profiles of Vertical Electrical Sounding (VES) measurements along with their inferred log profiles in the study area (from the measurement points of G7 and G9)

3.1.5 H/V microtremor measurements

Several studies (Ibs-von Seht & Wohlenberg, 1999; Özalaybey et al., 2011; Uebayashi et al., 2012, Eker et al., 2015) have shown that the resonance frequency obtained from microtremor measurements can be used to map the thickness of sediments. In this study, some microtremor measurements were recorded using a

single mobile station, and analyses of these records were processed by the H/V technique (Nakamura, 1989) to verify basin depth and the developed three 2-D Vs profiles. The spectral ratio between the horizontal and vertical components (H/V) of the microtremor measurements at the ground surface has been used to estimate the fundamental periods of the sites. Then, the predominant periods were calculated from the Vs profiles to estimate bedrock thickness using the quarter-wavelength method ($T_p = 4H / V_s$). The data was collected using a Güralp model PC-connected CMG-40TD seismograph with a frequency band of 0.033 Hz to 50 Hz and two horizontal and one vertical "servo type" velocity sensor. Data collection in this survey was carried out following the SESAME guidelines (SESAME, 2004). Microtremor recordings were typically recorded for 30 minutes with unprocessed waveforms and a 100 Hz sampling interval. The seismograph was warmed up for 5 minutes at each location before recording microtremors for 30 minutes. The data quality (measurements) was checked using a laptop PC during the recording process. In other words, in case there were any disturbances or adverse weather circumstances affecting the measurement process, the measurement was terminated, or the recording duration was increased to provide sufficient analysis windows after transient elimination.

After period analysis, a Fast Fourier Transform (FFT) approach was used on each selected window to waveform data (20 s) during data processing for each measurement point. The acquired Fourier spectrum was then smoothed with the suitable smoothing type and constant. The processed H/V measurements are shown in Figure 13.

The H/V spectral ratios were calculated at 0–10 Hz frequency intervals. The data indicated that the spectral ratio represented H/V curves with single, double, or broad peaks in the range of 0–10 Hz. Flat H/V curves were interpreted as “no-peak” values. Figure 13 shows the variation of the H/V spectral ratio curves obtained from the measurement points along the Vs profiles presented in Figure 28. In the meantime, Appendix C contains all of the processed H/V spectral ratio results acquired from the measuring points.

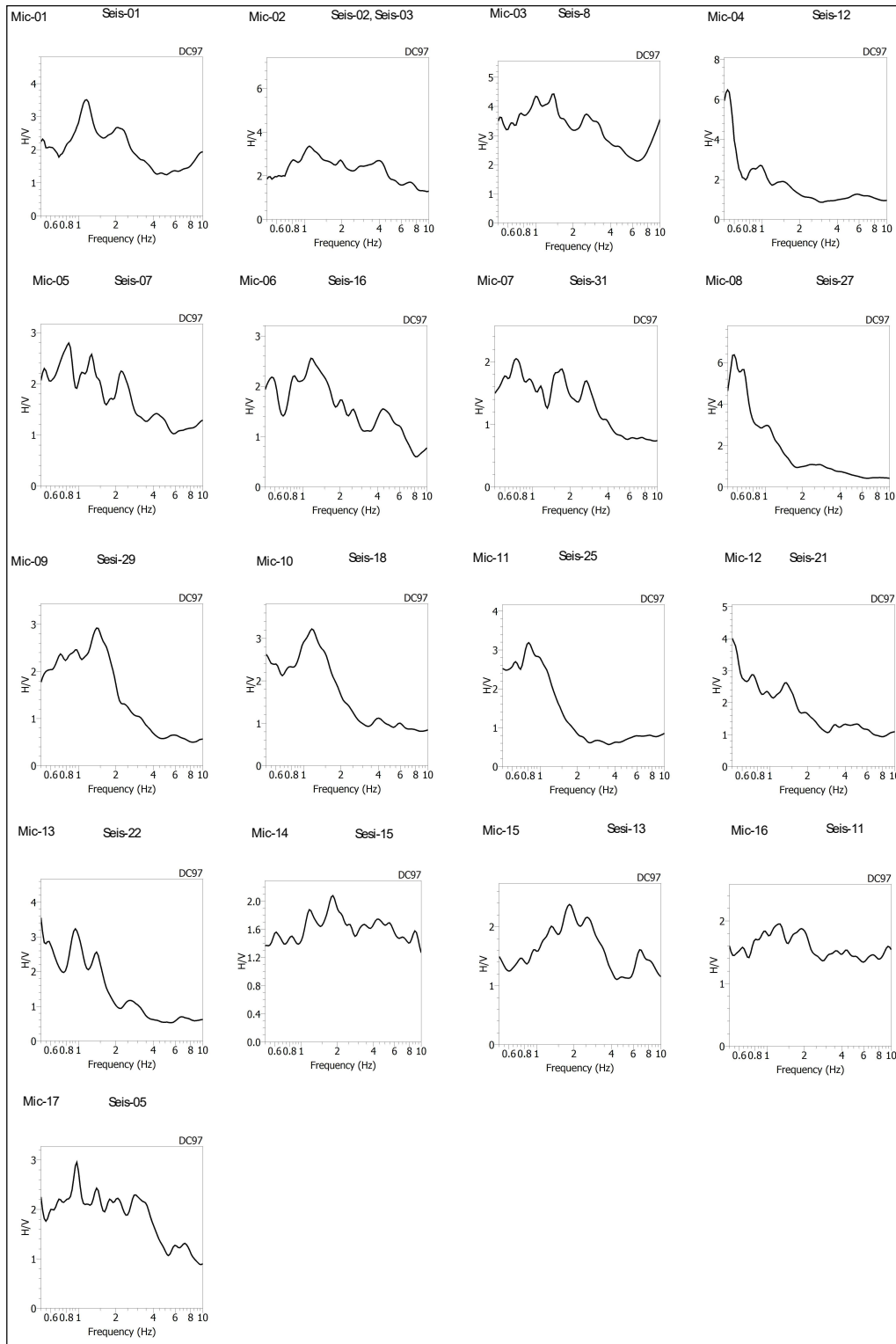


Figure 13. H/V spectral ratio curves that were selected to verify the given profile resulting from the measurements over the entire area

3.2 Procedure performed for 1D and 2D site response analysis

Soil response assessments involve the determination of nonlinear soil parameters and the evaluation of shear wave velocity profiles in the context of site effect characterization. There are numerous techniques available for simulating seismic response analyses that employ a variety of stress-strain constitutive models. These methods can be used to model the soil response in 1D, 2D, or 3D in the presence of an excitation. Dynamic soil response can be obtained through the use of linear (e.g., Boore, 1972; EPRI, 1988), equivalent linear (e.g., Idriss and Seed, 1967; Wallace and Rollins, 1996; Rathje and Bray, 2001; Ordonez, 2009; Barani et al., 2013), and nonlinear (e.g., EPRI, 1988; Dawson et al. 2001; Andrade and Borja, 2006; Gelagoti et al., 2010) techniques.

In general, it is considered that 1D analysis can cover critical response qualities associated with the underlying 3D problem. For many decades, one-dimensional analysis of horizontal shear wave vertical propagation and modeling of nonlinear soil responses using an equivalent linear approach have been used extensively in both scientific and engineering applications to determine the soil response to a possible excitation (Rathje and Bray, 2001; Chouinard et al., 2004; Cavallaro et al., 2008 ve 2012; Lanzo et al., 2008 ve 2012). However, the trustworthiness of 1D soil seismic response analysis results is questionable when estimating the accurate ground surface response (Kramer, 1996). Since the strata in the 1D analysis are considered horizontal in the vertical direction, the lateral and vertical abnormalities of subsurface layers and topography can be incorporated into a 2D/3D soil response analysis.

Seismic response analysis was carried out in this study using the 2D QUAD4M (Hudson et al., 1994) and 1D Shake2000 (Ordonez, 2000) software programs, which make equivalent linear assumptions and account for nonlinear stress-strain behavior of soils when investigating the effect of ground motions on basin/edge topography. However, due to the method's nature, seismic response analysis using an equivalent linear methodology results in over-attenuation, particularly at high frequencies, and

over-amplification of the soil response spectrum during big magnitude earthquakes (Kramer, 1996). In other words, due to the intrinsic linearity of equivalent linear analyses, false resonances (i.e., high levels of amplification caused by a strong component of the input motion coincident with one of the natural frequencies of the equivalent linear soil deposit) might occur. Such high amplification levels will not emerge in the field because the stiffness of nonlinear soil decreases throughout a major earthquake. When the peak shear strain is substantially much larger than the rest of the shear strains, using an effective shear strain in an equivalent linear analysis can result in an over-softened and over-damped system or an under-softened and under-damped system when the shear strain amplitude is almost uniform (Kramer, 1996).

Independent of dimensionality, one of the essential themes in soil response assessment is the characterization of soils to bedrock depth. Based on the shear wave velocity value from a seismological and geotechnical perspective, there are two bedrock conceptions. Seismic bedrock is one of them, while engineering bedrock is another. It is generally acknowledged that the seismic layer has a significant lateral extent and is more homogeneous and uniform in composition as compared to the underlying layers. According to Andrus et al. (2006) and Chapman et al. (2006), the lower bound for the shear wave velocity of seismic bedrock is 3500 m/s. Different shear wave velocity values are used to describe the engineering bedrock. For engineering bedrock used in geotechnical foundation design and characterization investigations, the lowest bound of the shear wave velocity value is between 500 and 760 m/s (e.g., Pitilakis, 2004; Boore, 2006; Havenith et al., 2007; Sitharam and Anbazhagan, 2008).

In this research study, the depth of bedrock was estimated to be greater than 200 meters in some areas of the region. However, the geophysical studies performed in this study could not characterize the layers to this depth. As a result, extrapolation was required to assign V_s data to the deeper layers and ultimately to the

characterization depth. A cut-off value of 1100 m/s was accepted and assigned to the bedrock to avoid increasing the uncertainty in the extrapolation step as a result of the significant lateral geological heterogeneities.

The rupture propagation can considerably affect ground vibrations close to a causative fault related to an earthquake. When the rupture and slip directions are coincident with respect to a site, and a considerable portion of the fault ruptures towards the site, the ground motion can display Forward directivity (FD) effects (Somerville et al., 1997). The FD effects occur when the fault rupture velocity is slightly less than the shear wave propagation velocity. As the rupture front propagates out from the hypocenter, a buildup of shear waves going ahead of the rupture front forms a shear wavefront. When a site is located at one end of a fault, and the rupture begins at the opposite end and proceeds toward the site, the arrival of the wavefront is seen as a big pulse of motion near the start of the record. Due to the radiation pattern of the fault's shear dislocation, this huge pulse of motion is oriented normal to the fault plane. FD generates large-amplitude, short-duration ground vibrations. These effects often have a long duration and are most readily visible in the velocity- or displacement-time history. The majority of energy in FD motions is concentrated in a small frequency range and is expressed as one or more high-intensity velocity pulses oriented in the fault-normal direction. Recent earthquakes, such as the 1994 Northridge, 1995 Kobe, and 1999 Kocaeli earthquakes, have demonstrated that these high-velocity pulses can cause catastrophic structural damage.

These investigations included the creation of prediction correlations for the period and amplitude of pulses with forward direction. However, they have omitted a measure of the prediction's uncertainty. In addition, the effects of local site effects on the features of pulse-type motions and the near-fault ground movements recorded during the 1999 Chi-Chi, Taiwan and 1999 Kocaeli and Duzce, Turkey Earthquakes were included in these studies to help comprehend the near-field site effects on ground motion.

This study aims to identify suitable rock-earthquake records for the study area, characterize local soils and determine nonlinear soil properties, conduct 1D and 2D soil response analyses, and compare the acquired findings. The analyses were conducted by considering the region's active tectonic structure and the relatively large ($M > 7$) magnitude earthquake potential as determined by a deterministic seismic hazard assessment approach. The related acceleration records were chosen based on the distinct earthquakes represented in the Pacific Earthquake Engineering Research (PEER) Center's NGA West-2 ground motion database. As a result, the performance of equivalent linear 1D and 2D analyses was compared at the same sites.

3.2.1 Procedure performed in numerical modeling

QUAD4M operates in the time domain and solves a dynamic equilibrium equation utilizing Newmark's unconditionally stable direct time integration, built on quadrilateral elements and employs a direct integration approach. Furthermore, QUAD4M incorporates a transmitting base to model the half-space beneath the mesh and eliminates the need for a rigid base assumption. Additionally, soil materials are treated as a single continuous linear viscoelastic material (Hudson et al., 1994). As with the Shake2000 program, each layer's shear modulus and damping ratio are altered (Ordonez, 2000). The analyses are performed until the effective shear stresses created at each layer are consistent with the layer's predetermined constant shear modulus and damping ratios. Shake2000 estimates the dynamic response of a layered system using a closed-form solution of a one-dimensional wave equation in the frequency domain and simulates damping independently of frequency (Ordonez, 2000). On the other hand, QUAD4M uses Rayleigh damping, which defines the viscous damping matrix as a linear combination of mass and stiffness matrices (Hudson et al., 1994).

A graphical interface called Visual-Q4M was used to generate complicated geometries considering lateral and vertical differences in lithologies, bedrock

surface, and topography. It can create complicated grids for use in FEM analysis to conduct QUAD4M analysis and provides graphical user interfaces for post-processing QUAD4M analysis results. Additionally, during the running stage of a study, it displays the strain check value after each iteration. As a result, it avoids acquiring misleading results due to the interpretation of an incomplete analysis.

For assessing soil response, two cross-sections representative of the basin's properties were produced E-W and NW-SE, respectively (Figure 14). As seen in this illustration, one is northwest-southeast (NW-SE), and the other is almost east-west (E-W). Four locations along the NW-SE segment have shear wave velocity measurements. On the other hand, the E-W segment contains seven shear wave velocity points. A total of 11 locations were subjected to a 1D seismic site response analysis, and these two sections were subjected to a 2D seismic site response analysis.

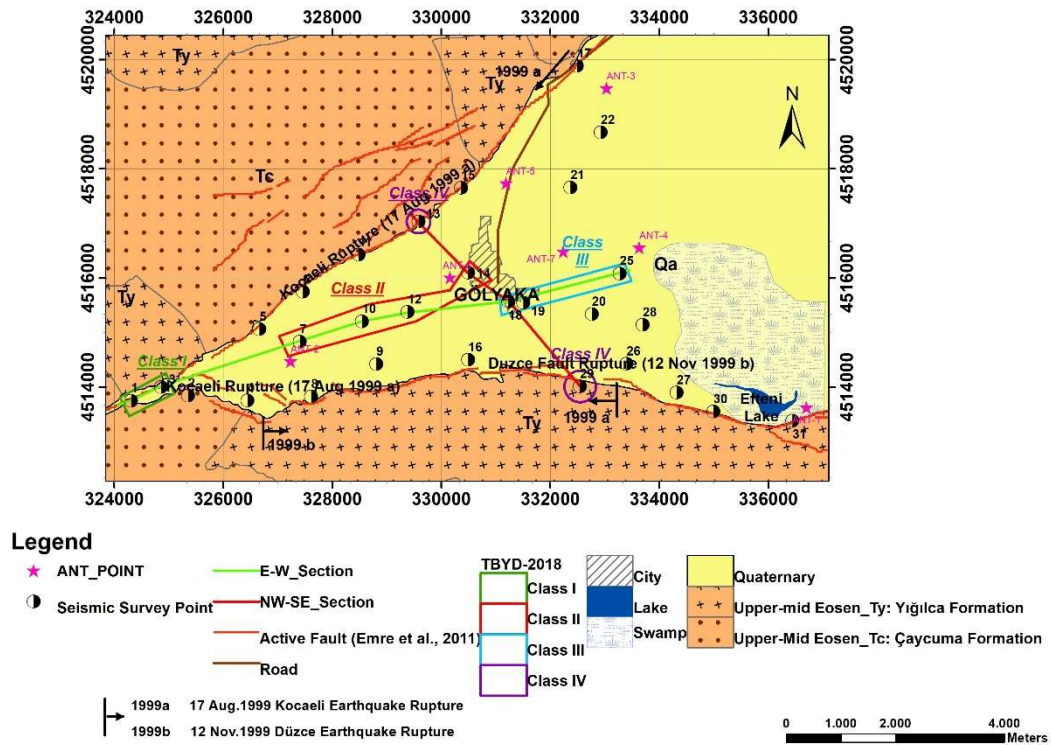


Figure 14. The cross-sections and measurement sites used in this study for a 1D and 2D site response analysis.

To model dynamic soil response behavior utilizing either the 1D or 2D analysis approaches mentioned previously, four major activities need to be accomplished as follows:

- development of a site-specific target spectrum,
- selection and scaling of input rock motions,
- characterization of a shear wave velocity profile,
- determination of nonlinear soil properties.

More details on the approach used to determine each of the aforementioned items may be found in the subsections that follow this chapter.

3.2.2 Development of a site-specific target spectrum

For almost 40 years, two approaches for determining design ground motion have been used in practice: deterministic (Krinitzsky and Chang, 1975) and probabilistic (Cornell, 1968) approach. Individual earthquake scenarios (with magnitude and location of the earthquake) are produced for each seismic source using the deterministic approach (Wells and Coppersmith, 1994). Rather than taking a probabilistic approach, this work takes a deterministic one by choosing a specific ground motion probability level which is often derived from the median (i.e., 50% likelihood of exceeding). In this dissertation, a deterministic seismic hazard analysis was conducted on only earthquake sources with destructive potential for the study area, following Reiter's (1990) four-step procedure:

The first stage was to classify and identify each seismic source capable of causing potentially damaging earthquakes in the research area. Although several distance definitions can be utilized depending on the attenuation relation standards (i.e., Joyner-Boore distance, rupture distance), the shortest distance between the fault zone and the study region was determined in the second phase. A characteristic earthquake was defined in the third phase based on its magnitude and distance from the study area. The fault zone segments nearest to the study area were chosen since they have

the most significant destructive potential for the study area. The third step was to assess seismic hazards based on the ground motion caused by the region's typical earthquakes in the research area. Cambazoğlu et al. (2016) have provided detailed information on characterizing earthquake sources using probabilistic approaches for the 1999 Düzce fault rupture.

A target spectrum was created for each site to select a range of input motions for 1D and 2D soil reaction assessment. After scaling the selected motions inside the suits, the suit with the seven input rock movements that best fit the target response spectrum was selected.

The deterministic method was used to obtain the region's target response spectrum by utilizing specified ground motion prediction equations based on the fault mechanism and regional tectonic circumstances. Figure 15 illustrates the produced target spectra. The distance between the sites and the fault segments was set to 2 km based on the average proximity of the sites. Calculations were performed using equally weighted GMPEs (Abrahamson-Silva-Kamai, 2014; Boore-Stewart-Seyhan-Atkinson, 14; Campbell-Bozorgnia, 2014; Chiou-Youngs, 14) for a possible earthquake ($M_w = 7.2$) along the NAFS, and a V_{S30} value of 760 m/s was used to represent the rock site.

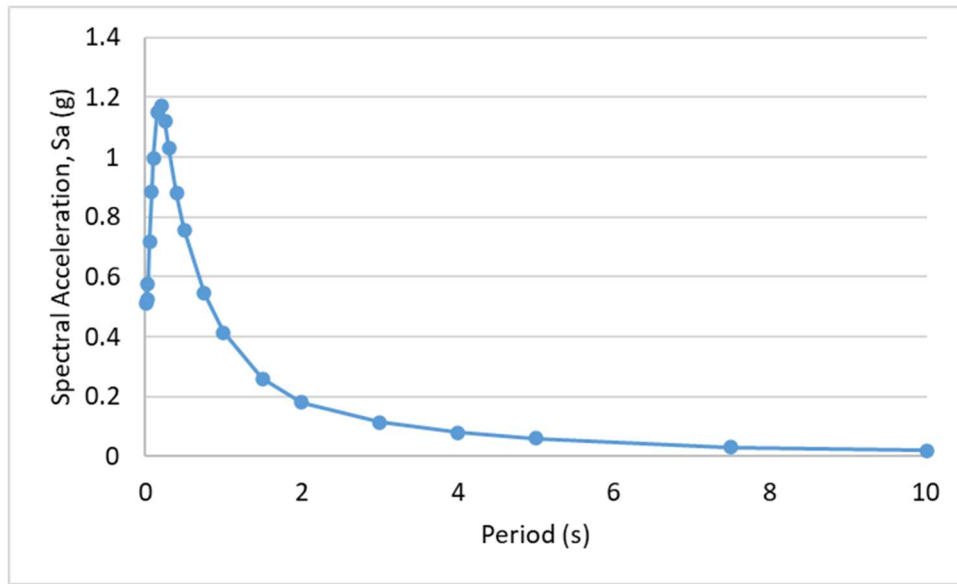


Figure 15. Site-specific target spectrum developed for the study area

3.2.3 Selection and scaling of the input rock motions

When superstructural information is ignored, the nonlinear behavior of soil, the characteristics of ground motion (i.e., intensity, duration, and the frequency content of ground motion), topography, subsurface geometry, and local soil condition all have a significant effect on the pattern of earthquake damage. The primary objective of a site response analysis is to generate a statistically reliable ground motion estimation based on the established target rock spectrum. In other words, the response spectrum computed is not strongly influenced by the input rock motions chosen (Rathje et al., 2010). Due to the non-linear behavior of soil, the calculated seismic site response may be influenced by the input rock motion characteristics. This effect can be minimized only by using a sufficient number of input rock motions either from earthquake records or through the creation of synthetic records (Bommer and Acevedo, 2004; ASCE 7, 2010).

To choose appropriate data from the Pacific Earthquake Engineering Research (PEER) Center's NGA West-2 ground motion database and to create appropriate suits for this investigation, the following criteria were used: Suits were formed by searching the NGA West-2 database (i.e., no aftershocks), selecting only one record from any single event, limiting the moment magnitude of the earthquake record of interest to 6.0 to 8.0, considering earthquakes that occurred within a distance of 0 km to 10 km, and setting the minimum and maximum shear wave velocity to 100 m/s and 1100 m/s, respectively.

Twenty earthquake records were chosen based on the criteria mentioned above. Table 1 summarizes these earthquakes. A total of twenty earthquakes were scaled, and seven of them were used to create suits using the criteria outlined above. Scaling was performed on the h2 components of each record.

Table 1. A summary of the pulse-like ground motion records that were chosen (PEER Ground Motion Database, NGA- WEST 2).

ID	Earthquake Name	Year	Station Name	Mw	Mechanism	Rrup (km)	V _{s30} (m/s)	PGA (g)
1	"Imperial Valley-06"	1979	"El Centro Array #10"	6.53	strike slip	8.6	203	0.23
2	"Imperial Valley-06"	1979	"El Centro Differential Array"	6.53	strike slip	5.09	202	0.48
3	"Imperial Valley-06"	1979	"Holtville Post Office"	6.53	strike slip	7.5	203	0.22
4	"Morgan Hill"	1984	"Coyote Lake Dam - Southwest Abutment"	6.19	strike slip	0.53	561	1.3
5	"Morgan Hill"	1984	"Gilroy Array #6"	6.19	strike slip	9.87	663	0.29
6	"Superstition Hills-02"	1987	"Parachute Test Site"	6.54	strike slip	0.95	349	0.39
7	"Kobe_ Japan"	1995	"KJMA"	6.9	strike slip	0.96	312	0.63
8	"Kobe_ Japan"	1995	"Takarazuka"	6.9	strike slip	0.27	312	0.62
9	"Kocaeli_ Turkey"	1999	"Izmit"	7.51	strike slip	7.21	811	0.23
10	"Chi-Chi_ Taiwan-04"	1999	"CHY074"	6.2	strike slip	6.2	553	0.33
11	"Bam_ Iran"	2003	"Bam"	6.6	strike slip	1.7	487	0.64
12	"Parkfield-02_ CA"	2004	"PARKFIELD - EADES"	6	strike slip	2.85	384	0.39
13	"Parkfield-02_ CA"	2004	"Parkfield - Cholame 1E"	6	strike slip	3	327	0.36
14	"Parkfield-02_ CA"	2004	"Parkfield - Cholame 3W"	6	strike slip	3.63	231	0.58
15	"Parkfield-02_ CA"	2004	"Parkfield - Fault Zone 1"	6	strike slip	2.51	178	0.84
16	"Darfield_ New Zealand"	2010	"DSLCL"	7	strike slip	8.46	296	0.26
17	"Darfield_ New Zealand"	2010	"HORC"	7	strike slip	7.29	326	0.48
18	"Darfield_ New Zealand"	2010	"LINC"	7	strike slip	7.11	263	0.39
19	"Darfield_ New Zealand"	2010	"TPLC"	7	strike slip	6.11	249	0.21
20	"Duzce_ Turkey"	1999	"IRIGM 487"	7.14	strike slip	2.65	690	0.3

Several suites having seven earthquake records were chosen and time-scaled in this analysis. The SeismoMatch software 2021 was used to select and linearly scale ground acceleration records. Rather than employing frequency domain spectral matching (e.g., Gasparini and Vanmarcke, 1976; Silva and Lee, 1987) or linear scaling of ground motions (Kottke and Rathje, 2009), this program makes use of the wavelets algorithm as proposed by Abrahamson (1992) and Hancock et al. (2006), which is based on the time domain technique proposed by Lilanand and Tseng (1988). The maximum and average mismatches were used to determine the suit best fits the target spectrum. The average misfit of the mean matched spectrum is 2.18 percent, while the maximum mismatch is 6.05 percent. The suit that best matches the target spectrum is depicted in Figure 16. Table 2 contains information about seven earthquake recordings included in the suit. In addition, Figure 17 and Figure 18 illustrate the original and matched accelerograms, respectively, of the seven records that comprise the best-fit suit, as well as the target spectrum.

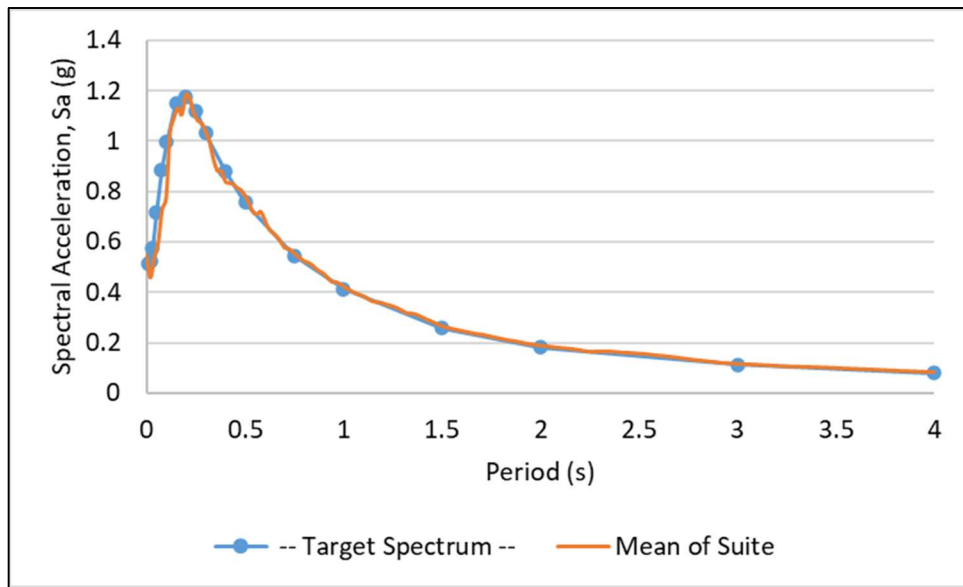


Figure 16. The mean match spectrum is calculated by averaging the spectra of the seven earthquakes and the target spectrum.

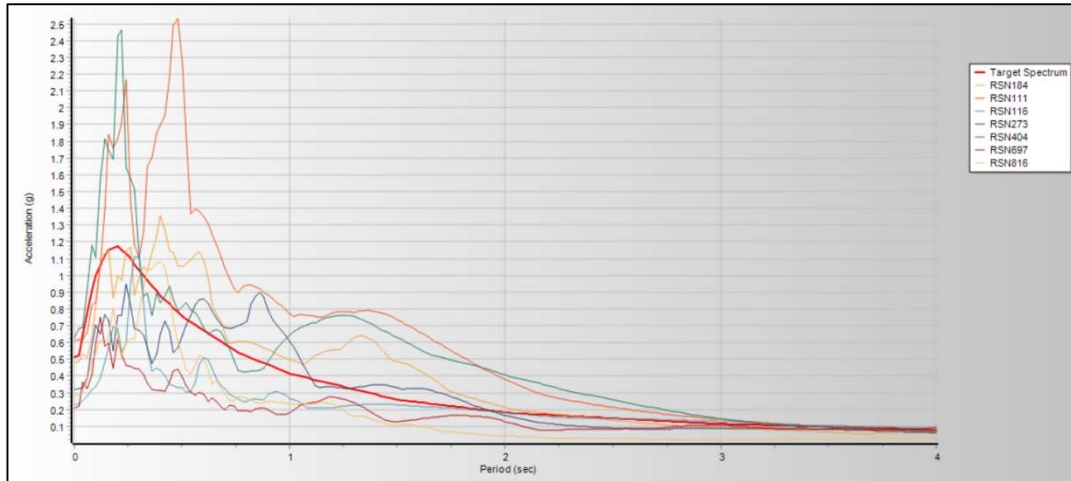


Figure 17. Target spectrum of the original accelerograms of the seven earthquakes. The abbreviations for these records are listed in Table 2.

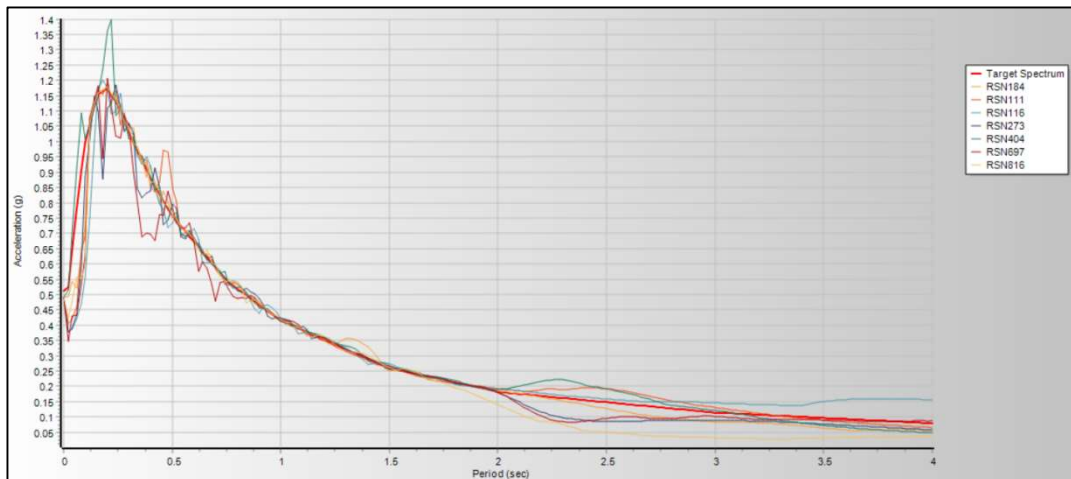


Figure 18. Matched accelerograms of the seven earthquakes matched the target spectrum. The records are abbreviated in Table 2.

Table 2. A summary of the seven earthquake records used to create the suit best matches the target spectrum.

ID	Record	Tp-Pulse Period (sec)	Earthquake Name	Year	Station Name	Mw	Mechanism	Rrup (km)	V _{s30} (m/sec)	PGA(g)	Scale Factor
1	RSN184	6.265	"Imperial Valley-06"	1979	"El Centro Differential Array"	6.53	SS	5.09	202	0.48	1
2	RSN1119	1.806	"Kobe_ Japan"	1995	"Takarazuka "	6.9	SS	0.27	312	0.62	1
3	RSN1165	5.369	"Kocaeli_ Turkey"	1999	"Izmit"	7.51	SS	7.21	811	0.23	1
4	RSN2734	2.436	"Chi-Chi_ Taiwan-04"	1999	"CHY074"	6.2	SS	6.2	553	0.33	1
5	RSN4040	2.023	"Bam_ Iran"	2003	"Bam"	6.6	SS	1.7	487	0.64	1
6	RSN6975	8.932	"Darfield_ New Zealand"	2010	"TPLC"	7	SS	6.11	249	0.21	1
7	RSN8164	10.052	"Duzce_ Turkey"	1999	"IRIGM 487"	7.14	SS	2.65	690	0.3	1

3.2.4 Geometries of the 1D and 2D soil profiles

To conduct 1D and 2D assessments of soil reaction, two cross-sections representative of the basin's properties were produced (Figure 19 and Figure 20). As seen in Figure 19 and Figure 20, the trends of the cross-sections are northwest-southeast (NW-SE) and almost east-west (E-W), respectively.

As indicated in this chapter, the blind method technique was used to derive the shear wave velocity (V_s) profile. After evaluating the results of these tests, it was discovered that practically all profiles, except one, had three distinct layers. As a result, 11 sites constructed their 1D shear wave velocity profiles using an idealization approach. The layer with shear wave velocity values larger than 760 m/s during the idealization process is considered bedrock, so the shear wave velocity bedrock half-space is assigned a V_s value of 1100 m/s. Then, using the neighboring measurement sites, geology, and vertical variation of the V_s across the profile, all 1D profiles were extrapolated according to this value.

Almost every profile revealed four layers, of which one was the bedrock. 2D V_s sections were produced by employing 1D profiles along the E-W and NW-SE

sections, respectively, as shown in Figure 19 and Figure 20. The mean values of the geotechnical and geophysical properties of the layers, such as unit weight, thickness, and shear wave velocity, were computed, together with their mean and standard deviations, and presented in Tables 3 through 8. These average values were applied to each layer in the 2D sections.

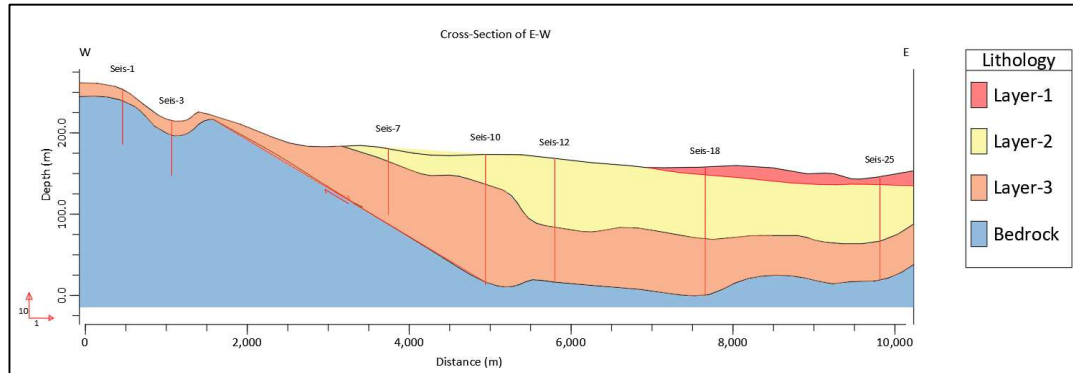


Figure 19. 2D soil model of the E-W cross-section

Table 3. Variations in layer thickness along the E-W segment on a lateral and vertical scale.

Thickness (m)								E-W section	
	Seis-1	Seis-3	Seis-7	Seis-10	Seis-12	Seis-18	Seis-25	Mean	Std.
Layer-1						9.6	10	9.8	0.28
Layer-2			15	37	85	76	69.4	56.5	29.42
Layer-3	15	18	77	120	67	70	47.7	59.2	36.46
Bedrock	-	-	-	-	-	-	-		

Table 4. Variations in the unit weights of the layers along the E-W section.

Unit weight kN/m ³								E-W section	
	Seis-1	Seis-3	Seis-7	Seis-10	Seis-12	Seis-18	Seis-25	Mean	Std.
Layer-1	-	-	-	-	-	17.6	17.4	17.5	0.14
Layer-2	-	-	18.4	18.3	17.8	18	17.8	18.1	0.28
Layer-3	19.2	19.1	18.9	18.8	18.5	18.5	18.5	18.8	0.30
Bedrock	-	-	-	-	-	-	-		

Table 5. Variation in the shear wave velocity of the layers along the E-W section in lateral and vertical directions.

	Vs (m/s)							E-W section	
	Seis-1	Seis-3	Seis-7	Seis-10	Seis-12	Seis-18	Seis-25	Mean	Std.
Layer -1	-	-	-	-	-	132	120	126	8.49
Layer -2	-	-	320	305	183	250	267	265	53.80
Layer -3	611	581	581	665	588	565	557	593	36.29
Bedrock	1100	1100	1100	1100	1100	1100	1100	1100	0.00

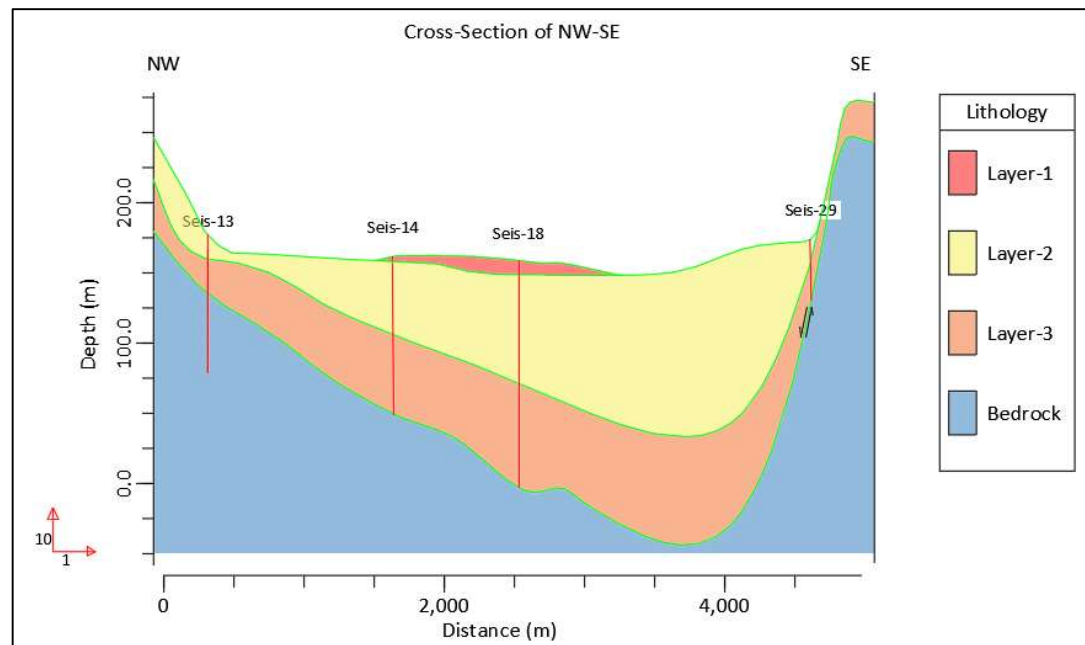


Figure 20. 2D Soil model of the NW-SE cross-section

Table 6. Variations in layer thickness along the NW-SE segment on a lateral and vertical scale.

	Thickness (m)				NW-SE section	
	Seis-13	Seis-14	Seis-18	Seis-29	Mean	Std.
Layer -1		3	9.6		6.3	4.67
Layer -2	17	52.2	76	16.5	40.4	29.01
Layer -3	23.5	56.6	70	26.6	44.2	22.79
Bedrock	-	-	-	-		

Table 7. Variations in the unit weights of the layers along the NW-SE section.

Unit weight kN/m ³					NW-SE section	
	Seis-13	Seis-14	Seis-18	Seis-29	Mean	Std.
Layer -1	-	17.6	17.6	-	17.6	0.00
Layer -2	17.9	18.1	18	18.2	18.1	0.13
Layer -3	19.4	18.6	18.5	18.9	18.6	0.40
Bedrock	-	-	-	-		

Table 8. Variation in the shear wave velocity of the layers along the NW-SE section in the lateral and vertical directions.

Vs (m/s)					NW-SE section	
	Seis-13	Seis-14	Seis-18	Seis-29	Mean	Std.
Layer -1	-	133	132	-	132.5	0.71
Layer -2	259	284	250	310	275.8	26.99
Layer -3	625	595	565	495	570.0	55.68
Bedrock	1100	1100	1100	1100	1100.0	0.00

The 1D and 2D profiles were constructed after the layers' geophysical, geotechnical, and geometric features were determined during the idealization of the 11 measurement locations. Matasovic and Ordonez (2012) claimed that strain-dependent attributes (e.g., shear modulus and damping values) rely on layer thickness. These qualities change with depth. Matasovic and Ordonez (2012) advised using thinner layers to capture significantly non-linear and/or non-uniform shear strain fluctuation over the soil profile. Layering a soil column in Shake2000 is also required to mimic vertical V_s depth fluctuations, although a relatively thick layer may mimic the soil column in Shake 2000 when the shear wave velocity is constant and the shear strain variation is essentially uniform (Ordonez, 2012). During this analysis step, each layer's shear wave velocity values are expected to be uniform and not to change appreciably vertically. The shear strain inside each layer is also assumed to be uniform.

To account for the linear rise in shear wave velocity with depth, some locations had their shear wave velocity profiles extended to 200 m (Table 3 and 6). The uncertainty of the modulus reduction and damping curves was also considered (Darendeli, 2001). A sensitivity study was also performed to evaluate the impact of the layer thickness and variations in shear wave velocity at the main layer's sublayers. These two model settings had no effect on the surface soil response. The primary layers were subdivided using Equations 1 and 2, where it was assumed that the shear strains behaved uniformly in the subsets of each layer.

$$H_{max} \leq V_s / (4 \times f_{max}) \quad \text{Eq. (1)}$$

$$f_{max} = \frac{1}{2 \times DT} \quad \text{Eq. (2)}$$

In the above equations, f_{max} is the maximum resolved frequency (Hz), and DT is the sampling interval of the records (s). In the 1D soil response analysis, a frequency threshold of 25 Hz was used. Table 9 and 10 show the maximum height of each sublayer determined by using the preceding formulae. Each main layer's sublayer count was determined by the H_{max} value.

2D soil response investigations started with 2D geometries of the soil models (Figures 19a-c), built from the lateral continuation of the soil layers described by the 1D shear wave velocity profile at the 11 sites (Table 3- 8). The mechanical properties of these lateral continuous soil layers were assigned using the mean values of the data from each site along the sections (Table 3- 8).

Table 9. The maximum height (m) along the E-W section for the 1D soil response study.

Maximum height (m) for 1D soil response analysis- E-W section							
	Seis-1	Seis-3	Seis-7	Seis-10	Seis-12	Seis-18	Seis-25
Layer -1	-	-	-	-	-	1.3	1.2
Layer -2	-	-	3.2	3.1	1.8	2.5	2.7
Layer -3	6.1	5.8	5.8	6.7	5.9	5.7	5.6
Bedrock	11.0	11.0	11.0	11.0	11.0	11.0	11.0

Table 10. The maximum height (m) along the NW-SE section for the 1D soil response study.

Maximum height (m) for 1D soil response analysis- NW-SE section				
	Seis-13	Seis-14	Seis-18	Seis-29
Layer -1	-	1.3	1.3	-
Layer -2	2.6	2.8	2.5	3.1
Layer -3	6.3	6.0	5.7	5.0
Bedrock	11.0	11.0	11.0	11.0

The geometry of the individual soil layers (i.e., those that lack continuity in the lateral direction) was modeled using the region's geological background information. This information is vital in developing the geometric model because the study area is a fault-controlled basin with rivers and lakes controlling the depositional and/or erosional settings. Variations in the data were also considered, most notably during the modulus reduction and damping curves, as discussed in the following portions of this chapter.

After creating the geometry, both sections' finite element (FE) meshes were created to conduct 2D seismic response assessments using the finite element method (FEM)-based QUAD4M. Quadrilateral and triangular elements were chosen due to the complicated geometries of the layers creating the sections. Equation 3 was used to determine the maximum height of the elements. The maximum value of the ratio between the horizontal and vertical sizes of the elements was constrained to less than three to improve the accuracy of the results. FE meshes were generated following these considerations (Figure 21). Table 11 details the geometric model and mesh attributes of the parts.

$$H_{max} \leq C \times \frac{V_s}{f_{max}} \quad \text{Eq. (3)}$$

where H_{max} represents the maximum height of a finite element (m), V_s represents the layer's shear wave velocity (m/s), f_{max} represents the maximum resolved frequency

(Hz), and C represents a constant that ranges between 1/5 and 1/10 according to various studies (e.g., Kuhlemeyer and Lysmer, 1973; Lanzo and Silvestri, 1999; and Ordóñez, 2009). The C value is set to 1/5 in this study.

Table 11. Summary of geometry and mesh characteristics

Sections	Min. Height (m)	Max. Height (m)	Min. Length (m)	Max. Length (m)	Node No	Element Nos
E-W	0	261.7	0	10000	22384	21312
NW-SE	32.8	350.29	0	5000	24614	23526

As indicated in this section, since the deconvolution procedure was used, transmitting boundary conditions were applied to the base of the soil models. Additionally, to mitigate the effect of intentionally reflected waves, various studies reported building their models with lateral extension values ranging from 200 to 800 m (Augello et al., 1998; Rathje and Bray, 2001; Pagliaroli, 2006). The primary reason for this large range is connected to the goal of the seismic response analysis and the geometry of the models used in this research. To circumvent this problem, Bouckovalas et al. (2006) proposed that the overall lateral extent of a model be at least five times the thickness of the soil column. The side boundaries of both models were extended 500 m in both directions in this study, taking into account lithological changes and bedrock geometry to reduce the influence of the side boundaries, which is the interference between the input motion and the artificially reflected waves.

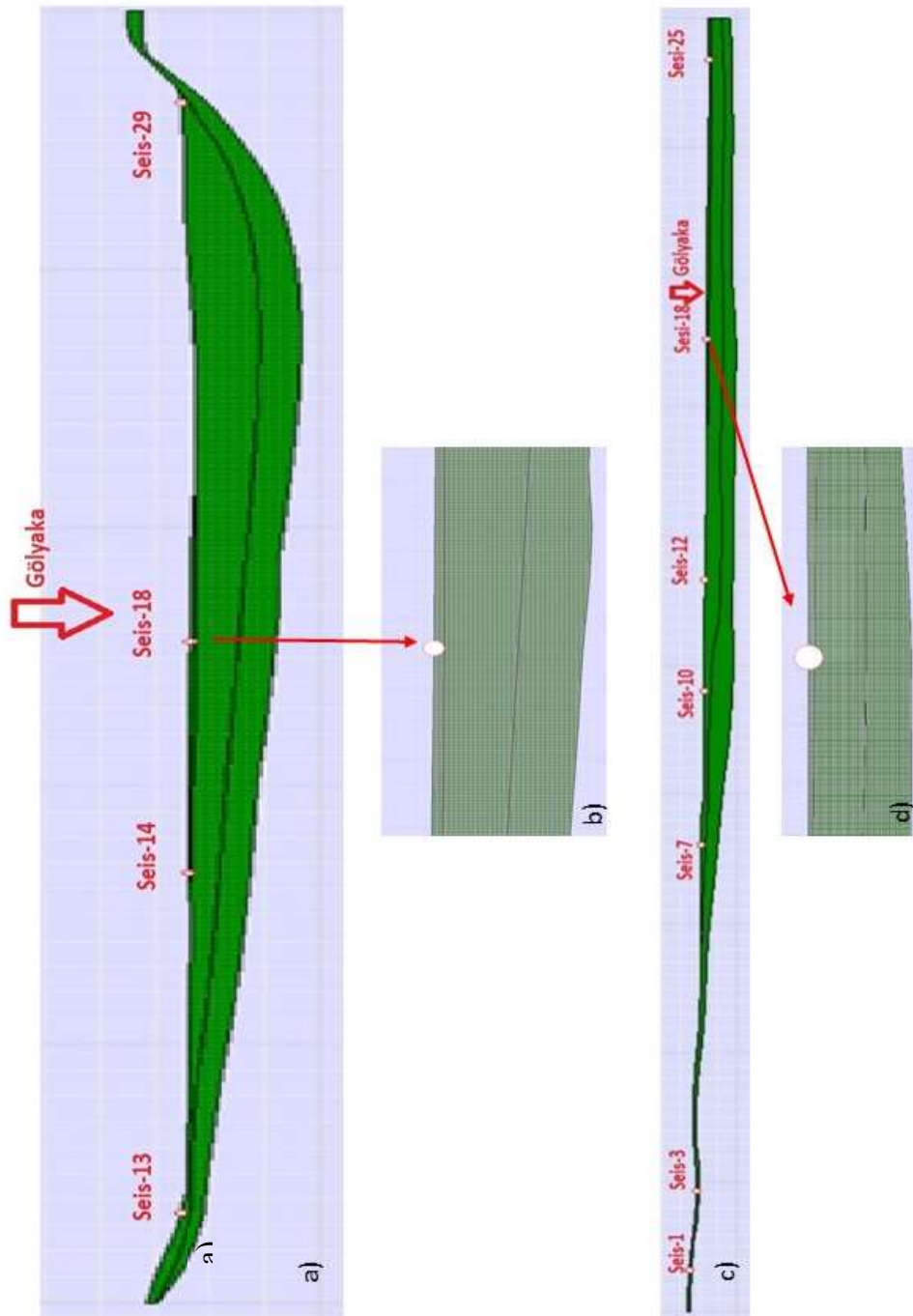


Figure 21. a) and c) Soil model of NW-SE and E-W sections, respectively. b) and d) a close view of these sections to show the lateral and vertical variations of the layers.

3.2.5 Characterization of non-linear soil properties

The changes in the normalized modulus reduction and material damping curves as a function of the strain level (i.e., the G/G_{\max} - γ and D - γ curves) serve as key input parameters for any numerical ground motion analysis. Comparing the observed shear moduli and standard degradation curves also requires the value of the small-strain shear modulus (i.e., G_{\max}), which is typically used to normalize the shear modulus (Darendeli, 2001; Brennan et al., 2005). Most field seismic surveys can be undertaken to determine the shear wave velocity at shear strains less than 3×10^{-4} percent. As a result, the G_{\max} value in this study was determined using the findings of the surface wave measurements, which is the most reliable method for determining the in situ value of G_{\max} for a particular soil deposit (Kramer, 1996), using Equation 4.

$$G_{\max} = \rho \times V_s^2 \quad \text{Eq. (4)}$$

where ρ is the material density calculated by dividing the total unit weight of the soil by gravity (9.807 m/s^2) and V_s is the shear wave velocity in meters per second (m/s).

The most acceptable curves for these soil parameters were calculated using data collected from prior geotechnical investigations, seismic characterization studies conducted throughout this project, and experimental results published in the literature. Numerous parameters affect the variance of these curves, which is necessary for determining the proper G/G_{\max} - γ and D - γ curves for the soil layers. These parameters include the mean effective confining stress, the soil type and plasticity, the loading frequency and the number of cycles, the degree of saturation, the over-consolidation ratio (OCR), the void ratio, the grain size distribution, and characteristics, as well as the mineralogical properties. According to Darendeli's (2001) study, not all characteristics effectively influence non-linear soil behavior. Darendeli (2001) states that the most significant parameters affecting the G/G_{\max} - γ and D - γ curves are the mean effective confining pressure, soil type, and plasticity.

The laboratory test results and borehole data in the Quaternary and Pliocene units were analyzed, and the resulting information was combined with the results of the geophysical surveys conducted in the area to select predefined experimental curves from the literature (e.g., Seed et al., 1986; Vucetic and Dobry, 1991; Darendeli, 2001). Based on available geotechnical data, the soil layers above seismic bedrock were composed of intermediate plasticity clay (PI=10-20 percent) and sand. The non-linear properties of the soils were determined using the soil model of Darendeli (2001) for each layer, which was developed using data on soil class, soil plasticity, and mean effective confining stress values.

As previously indicated, the findings of the geotechnical laboratory tests up to a depth of 15 m were used to calculate the unit weight, soil type, and plasticity values of the soil layers at the 10 sites. The other soil layer attributes were assigned based on the fluctuation of the shear wave velocity profiles and the local geology. To determine the mean effective confining stress for each site, the thickness and unit weight of the soil layers were determined (Table 3- 8), and Equation 5 was used.

$$\sigma'_m = \sigma'_v \times \left(\frac{1+2K'_0}{3} \right) \quad \text{Eq. (5)}$$

where σ'_m defines the mean effective confining stress, σ'_v defines the vertical effective stress, and K'_0 defines the effective earth stress at rest coefficient.

For typically consolidated soils, the K'_0 value depends on the effective angle of internal friction. For over-consolidated ones, the OCR value is also integrated (e.g., Pruska, 1973; Mayne and Kulhawy, 1982). However, in this investigation, the OCR and effective angle of internal friction are not enough to characterize the entire region. Instead of assuming OCR and angle of internal friction values, the effective vertical stress for each layer was determined and used to generate curves together with soil type and plasticity in 1D and 2D site response analyses. As indicated

previously, the approach chosen during the determination step of the geotechnical characteristics of the strata does not affect the 2D analysis.

The normalized modulus and material damping curves created by Darendeli's (2001) work are shown in Figures 20 to 24. These curves were utilized as input parameters for a one-dimensional analysis of soil response. As illustrated in these images, these curves were categorized according to the site's layer numbers, with Layer 1 being the shallowest part of the soil profile and Layer 3 representing the strata just above bedrock.

The behavior of bedrock was studied in 1D response analysis by utilizing the G/G_{\max} - γ and $D-\gamma$ curves of Schnabel (1973). The fluctuation of these curves is not depicted, as they are unaffected by any of the previously stated characteristics, which implies that these curves are the same at all locations.

Based on the mean values of the parameters listed in Table 3 through 8, the normalized modulus and material damping curves were created in 2D soil response analysis using Darendeli (2001) model.

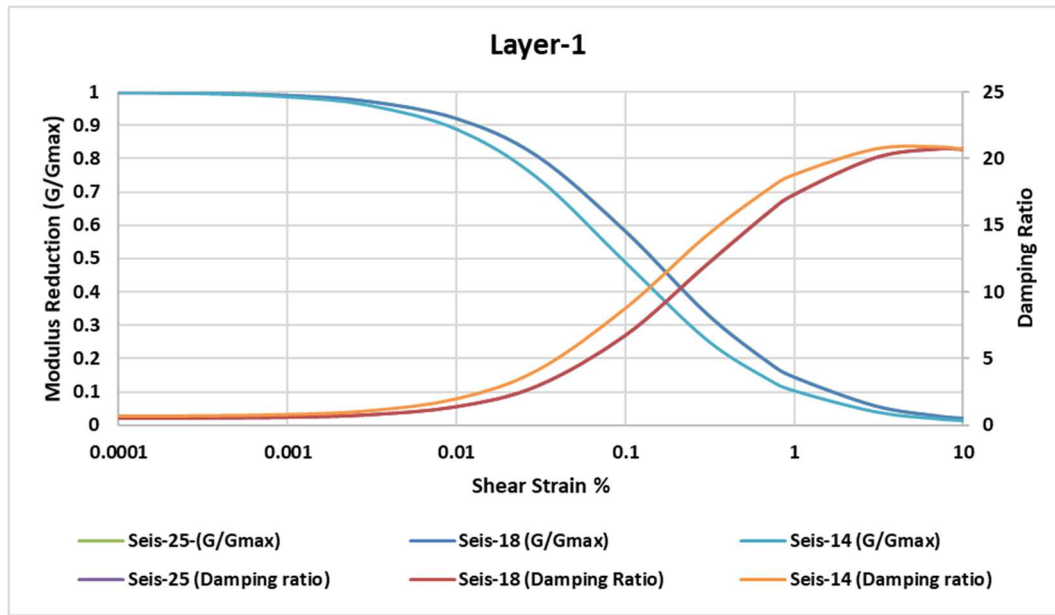


Figure 22. The first layer's normalized modulus and damping curves utilized in the 1D site response assessment.

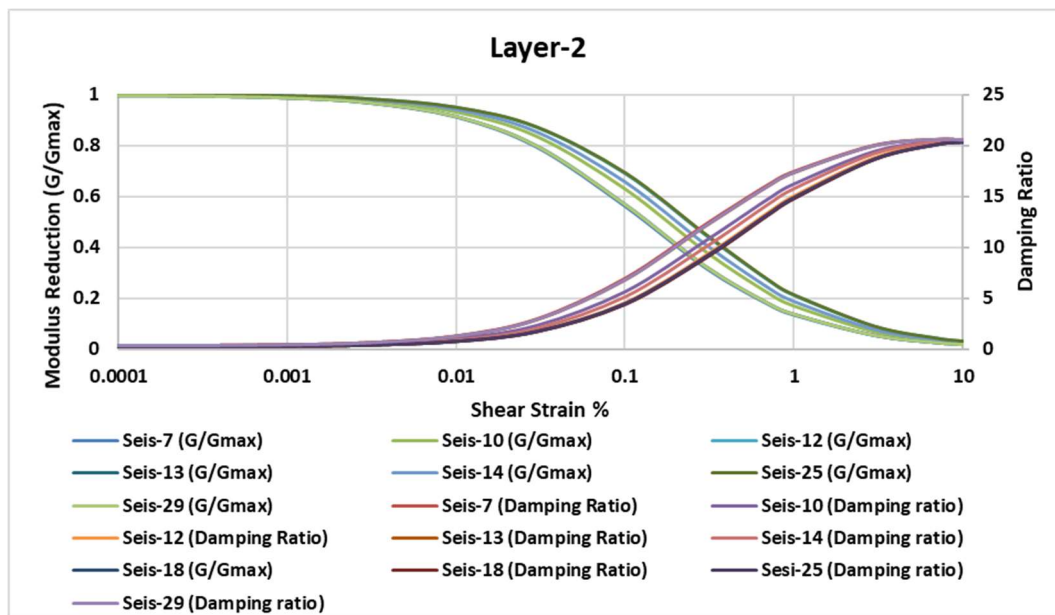


Figure 23. The second layer's normalized modulus and damping curves were utilized in the 1D site response assessment.

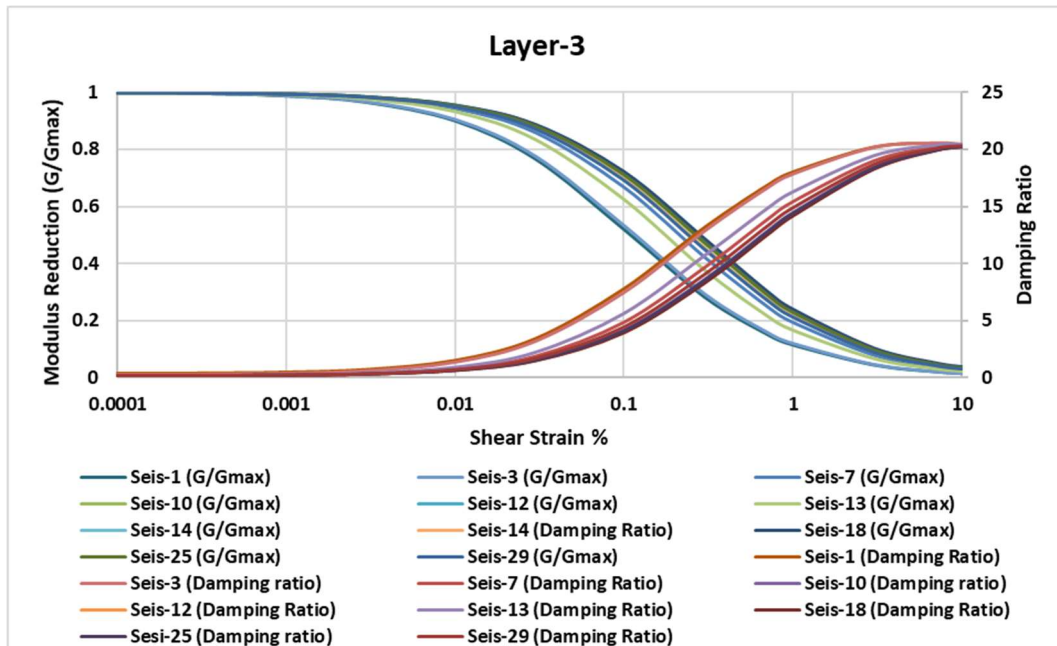


Figure 24. The third layer's normalized modulus and damping curves were utilized in the 1D site response assessment.

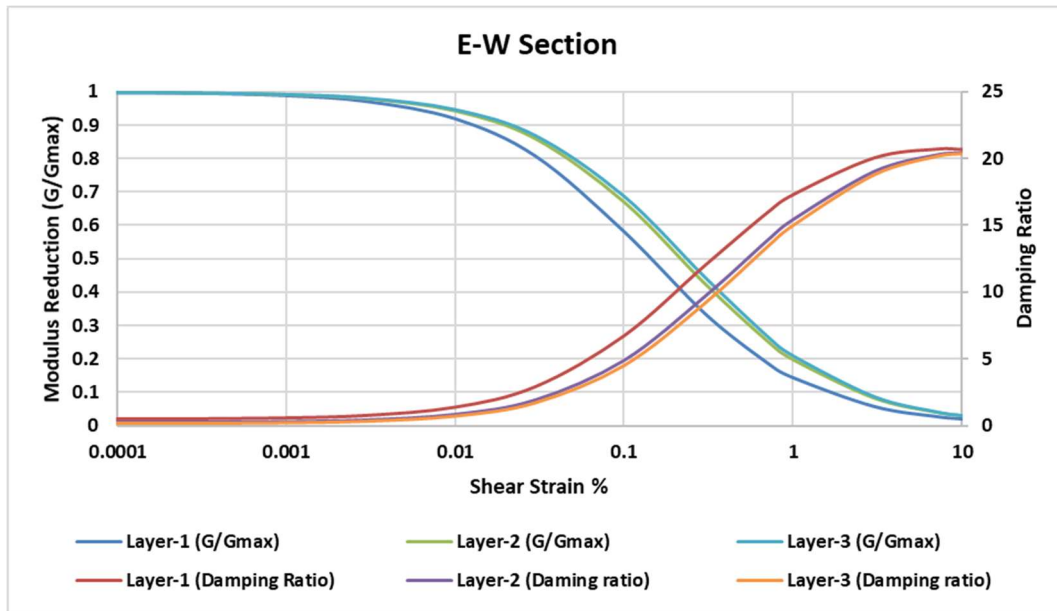


Figure 25. Material modulus reduction and damping curves for all layers were used in the 2D site response analysis

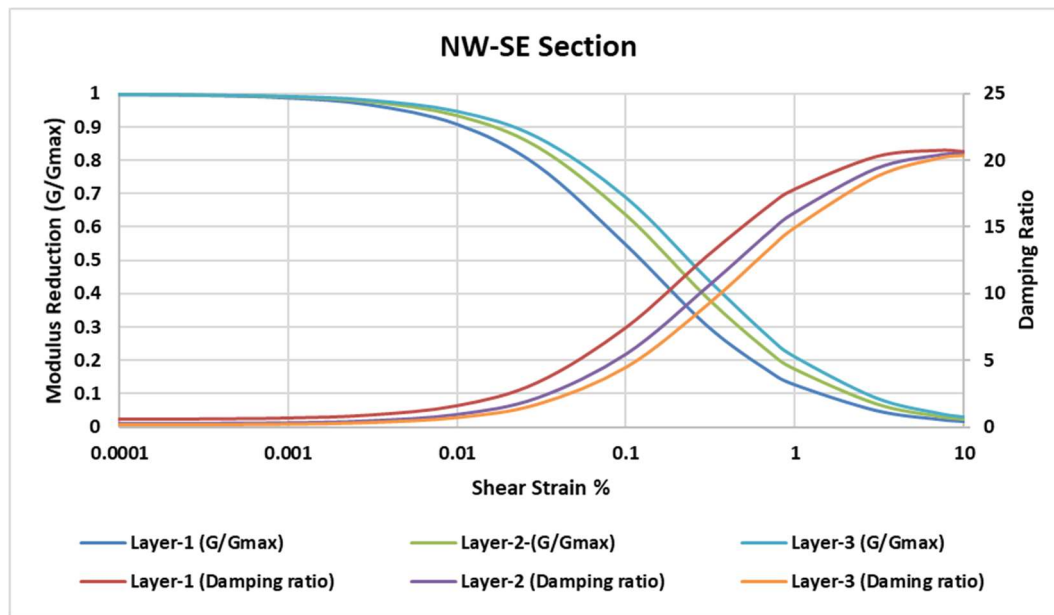


Figure 26. Material modulus reduction and damping curves for all layers were used in the 2D site response analysis

CHAPTER 4

SITE CHARACTERIZATION AND BASIN MODELING

This section presents a discussion of the results of the geotechnical and engineering geological boring and geophysical data (i.e., surface seismic testing, VES, H/V microtremor measurements) along with the geology and topography of the basin to determine the presence of geological heterogeneities and the geometry of the basin in the Gölyaka region. Based on these results, a dimensional basin model has been developed and verified.

The shallow geotechnical boring profiles along with the deep engineering geological boring profile (about 168.5 m) indicated that clay, gravel, silt, and sand-size sediments were present at shallow depths, whereas a thick layer of clay (about 61 m thick) was present in between 64 and 125 m (Figure 7 and Figure 8). Finally, a sand layer about 43 m thick that underlined the clay layer reached down to a depth of 168 m. The laboratory index testing results obtained from the geotechnical boring data in the study area implied that the soil possessed low plasticity down to a depth of 15 m. According to the geotechnical laboratory data, the basin's center was mainly composed of gravelly sandy silt and clay, and the clay content increased towards the northern boundary. At the same time, claystone was reached at a relatively shallow depth (i.e., at a depth less than 10 m), especially towards the northwestern part of the study area. From the deep engineering geological borehole data, it can be inferred that the thickness of the alluvial deposits increased significantly towards the east and the center of the basin, and this observation presented consistency with the Vs profiles.

Preparing a well-developed basin model to define the topography and basin structure accurately, and thus to determine the spatial distribution both horizontally and vertically to evaluate the heterogeneity of the sediments, a 3-D basin model has been

developed in the tectonically active Gölyaka basin. The model was developed with high-resolution Vs profiles obtained through surface wave methods using active MASW and passive MAM measurements (Figure 27). Therefore, the vertical and horizontal variations of the shear wave velocity models have been developed to characterize the sedimentary units and differentiate the sediment type. While creating 3D Vs models, the basin was developed from 1D Vs profiles by utilizing the anisotropic inverse distance weighting (IDW) method with a high fidelity option. Then, the upper surface boundary of the models was adapted according to the topography. The site's digital elevation map (DEM) was generated from the 1:25,000 topographic map of the General Command of Mapping and was later exaggerated in the vertical direction. The bottom surface of the models was extracted according to the Vs profile depths. In the development of the interpolated models, the combined results of the surface wave measurements of MASW and MAM measurements (i.e., Seis-01, -02) were used in conjunction with the Vertical Electrical Sounding (VES) measurements and the deep engineering geological data to provide a well-developed basin geometry for the Gölyaka basin.

Using the Vs results of 1100 m/s obtained from the shallow parts of the western boundary of the basin, the model was interpolated by considering the deep engineering geological borehole logs in terms of borings where the bedrock was not encountered down to a depth of about 260 m. Additionally, the results of the VES measurements indicated that the possible alluvial thickness is approximately 200-300 m, except for the measurement at G7, which indicated a low apparent resistivity and thus a depth of nearly 300-400 m. Also, according to the results of the VES measurements, the possible alluvial thickness was determined to be about 200-300 m, apart from the measurement taken at G7, which indicated a low apparent resistivity and hence, a depth of almost 300-400 m. This anomaly could be attributed to the step-over faulting mechanisms of the Düzce Fault segment or the presence of a bedrock formation of Eocene age (i.e., marl, claystone, or sandstone). Similar to the engineering geological boring data, by the aid of the information obtained from

the VES results, the Vs profile depths were comparatively interpolated down to the depth where an 1100 m/s shear wave velocity was attained (Figure 27).

An evaluation of the surface seismic results revealed that the shear wave velocities in the upper 10-15 m of the alluvial deposits were less than 180 m/s. These velocity values were recorded in the Holocene alluvium or the relatively high altitudes around the basin-ridge consisting of thicker alluvium or terrace deposits. For both lithologies, the Vs results were less than 150 m/s, which implied a shallow groundwater level. Considering the heterogeneity of the site, the seismic surface wave testing method by itself was not deemed to be satisfactory. For this reason, the surface seismic testing results and the collected data obtained through the boring studies (i.e., geotechnical and engineering geological deep boring results, the thickness of the subsurface lithology, groundwater levels) along with the VES results have been evaluated and compared in their entirety. The results of the combined active and passive surface wave methods in Plio-Quaternary sediments have been determined and utilized in developing the 3-D basin model (Figure 27), which indicated that the Vs results varied considerably as anticipated depending on the thickness of the alluvial layer. As the thickness of alluvium increased towards the east, the Vs results decreased in accordance. However, the shear wave velocity increased towards the west of the basin (i.e., towards the Upper-mid Eocene sedimentary deposits), where the depth of bedrock decreased rapidly at about 30-40 m, where shear wave velocity values greater than 1100 m/s were observed in the engineering bedrock. When these Vs measurement results were examined in the basin where the valley expands, it was observed that the thickness of the engineering bedrock in the Vs profile had not been encountered down to a depth of approximately 200-250 meters. Therefore, the engineering bedrock was not observed in the middle of the basin depth (i.e., at a depth of about 50-100 m) due to the penetration of these sediments that possess lower shear wave velocity values at this depth.

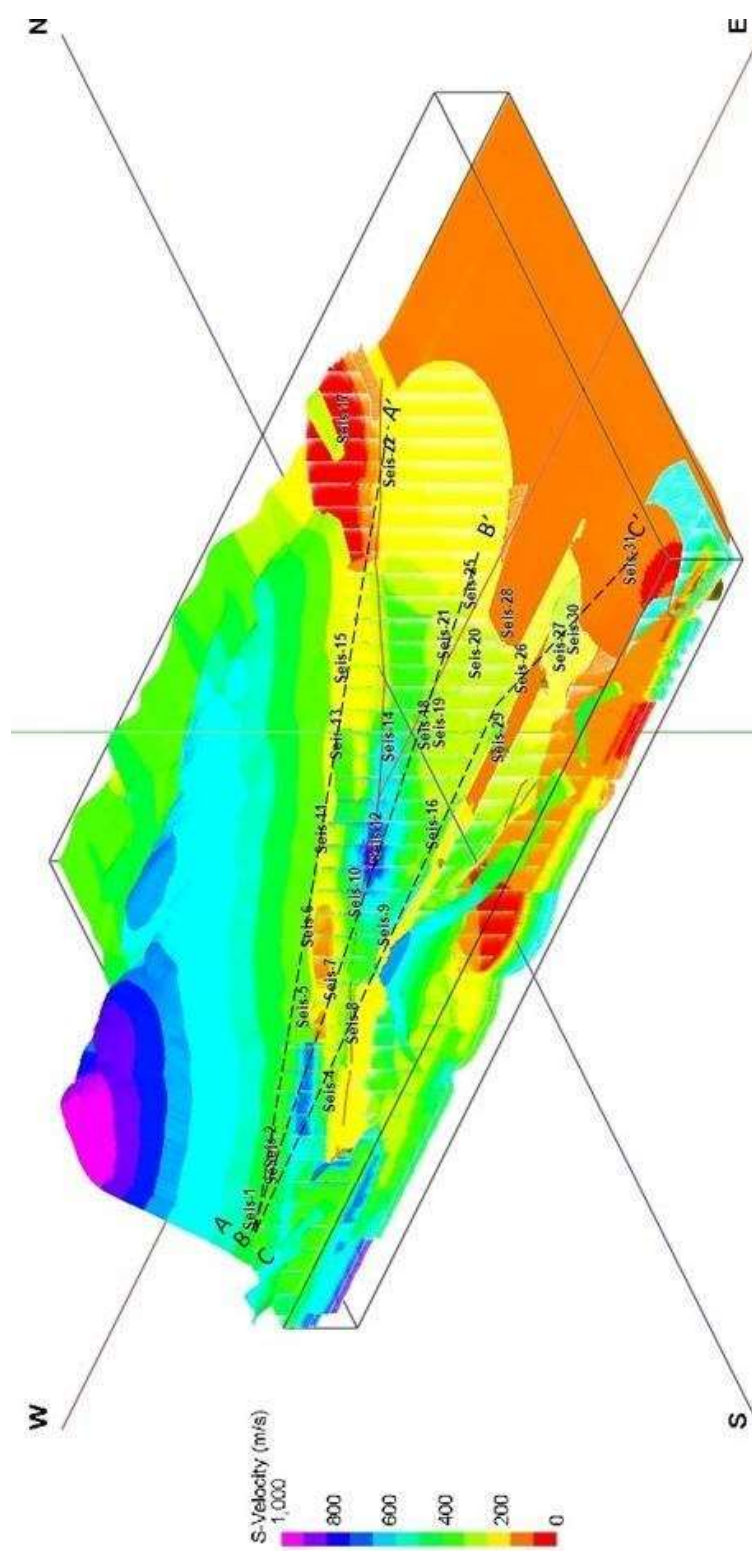


Figure 27. A 3-D basin model of the Vs results for the study area (Vertical Exaggeration: 5)

According to Dreger et al. (2007), the complexity of the surface seismic wave model in the form of velocity contrast with low velocity can be expected at sites located near a fault or within the low-velocity fault zone. The V_s results indicate that these conditions prevail in the study area, especially near the faulting area at the southern edge and to the southeastern part of the basin. Furthermore, as previously stated, these complexities in velocity contrast were observed in the center of the basin, where layers with lower V_s values were obtained in the middle of the section.

A comparison of the west and east parts of the plain (Figure 27) indicates that lower V_s results are relatively concentrated towards the eastern and southeastern sides of the plain. One of the possible reasons is that Efteni Lake changed its course from the east and the north to the southeast, where the present lake and Düzce faults are located. The presence of unconsolidated lacustrine sediments with various thicknesses, horizontal variation in material properties, and their thicknesses and different consolidation degrees might be other reasons for observing different V_s results or velocity contrast in the basin center and at the edges. Based on the coherency of the data, the V_s results were observed to be between 250 and 560 m/s and 150 and 360 m/s in the western and eastern parts of the basin, respectively. However, this coherency tended to become incoherent, particularly in the proximity of the fault.

The vertical and lateral variations of the V_s profiles across three sections were developed from the 3D basin model to characterize the sedimentary units and differentiate the sediment type. The trends of these sections are given in Figure 28 as (a) the northern margin (along the 1999 Kocaeli Fault rupture), (b) the basin center, and (c) the southern margin (along the 1999 Düzce Fault rupture) of the Gölyaka basin. In preparation of the sections, the reliability of the results was ensured by taking sections along the route where the combined results of the MAM and MASW measurements in the study area were taken (i.e., Seis-01, -02). The thicknesses of the deposits according to the V_s values are given in each section. Section A-A' (Figure 28) passes through the northern boundary along the 1999 Kocaeli earthquake fault section, and especially the products of marginal

depositional system can be easily determined with the help of the information along this section. The alignment of the C-C' section that passes through the southern boundary along the 1999 Düzce earthquake fault section was selected to examine the variation in the shear wave velocity of the deposited sediments at different boundaries and lithology ages (Figure 28). The B-B' section that passes through the basin's center also provided information regarding the sedimentation systems that dominated the Quaternary period (Figure 28).

The middle of the depositional system, which is dominant at the side boundaries of the main course of the Büyükmelen river, consists of alluvial fan and terrace sediments deposited by debris flow. Because of the nature of the boundary depositional setting, the grain size of the sediments is coarser than those located on the southern side and those that are present towards the eastern sedimentation system that consists of fine-grained alluvial plain sediments such as sand, silt, and clay. Thus, the V_s results of the marginal depositional system are higher than those at the center. The V_s profiles of the models at the Seis-20, Seis-25 sites are located at the Büyükmelen river course, where it migrates towards the region's north (Figure 28 b). Due to the heterogeneity of the alluvial deposits, it was almost always observed that the layers with coarse-grained materials having high shear wave velocity displayed lateral transition into layers of fine-grained materials having relatively low-velocity results.

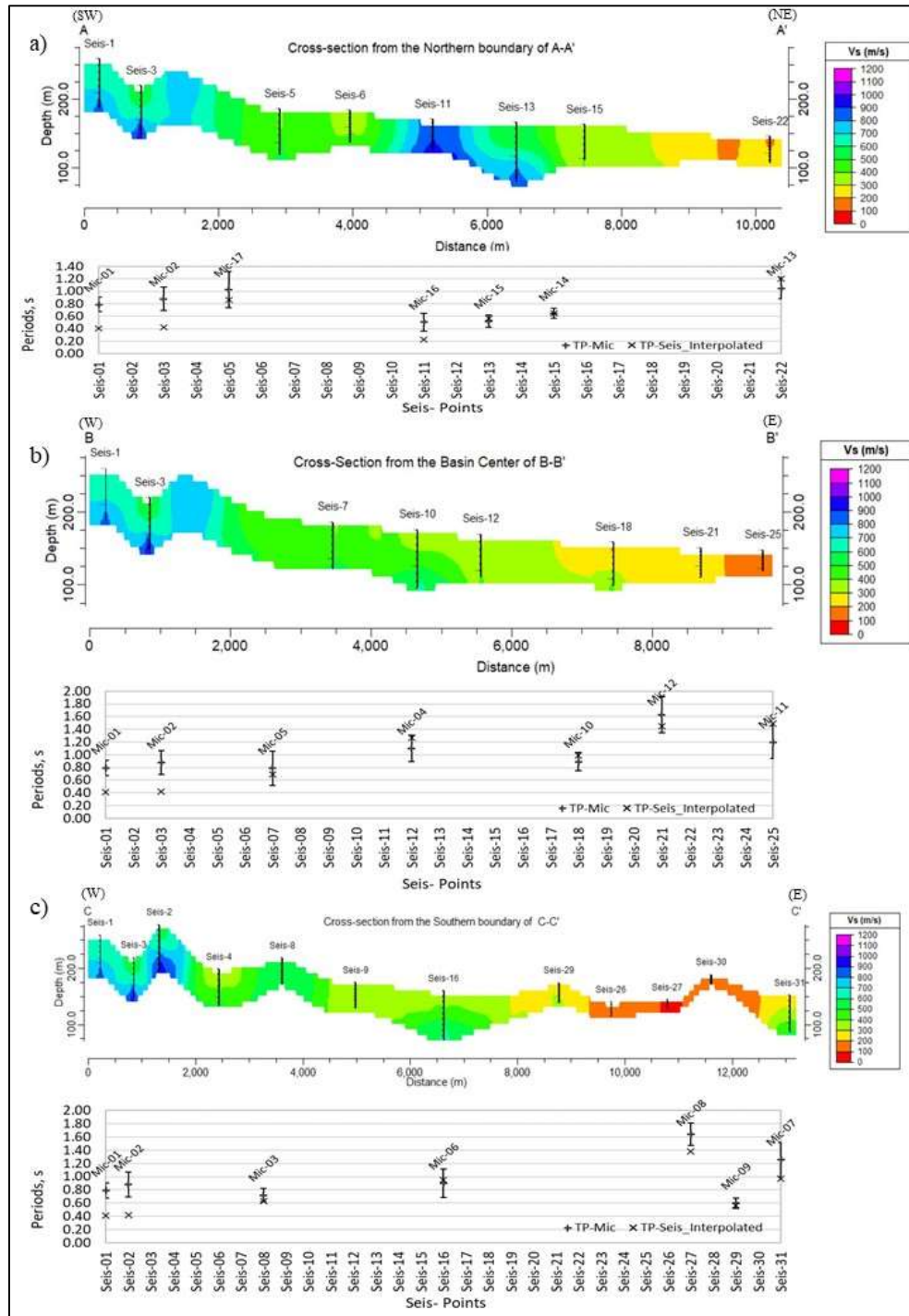


Figure 28. A comparison of the three interpolated 2-D cross-sections of the Vs profiles along with the microtremor measurements that present the northern (a) and southern (b) margin along with the basin center (c) of the Gölyaka basin (Vs Profile Vertical Exaggeration: 10)

The saturation of the sediments formed due to the presence of the course of the Efteni lake towards the south is also added to this. The reason for these lateral transitions could have been either due to a wedge-type topography, near-field faulting, or stratification based on the depositional setting that controls the depositional environment, namely, the shear zone or the braided river system. Furthermore, the shear zone caused by faulting could be seen on Seis-11, Seis-26, Seis-27, and Seis-30 in the two sections that pass through the northern and southern boundary (Figure 28 a and Figure 28 c). It should be noted that the heterogeneity in the measurements along both sections could be attributed to the deformation created by faulting, which implied that stiffer material was sitting next to the softer and saturated soil or vice versa. In other words, these sediments represented themselves as low shear wave velocity sediments (<180 m/s) bordering higher velocity sediments (>500 m/s).

The VES results have also provided invaluable information to determine the thickness of the alluvial deposit and the depth of the engineering bedrock along with the faulting zone based on the geology and topography in the Gölyaka basin (Figure 7). In addition, the results of this comprehensive survey were also used as complementary data for developing a well-developed 3-D geometry of a basin model of the Gölyaka basin. The enlarged spatial distributions of the VES measurements and their profile locations (i.e., A1, A2, A3) used for preparing the cross-sections are given in Figure 29. Based on these results, a fence diagram given in Figure 30 was developed from the VES measurements to prepare a 3-D VES model obtained from the 1-D VES profiles. This diagram illustrates the horizontal and vertical heterogeneity in both the N-S and E-W directions. In Figure 30, it is observed that the thickness of the alluvial deposit varies considerably in the basin. The estimated most immense alluvial thickness is about 200-350 m in the basin's center. As the resistivity increases from the center to the edge of the basin, the thickness of the alluvium decreases. Although the resistivity of the sub-surface sediments is generally less than about 20 Ohm.m, the resistivity values of the bedrock (i.e., fractured sandstone/andesite) increase with depth (~ 200 Ohm.m) in the study area. In particular, near-field faulting and geological observation can be identified from the

resistivity diagram in the measurement point of G10 illustrated in the VES profiles (Figure 29) and the fence diagram of the VES model (Figure 30).

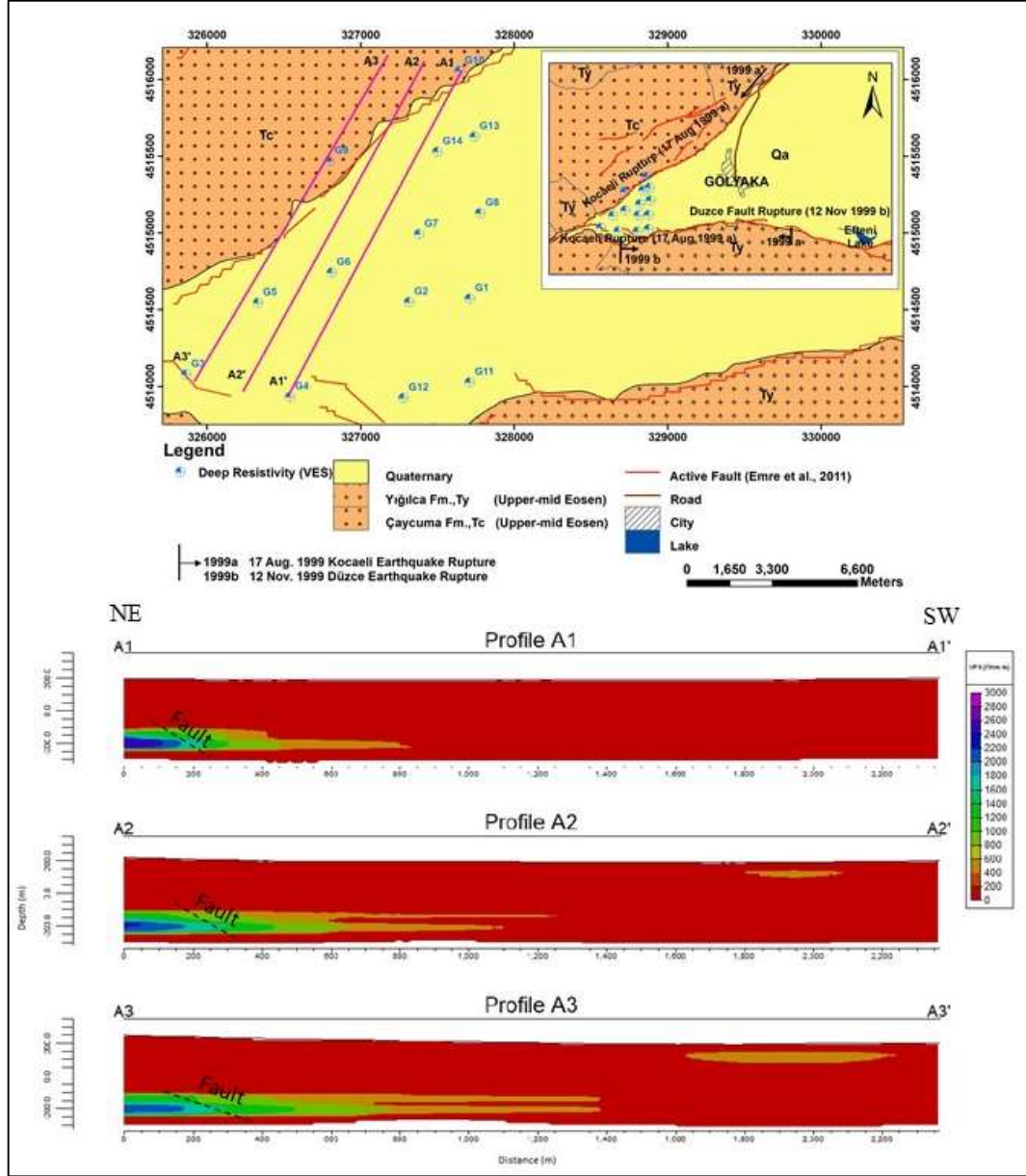


Figure 29. Enlarged Fig. 2 shows the spatial distributions of the VES measurements and three parallel profile locations (i.e., A1, A2, A3). It should be noted that the apparent resistivity contrast in the A1, A2, A3 points of the profiles are due to the zone of faulting

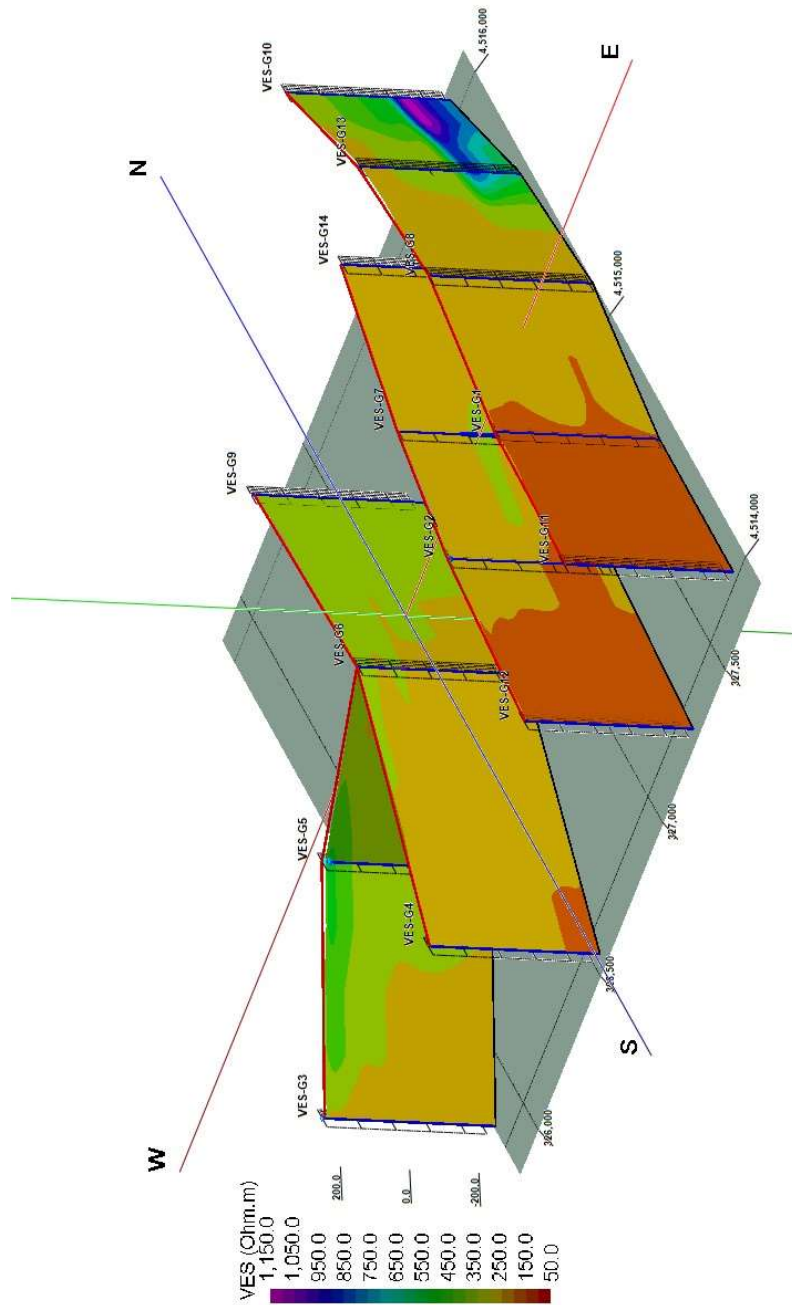


Figure 30. A 3-D fence diagram of the VES model. It should be noted that the apparent resistivity results decrease due to the zone of faulting in the northeast section

As illustrated in Figure 30, an anomaly was observed towards the basin's center where the G7 measurements were taken. Because of the presence of gravel and the blocky content of the Quaternary alluvium, the measured point indicated a high resistivity layer from the surface down to a depth of 300 m, but a low resistivity layer was observed beyond this depth. Based on the surrounding VES measurements, faulting or Eocene-age formation (i.e., marl, claystone, and sandstone) might be present at a depth beyond 300 m. Meanwhile, the Seis-7 measurement point, which is close to the point of G7, illustrates shear wave velocity values between 350 and 600 m/s down to a depth of 70 m, which is a good indicator for coarse material at this depth (Figure 28b).

Examining the VES locations G13, G8, and G1 at the east of the 3-D fence diagram indicates that the higher resistivity results start from the surface and continue down to 200-350 meters due to coarse-grained materials preventing electrical conductivity in the Quaternary unit. It is strongly believed that the progression in the lower resistivity layers in the lower layers is due to the transition to the Eocene aged units (i.e., marl, mudstone, sandstone). The VES point of G9 at the northern part of the diagram presents highly variable resistivity values as it progresses over the Quaternary unit at shallower depths (i.e., at a depth of 35 m). The higher resistivity value (312 Ohm.m) after 35 meters suggests that it has entered into the Yığılca unit (i.e., andesite, basalt), which can be accepted as bedrock. Likewise, the decrease in resistivity after 140 meters at the VES point of G6 most probably indicates a fault between points G9 and G6. The VES points G4, G11, and G12, which are in the same direction as the Düzce Fault, remained in the diagram's south. An anomaly observed at the VES point of G4 may indicate a different unit with high resistivity. The resistivity increase towards depth in the VES measurements of the G11 and G12 most probably indicates that bedrock was encountered at a shallower depth and progressed in this unit.

As mentioned in the previous section, during the development of the 3-D basin model, the surface seismic measurements have been analyzed and processed comparatively with the VES measurements and the deep engineering geological

results to provide a well-developed basin geometry of the Gölyaka basin. Then, by the aid of the information obtained from the VES results, the Vs profile depths were interpolated with depth through considering the bedrock geometry. Regarding this procedure, it needs to be mentioned that while the depths of the observed Vs profiles are about 70-90 m at the most, the deep VES measurements covered a depth of more than 300 m. Therefore, deep VES surveying results has been complementary to the depth-related processing of the shear wave velocity profiles conducted in the study area to observe the vertical and horizontal heterogeneity of the basin. This method enabled the detection of faults at the measurement point G10 in the profiles illustrated in Figure 29. Furthermore, the possible bedrock depth and/or possible faulting due to the over-step mechanism of the Düzce fault observed at the measurement point G7 is also presented in Figure 30. As a result, it can be inferred from the deep VES results that the results provide useful information to estimate the thickness of the alluvial deposit through the bedrock and evaluate the lateral variation of the basin complexity in the tectonically active near-fault region. Then, these results were used complementarily to develop a 3-D geometry of the basin model of the Gölyaka basin.

The H/V microtremor measurements available at the study area were used to verify basin depth and developed 2-D Vs profiles along the three sections in the Gölyaka basin (Figure 27). The experimental data obtained by microtremor measurements were complementarily used in conjunction with the available engineering geological, geotechnical, and surface seismic test results to obtain reliable and comprehensive information from the H/V microtremor measurements based on fundamental frequencies in those areas. In this regard, the fundamental periods obtained from the microtremor measurements have been compared with the 2-D VS profiles throughout the developed cross-sections (i.e., Figure 28).

Section A-A' in Figure 28 (a) runs through the northern boundary of the basin where the bedrock depth is just beneath a few meter thick sediments towards the west of the profile. As seen on the profile at Seis-1 and -3, the Vs values of about 1100 m/s were obtained, and the bedrock depth is relatively shallow. At these two points, the

predominant periods calculated from the Vs profiles ($T_p \sim 0.41$) having shallow bedrock thickness using the quarter-wavelength method ($T_p = 4H/V_s$) were not concordant with the fundamental periods measured by the H/V microtremor survey at the points of Mic-01 ($T_p \sim 0.79 \text{ s} \pm 1\sigma$) and Mic-02 ($T_p \sim 0.88 \text{ s} \pm 1\sigma$), which gave relatively higher anomaly results. In addition, the fundamental period measured at the Mic-16 measurement point ($T_p \sim 0.51 \text{ s} \pm 1\sigma$) inferred higher period values than those calculated from the Vs profile of Seis-11 ($T_p \sim 0.2 \text{ s}$). All these results are probably due to the non-linear behavior of soils, such as shallow bedrock depth (impedance contrast), material deformation (velocity contrast), and basin edge effects. In addition to these results, thicker sediment deposits lead to higher fundamental periods towards the center of the basin from the northern border, as clearly observed in Mic-13. Here, the predominant period value calculated from the Seis-22 Vs profile of the 3D basin model ($T_p \sim 1.2 \text{ s}$) was consistent with the measured H/V results from microtremors. This result verified the estimated thickness of the 3D basin model at this location. In Figure 28 (b), section B-B' runs through the basin's center, where the deposit thickness or basin depth increases rapidly from the west towards the center. Here, the bedrock depth rises significantly from about 60 m at points Seis-01 and -03, at about 170 m at point Seis-07, and about 250-300 m at points Seis-10, -12, -18, -21, and Seis-25, respectively. At the sites where the estimated bedrock is present at a depth of more than 250-300 m (i.e., the location of microtremor measurement points of Mic-04, -10, -11, and -12 at the center of the basin) around the Gölyaka basin with thicker deposits, the fundamental period takes on relatively higher values as compared with those at the edge of the basin ($T_p \sim 1$ to 1.7 s) (Figure 13). The predominant period calculated from the Vs profiles of Seis-21 ($T_p \sim 1.45 \text{ s}$) is well suited within the lower limit of the period as estimated from the microtremor results of Mic-12 ($T_p \sim 1.63 \text{ s} \pm 1\sigma$).

Similarly, at Mic-10, -11, -12 towards the east of the basin where the thicker deposits exist, the higher fundamental periods (1.1 to 1.7 s) observed verify the estimated bedrock depth. Section C-C' in Figure 28 (c) runs through the southern boundary of the basin along the Düzce fault rupture. Since the trend of this cross-section is not a

straight line, the bedrock depth increases drastically from about 70-90 m along the southern boundary to about 200 m just a few tens of meters distant from the basin edge at the measurement point Seis-27. The rapid deepening of the bedrock at this point has inferred the presence of faulting with a sharp dip. A comparison of the fundamental period obtained from microtremor measurements (Mic-08; $T_p \sim 1.64 \text{ s} \pm 1\sigma$) with the predominant periods obtained from the Vs profiles ($T_p \sim 1.38 \text{ s}$) depend on interpolated data from the basin model verifies the estimated deep bedrock depth.

In summary, these high predominant period results are most likely to the thick unconsolidated and soft sediments of the Efteni lake deposits and the tectonic activity-related deformation that controls these deposits. In general, the determined fundamental periods from the microtremor measurements with one standard deviation ($T_p \sim 0.6 \text{ to } 1.2 \text{ s} \pm 1\sigma$) at points of Mic-03, -06, -07, -09 are consistent with the predominant periods estimated from the Vs profiles in the basin at points of Seis-8, -16, -29, -31. Hence, these results confirm the estimation of the bedrock depth of the basin model at these locations (about 70-90m).

As a result of the evaluation of three sections taken from the basin, it has been observed that there is an inconsistency between the dominant period values obtained by seismic measurements at the basin edge, where the bedrock depth is known, and the dominant period values measured directly by the microtremor method. These results are consistent with the basin edge effects observed at the basin's boundary, where a distinct impedance contrast between the layers is encountered. Notably, they do not affect the estimated basin depth due to the non-linear topography and heterogeneity along the active fault zone. On the other hand, although the estimated basin depth at the basin center is not precisely known, the predominant periods estimated by interpolated results from the basin model have proven to be consistent with the data obtained by the microtremor measurements. These results confirm the suitability of the microtremor method as complementary along with the other methods mentioned above used in determining the bedrock depth model and for developing a well-developed 3-D geometry of a basin model of the Gölyaka basin.

CHAPTER 5

1D AND 2D NUMERICAL ASSESSMENTS OF SITE EFFECTS

As described in Chapter 3, two cross-sections were developed with many considerations to conduct 1D and 2D site response analyses. The NW-SE and E-W trending sections were created to describe the sedimentary deposits in the basin adequately. The E-W trending section lies parallel to the NAFS, the region's principal fault system. This section contains the analysis points Seis-1, Seis-3, Seis-7, Seis-10, Seis-12, Seis-18, and Seis-25. On the other hand, the other cross-section runs almost perpendicular to this fault system (NW-SE). Analysis points, Seis-13, Seis-14, Seis-18, and Seis-29, are located along the NW-SE section. Seis-18 point is the only point that these two sections share. The 1D shear wave velocity profiles, which were employed to generate these cross-sections, were used to characterize a total of 10 individual sites.

Before conducting the ground response evaluations, seven earthquakes were initially specified as the input rock motion based on the target spectrum presented in this work. Chapter 3 explains the technique for selecting and scaling these earthquakes. Shake2000 (Ordones, 2000) and QUAD4M (Hudson et al., 1994) software programs were used to conduct 1D and 2D site response analyses, respectively. As discussed in Chapter 3, these two software packages make equivalent linear assumptions and consider the nonlinear stress-strain behavior of soils in the presence of possible ground motion. Additionally, as described in Chapter 3, the pre-and post-processor VisualQ4M (using QUAD4M code) were employed to do two-dimensional site response analysis.

1D studies were performed at each site using the selected seven earthquakes to assess the variability in soil responses based on the input ground motion data. In other words, whether or not the soil responses at each site were statistically stable has been

assessed. A total of 70 runs, using the selected seven earthquakes for each site at ten different locations, were carried out in Shake2000 software to evaluate the 1D site responses. Each seismically and geotechnically defined sector's 2D site response analyses used these seven input rock motion data by utilizing Visual Q4M (QUAD4M code). About 14 runs were performed to assess the two-dimensional soil response along two sections.

The surface layers' amplitude and acceleration response spectra were studied to establish whether or not the soil responses are stationary. It should be noted that all spectral accelerations were calculated using a damping ratio of 5%.

The results of 1D and 2D numerical response analyses are compared. Figure 31 through 35 show the spectral acceleration and mean spectrum variations concerning the input motions used at these sites, respectively. The velocity spectrum and mean variations for 1D and 2D response analysis are shown in Figure 35 through 39, respectively. These spectrums (acceleration and velocity) reference the input motions employed at these sites for 1D and 2D response analysis. As seen in these figures, the sites' responses are constant regardless of the input motions chosen. This stable behavior means that the mean values of the soil reactions to ground motions may be utilized to calculate the site's 1D and 2D seismic responses. The acceleration and velocity spectrums are used to investigate ground motion variations in the Gölyaka basin.

The results of the 1D and 2D numerical studies were classified according to the site class (TBDY 2018, Turkish Code) and their relative positions in reference to the basin after evaluating and correlating the spectrum acceleration curves' behaviors. In addition, the 1D and 2D seismic responses of the sites have been investigated concerning the variation of the input rock motions obtained by choosing and scaling seven ground motion records using the time-domain spectral matching technique. When the results of the 1D and 2D numerical response analyses are compared, four parts are recognized in connection to basin location and site class as described by the TBDY 2018 Turkish Code. According to location and site class, these four areas are

as follows: very dense/weathered rock sites in the basin's western portion, stiff sites in the basin's center, soft/weak sites in the basin's deepest region, and the basin's northern and southern boundaries (Basin edge effect).

A dense and weathered rock site in the western part of the basin reveals short dominant periods ($T \sim 0.25s$) and higher spectral acceleration values. The amplitude of the acceleration spectrum is about 2g (Figure 31). In the center of the basin, the stiff site, longer dominant periods ($T \sim 1s$ and $1.5s$), and higher spectral acceleration values ($Sa \sim 1.2g$ and $2g$) have been observed, except for Seis-12, which shows small spectral acceleration ($Sa \sim 0.45g$) at short period ($T \sim 0.5s$) in the 1D results (Figure 32). The longer periods ($T \sim 1s$ and $1.5s$) and lower spectral acceleration for 1D have been recorded in the deepest region of the basin where soft ground exists, compared to 2D with higher spectral acceleration ($Sa \sim 3g$) and shorter period (Figure 33). Finally, the northern and southern boundary of the basins where the very dense site (Seis-13) and stiff site (Seis-29) exists, the results show that short period ($T \sim 0.5s$) with higher spectral acceleration value ($Sa \sim 1.5g$ and $2g$) have been observed. (Figure 34). Seis-13 shows a higher spectral acceleration value in 2D numerical response analysis results in this class.

Figure 31 shows the 1D and 2D results for Seis-1 and Seis-3 points located in the western part of the basin at a very stiff /weathered rock site. The bedrock depth at these two places is shallow (about 15 m). The amplification and spectrum amplitude is considerable due to the velocity contrast between soil and bedrock for both 1D and 2D analysis results. Maximum horizontal acceleration (MHA) results from these two sites (Seis-1 and Seis-3) are comparable with those from the 2D analysis. At these sites, MHA was obtained at period (T) 0.2 seconds with spectral acceleration (Sa) of 2.5g and 2.2g for 1D and 2D analysis, respectively.

Dominating longer periods and moderate spectral acceleration values were observed at a stiff soil site in the basin's center (Figure 32). The acceleration spectrum has an amplitude of roughly 1.2g for 1D results and about 2g for 2D results. Because of the 2D effects and deep bedrock depth at these locations, the amplification and spectrum

amplitude is considerably higher in 2D results than in 1D results. MHA data from these four sites (Seis-7, Seis-10, Seis-13, and Seis-14) are equivalent to those from the 2D analysis. Aside from Seis-12, de-amplification was observed in 1D results compared to 2D outcomes. These effects can be because of 2D effects and velocity contrast at this site due to the relatively short distance from the material deformation resulting from the basin's northern boundary faulting. MHA was obtained at these sites at the 1s and 2s periods with S_a of 1.3g and 2.0g for 1D and 2D analysis, respectively. When comparing the 1D and 2D results in Seis-12, as shown in Figure 32, the 2D effect is more pronounced, with the second peak appearing in the 1.5s period compared to the 1D data. For these sites, when compared to 2D results with higher spectral amplitudes, the spectral acceleration amplitude in 1D is low.

The computing results of 1D and 2D at soft/weak soil sites in the basin's deepest section (Figure 33) show longer dominating periods and small spectral acceleration values for 1D results compared to short period and large spectral acceleration values for 2D results. The acceleration spectrum has an amplitude of around 0.8g for 1D results and S_a of 2.5g and 3g for 2D results that exhibit 2D effects. The bedrock depth is deepest at these locations, and the amplification and spectrum amplitude is significantly greater in 2D results than in 1D results due to the 2D effects. Additionally, a second peak at period 1.5s with S_a of 1g was observed. Spectral acceleration (S_a) results from these two sites (Seis-18 and Seis-25) are low for 1D results compared to 2D analysis. The S_a was obtained at these sites between periods 1s and 1.5s, and S_a of 0.8g and 0.6g for 1D analysis. For 2D results, periods of 0.5s and S_a of 2.5g and 3.0g for 2D analysis. When comparing the outcomes of 1D and 2D at these two sites, as shown in Figure 33, the 2D effect is visible as a second peak in a period of 1.5s in the 2D data compared to the 1D results. Compared to the spectral acceleration at Seis-25, the S_a in 1D is small.

Figure 34 illustrates the two sites that located the basin's boundary, one at the northern at a very dense site and the second at the southern boundary at a stiff site. By comparing the results of 1D and 2D response analysis, these two show similar behavior in spectral acceleration. They show the maximum spectral acceleration of

2g at a short period of 0.5 seconds for both 1D and 2D results. However, Seis-13 at the northern boundary implies higher S_a than Seis-29 at the southern boundary with S_a of about 2g. These two sites exhibit S_a of changing for longer periods in 1D results.

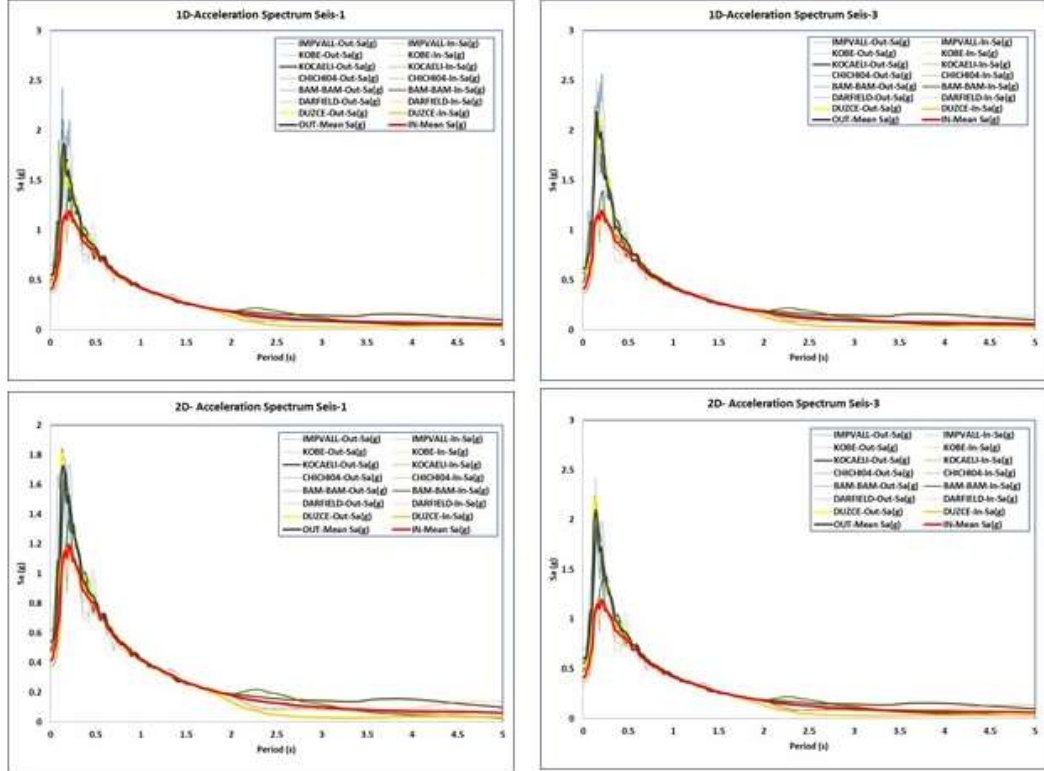


Figure 31. Stability of the site responses by evaluating the variations of the acceleration spectrum after computing 1D and 2D analyses for seven earthquakes in a very dense/weathered rock site near the 1999 Kocaeli EQ earthquake fault rupture in the western part of the Gölyaka basin.

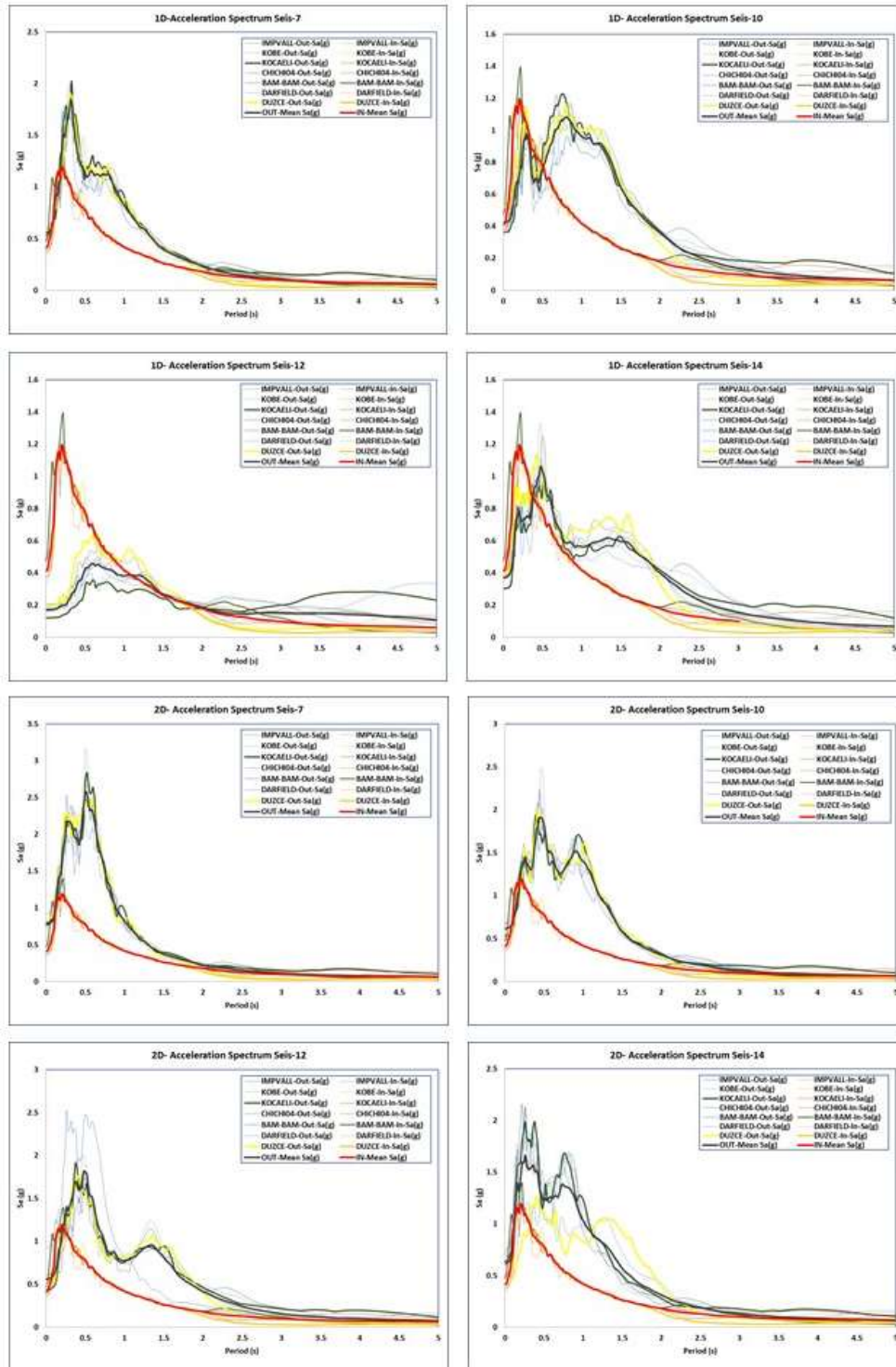


Figure 32. Stability of the site responses by evaluating the variations of the acceleration spectrum after computing 1D and 2D analyses for seven earthquakes located in the center of the basin at stiff soil sites.

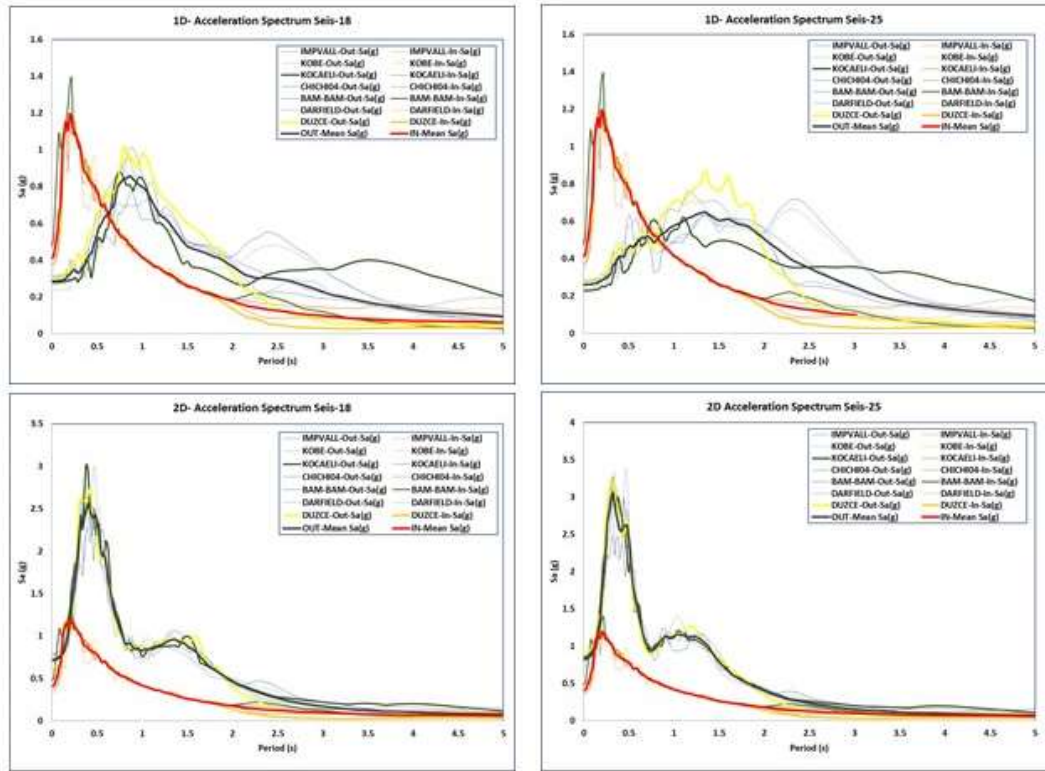


Figure 33. Stability of the site responses by evaluating the variations of the acceleration spectrum after computing 1D and 2D analyses for seven earthquakes in the deepest part of the Gölyaka basin at the soft/weak soil site (Seis-18 located in the center of the Gölyaka county)

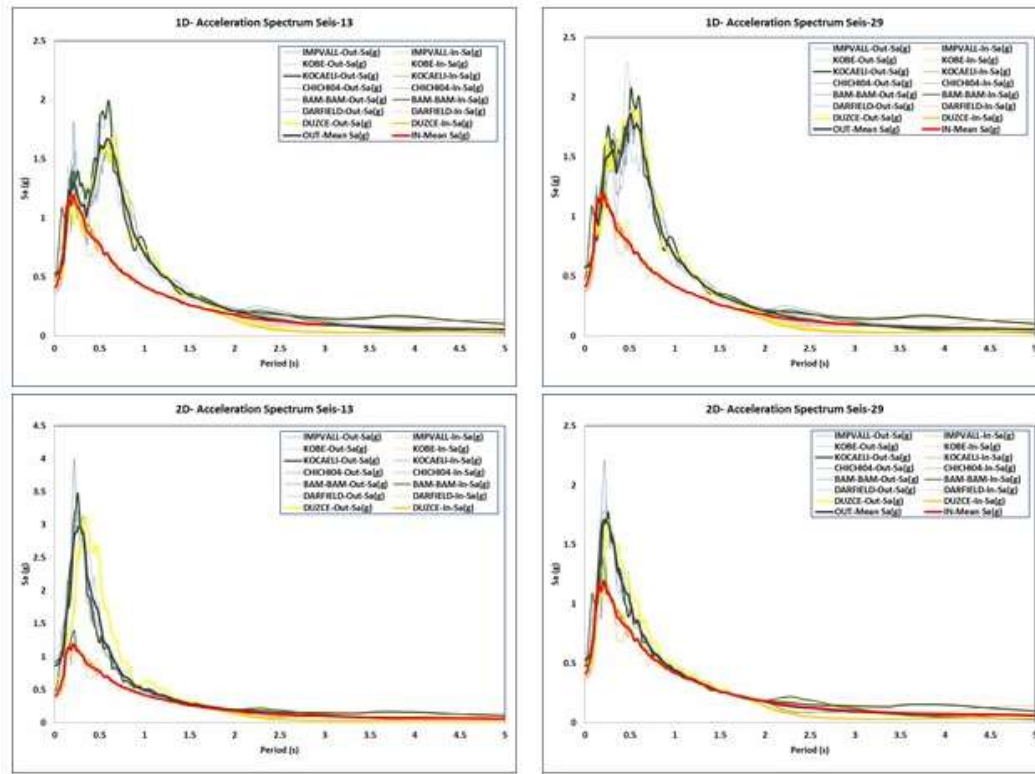


Figure 34. Stability of the site responses by evaluating the variations of the acceleration spectrum after computing 1D and 2D analyses for seven earthquakes in the northern and southern boundary of the basin at very dense/weathered rock (Seis-13) and stiff soil sites (Seis-29)

When the 2D response analysis results are examined individually at each of the defined locations, it is evident that the spectral peaks of the 2D site response analyses are larger than those of the 1D studies at all sites (Figure 31 through 35). The comparison of the spectral curves shows that 1D numerical analyses can approximate the similar behaviors of the spectral curves derived through 2D response analysis. However, the results of the 1D analysis indicate that it is underestimated for design purposes, most notably by omitting 2D effects. The maximum spectral values are notably different when the response spectra of the sites are compared. According to the 1D analysis results, a shift toward longer periods may be observed in the 2D response spectrum. According to Jibson (1987), Geli et al. (1988), and Rathje and

Bray (1989), this response may be related to the topographical elevation of the site and its immediate surroundings (2001).

By comparing the results of 1D and 2D site response studies, we could determine the effect of near-field directivity. These effects typically have a long duration and are most readily visible in the velocity- or displacement-time history. As indicated in Figure 35, no directivity effects were detected in the velocity spectrums of both 1D and 2D outputs for sites with a very dense site. These effects may be due to these sites located next to the 1999 Kocaeli and Düzce fault rupture. However, as illustrated in Figure 36 and Figure 37, at these sites (Seis7-10-12-13-14-18-25), where they were positioned in the direction of fault rupturing, velocity spectral with greater periods were detected at all of these locations at longer periods ($> 1.5s$), Especially for Seis-18 and 25 at soft soil sites. On the other hand, 1D results (Figure 38) for sites located at the northern and southern border of the basin showed higher spectral values than 2D in short periods. It might be related to the basin edge effect and non-linearity located next to the fault rupture.

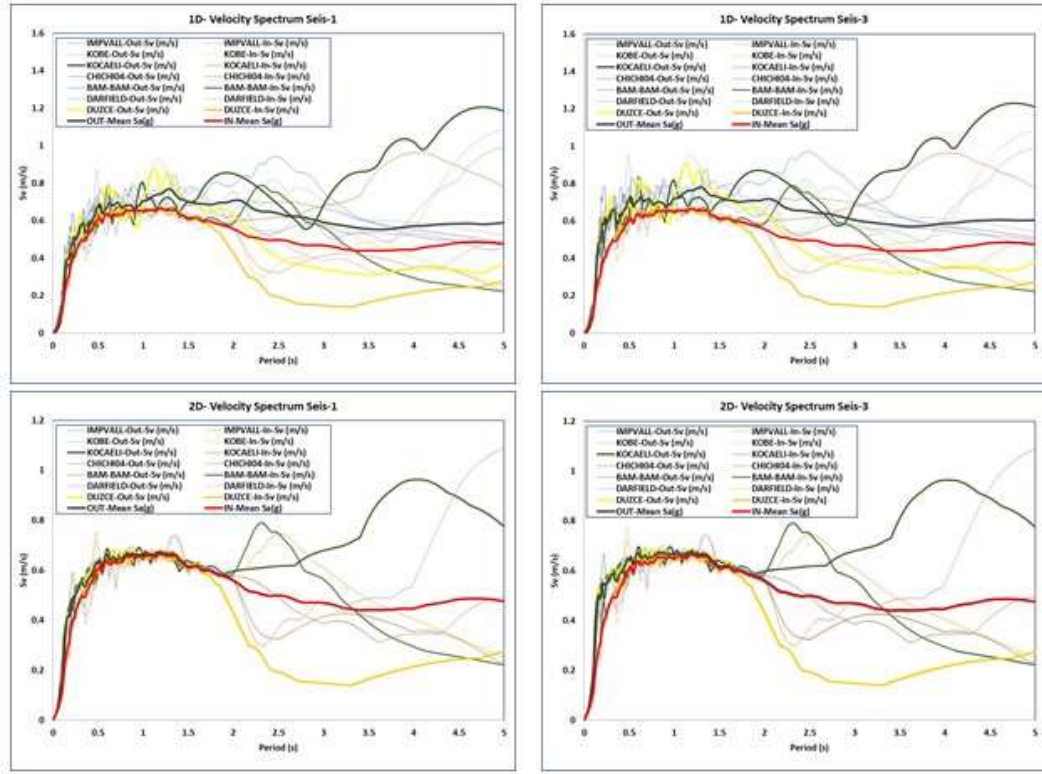


Figure 35. The shapes of the velocity spectra for sites at the western part of the Gölyaka basin near the 1999 Kocaeli EQ fault rupture on very dense/weathered rock site after performing 1D and 2D numerical site response analyses

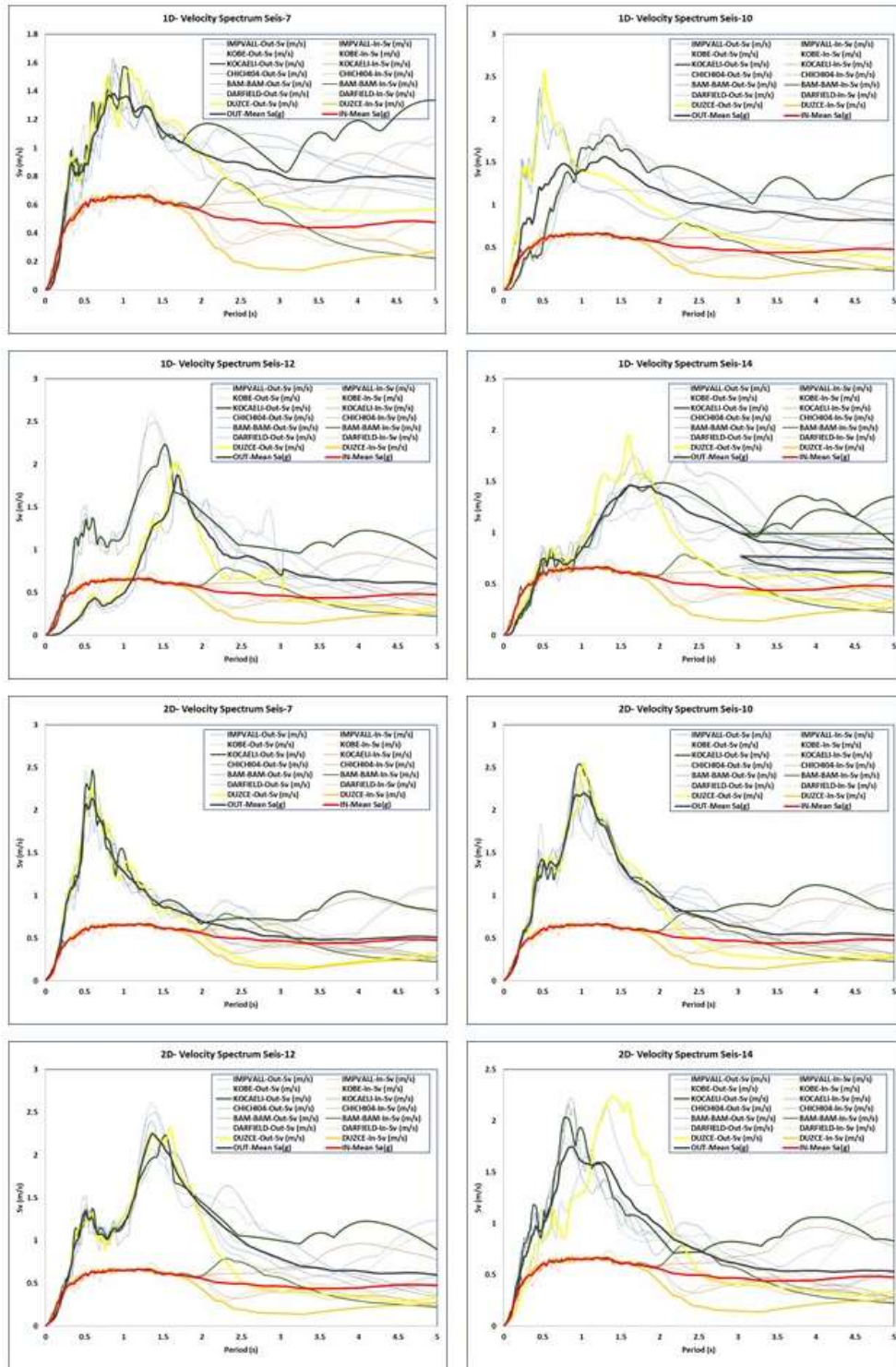


Figure 36. The shapes of the velocity spectra for sites at the basin center after performing 1D and 2D numerical site response analyses (Directivity effects).

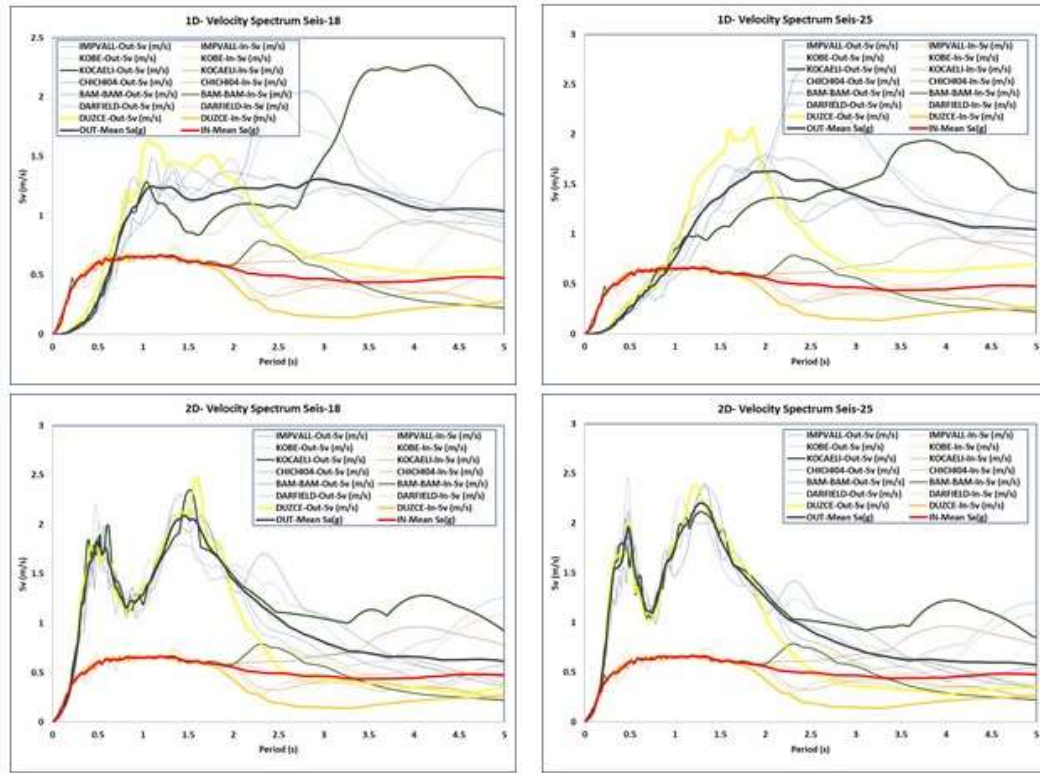


Figure 37. The shapes of the velocity spectra for sites at the deepest part of the basin after performing 1D and 2D numerical site response analyses (Directivity effects).

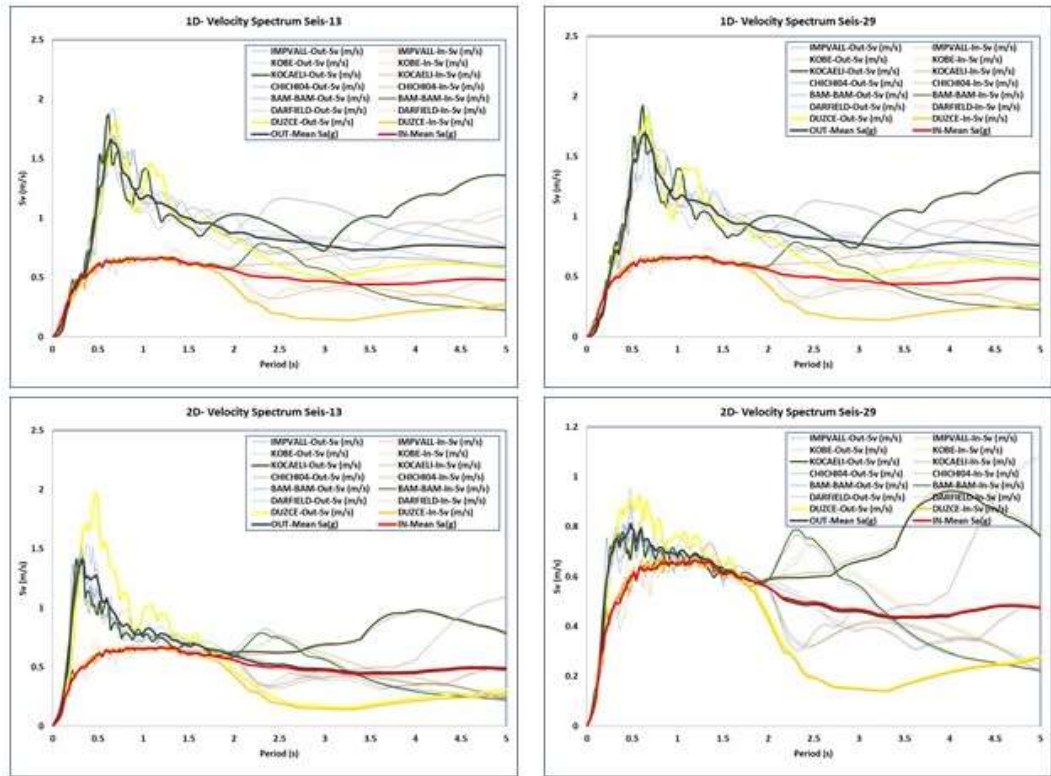


Figure 38. The shapes of the velocity spectra for sites at the northern and southern boundary of the basin at very dense/weathered rock (Seis-13) and stiff soil site (Seis-29) after performing 1D and 2D numerical site response analyses (Directivity effects).

CHAPTER 6

RESULTS AND DISCUSSION

This chapter compares and analyzes the ten different seismic site response analyses generated using both 1D and 2D numerical methods. Furthermore, these obtained results were checked and validated against recorded weak motion (small magnitude earthquake, $M_w=3.7$) during fieldwork.

6.1 Comparison and evaluating 1D and 2D site response analysis

Four parts are identified by comparing 1D and 2D response analysis results based on the position of the 1D data concerning basin location and site class, as defined by the TBDY 2018 Turkish code. These four sections can be classified as highly dense/weathered rock in the western part of the basin, stiff soil in the center of the basin, soft/weak soil in the deepest part of the basin, and the northern and southern boundaries of the basin.

The acceleration and velocity spectrum mean values for two sites (Seis-1 and Seis-3) located in the western part of the basin along the E-W section are shown in Figure 39. According to the TBDY 2018 Turkish code, these two sites can be categorized as very dense/weathered rock sites based on their VS30 values. As indicated in Figure 39, the maximum horizontal acceleration amplitude (MHA) of 2D numerical analysis is greater than that of 1D response analysis when the input motion is considered. Additionally, as can be observed from the results in both 1D and 2D analysis, the velocity spectrum at these places exhibits a minor fluctuation with respect to the input velocity spectrum. There is no evidence that both response analysis results observed forward directivity effects at the near-fault region.

As determined by the 1D and 2D numerical computations results, the second classified section is located in the basin's center at a stiff soil site (Figure 40). By comparing the 1D and 2D analysis results, 2D basin effects in spectral acceleration have been detected. Additionally, near-field directivity effects were observed at the longer periods (i.e., 1s and 1.5s), and due to the nature of directivity, this velocity pulse has a longer period (Figure 40). These two phenomena (2D basin effects and directivity) are readily apparent in all four locations depicted in Figure 40, particularly in Seis-10 and Seis-14. These two sites are positioned far from the Düzce faults and in the general direction of the 1999 Kocaeli and Düzce fault rupture.

Figure 41 shows the results of 1D and 2D numerical computations for the third categorized region in the basin's deepest section at soft/weak soil site. When the 1D and 2D analysis results are compared, 2D basin effects in spectral acceleration for short periods are detected. The 1D results show that the acceleration spectrum changed towards longer periods, and the spectral amplitude was moderate, but for longer periods (1s and 2s), the 1D and 2D spectral amplitudes were comparable. Furthermore, near-field directivity effects were observed at longer periods (1s and 1.5s), and as a result of the directivity characteristics, this velocity pulse has a longer period by definition, particularly for 1D analysis results. These two phenomena (2D basin effects and directivity) are easily seen in two locations depicted in Figure 41, especially for recorded 1D results with a longer velocity pulse in the spectrum. These two locations are far from the Düzce faults and in the direction of the 1999 Kocaeli and Düzce fault rupture. Furthermore, a 3D effect can be observed by comparing the acceleration and velocity spectrums in the E-W and NW-SE sections for the analysis point of Seis-18. These two sections share the analysis's sole points. This location has minimal variation in both spectrums.

Figure 42 illustrates 1D and 2D mean acceleration and velocity spectrum for the two sites located on the northern and southern boundary of the basin. Seis-13 is located in the northern boundary at a very dense site and Seis-29 on the southern at stiff soil and the 1999 Düzce fault rupture. Although these two sites show similar behavior for acceleration and velocity spectrum, 1D results show higher spectral velocity

when comparing the 2D results, and this may be due to basin edge effects and the proximity of these sites to the fault. In addition, there is a shift to longer periods for the spectral velocity in Seis-13, where the distance to the Düzce fault is far.

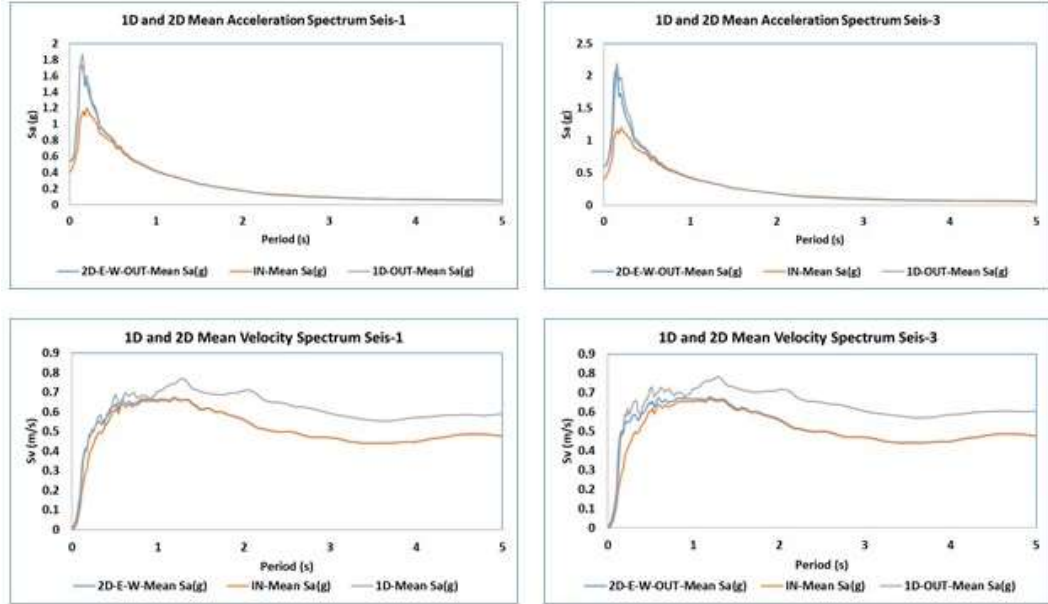


Figure 39. 1D and 2D acceleration and velocity site response spectra in the western part of the basin with very dense/weathered rock soil profiles where the 2D and directivity effects are not observed.

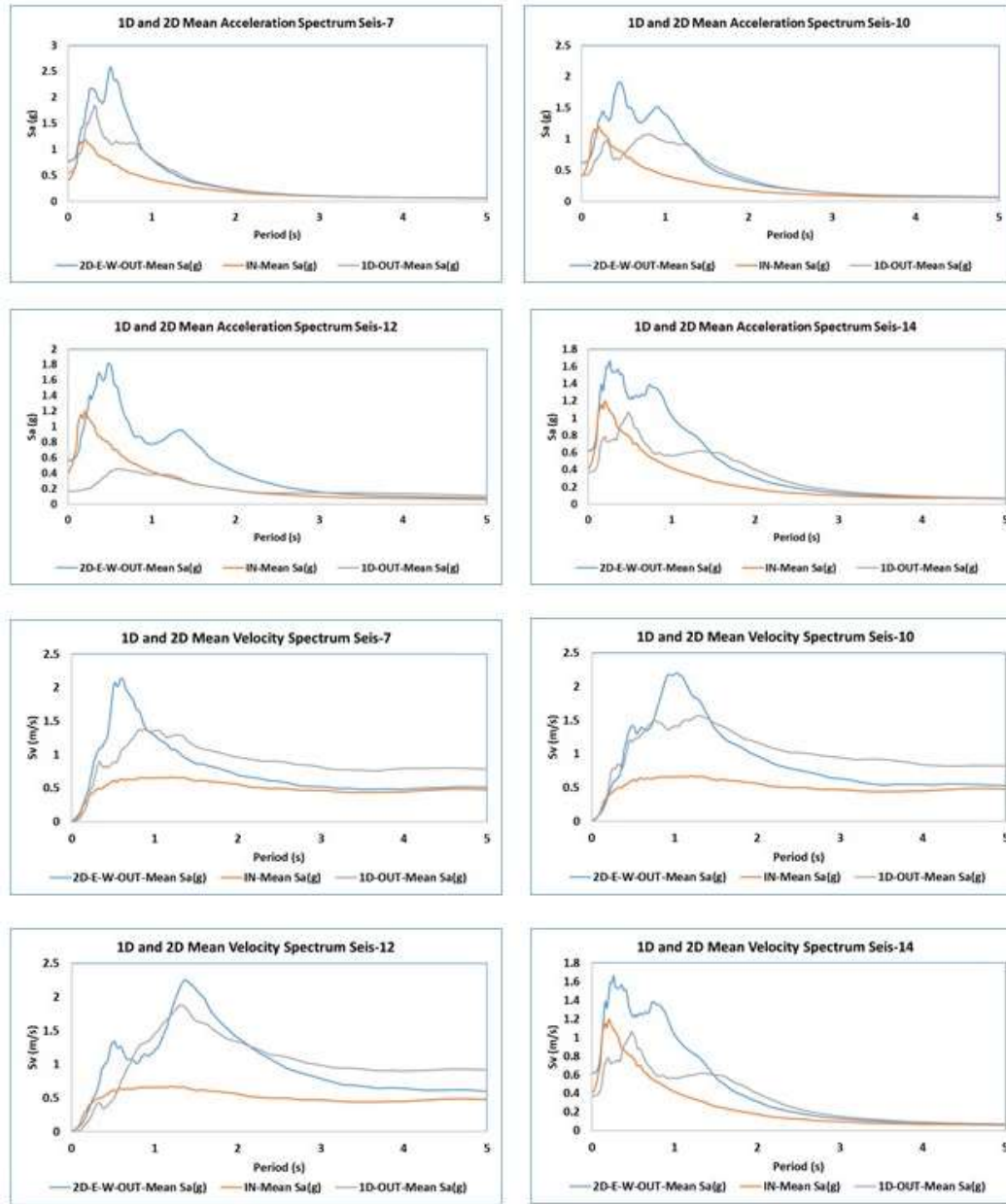


Figure 40. 1D and 2D acceleration and velocity site response spectra in the basin's center at stiff soil profiles where the 2D and directivity effects are evident, especially for Seis-10 and Seis-14.

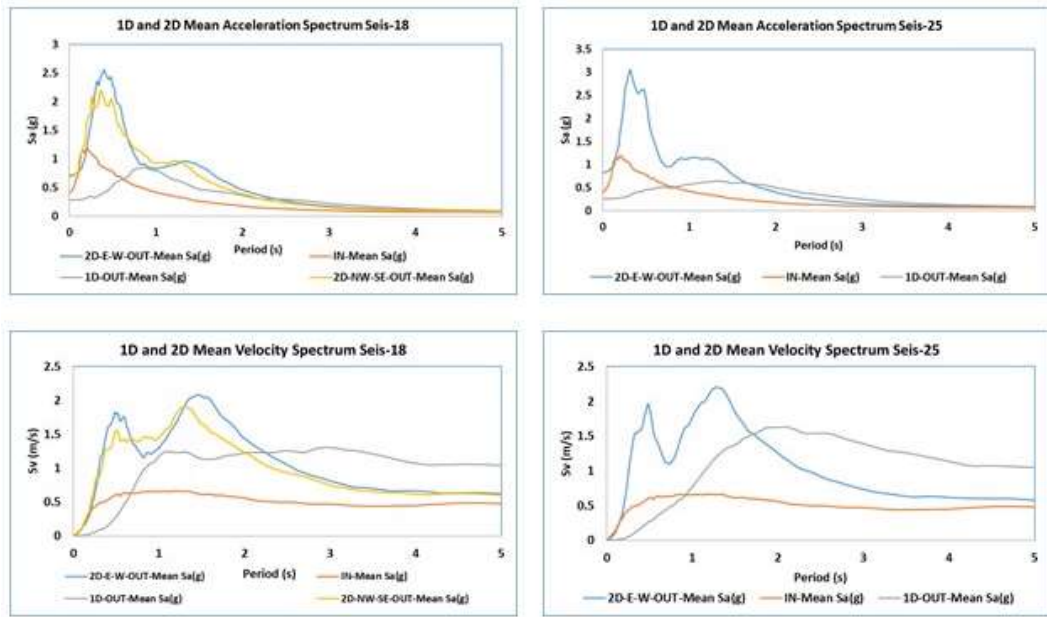


Figure 41. 1D and 2D acceleration and velocity site response spectra in the deepest part of the basin with soft/weak soil profiles where the 2D and directivity effects are evident

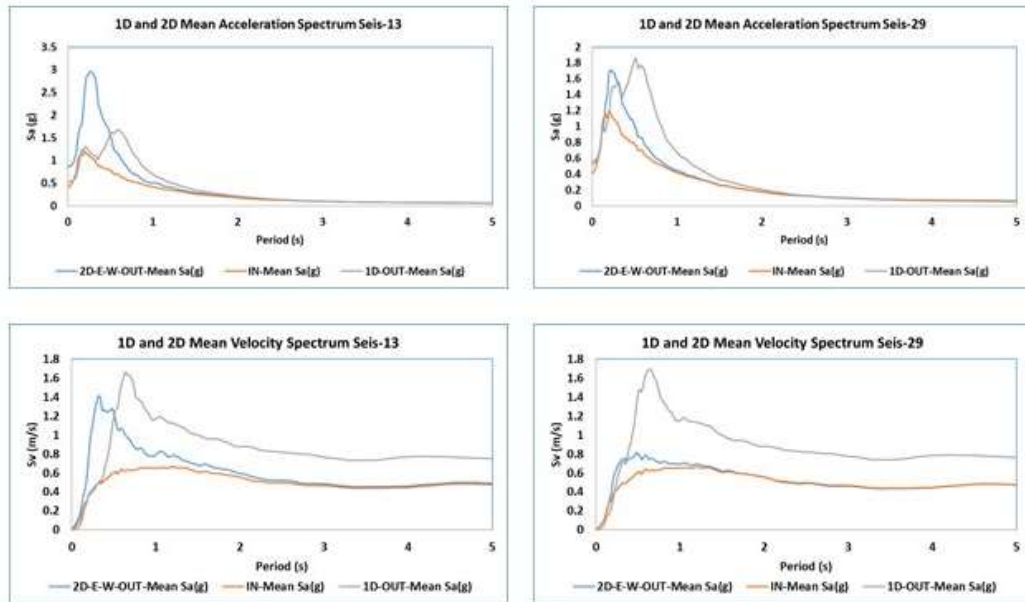


Figure 42. 1D and 2D acceleration and velocity site response spectra in the western part of the basin with very dense/weathered rock soil profiles show the 2D and directivity effects, especially for Seis-10 and Seis-14.

6.2 Validation of the weak motion records along with the site response analyses

In this study, the weak ground motion (small magnitude earthquake, $M_w=3.7$) was recorded only at six temporal stations out of 7 measurements during the field measurement where the location of the measurement locations are illustrated in Figure 13. At the time of this event, station two had been disassembled. Therefore, the recorded motion was obtained at Stations-1-3-4-5-6 and 7. According to Kandilli Observatory and Earthquake Research Institute (KOERI), this event occurred on 2016.09.02 (date) at 19:24:57.53 (local time) at a depth of 9 km in Şirinsulhiye-Kartepe (Kocaeli) at 2.7 km northeast with geographic latitude and longitude of 40.7097, 30.1263.

In the case of weak motion, the amplification is always more robust at younger sediment sites for all frequencies up to 12 Hz (Aki, 1993). Phillips and Aki (1986) conclude that, in terms of weak motion, amplification due to the low impedance of younger sediments continues to outweigh de-amplification due to high absorption, at least up to 12 Hz on the average in central California. Rogers et al. (1984, 1985) also discovered a significant association between the amplification factor and the data for weak motion (NTS) and strong motion (San Fernando) in the frequency range of 0.1 to 5 Hz. Tucker and King (1984) stated no discernible variation in the spectral ratio of the valley's edge to its center between weak (10^{-9} - 10^{-3} g) and strong (0.04-0.2 g) acceleration in the frequency range 0-50 Hz. According to Aki (1993), the local site's influence on strong ground motion is far more complicated than most seismologists have addressed. The non-linearity would prevent the weak motion amplification factor from being used directly to predict strong ground motion. This fact does not negate the importance of the amplification factor for weak motions; on the contrary, weak motion amplification may be helpful in the non-linear regime. If the significant weak motion amplification factor is not linearly amplifying the strong motion, it will manifest in the site damage caused by the very non-linear effect. Indeed, several studies published since Borchardt (1970) have demonstrated a

significant positive correlation between the weak-motion amplification factor and the site-dependent component of the distribution of earthquake intensity, which may be a more versatile seismic hazard parameter than peak ground acceleration.

Figure 14 illustrates the spectral acceleration and velocity spectrum of the Seis-14 and Seis-25. A significant spectrum similarity was observed by comparing the 1D and 2D site response analysis results along with the recorded weak motion. At Seis-25 point in the 2D analysis, the results displayed much better agreement with the spectrum of weak motion, whereas compared to the 1D results, different site response behavior was observed because of the non-linearity resulting from strong ground motion. Furthermore, the 2D effect has represented the second peak at station 4 in both components ($x=E$ and $y=N$). 1D and 2D results at Seis-25 point have represented directivity effects with velocity spectrum impulse at 2s and longer periods.

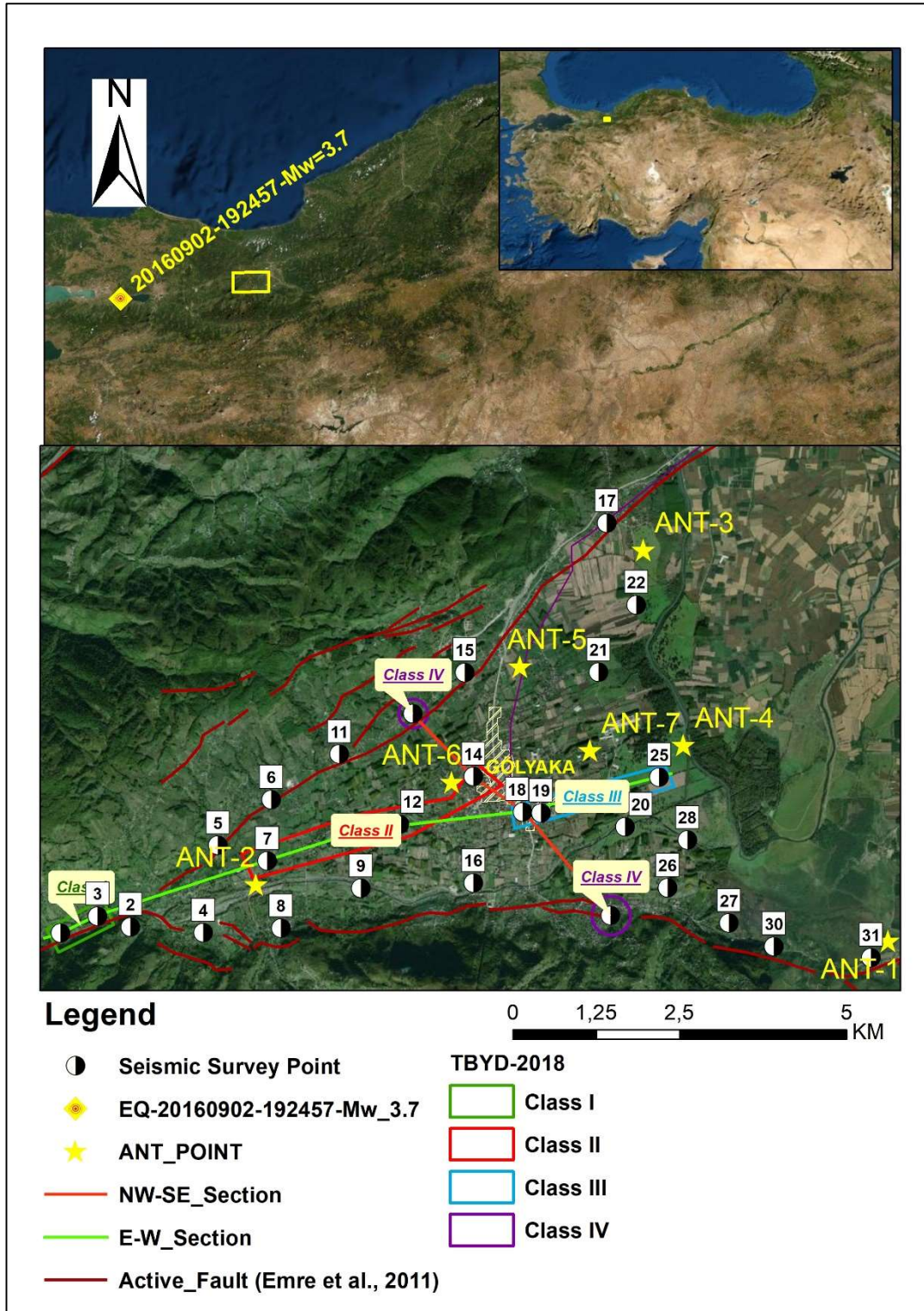


Figure 43. A view of the epicenter location and of the recorded weak motions (Kandili record_02.09.2016)-Mw= 3.7.

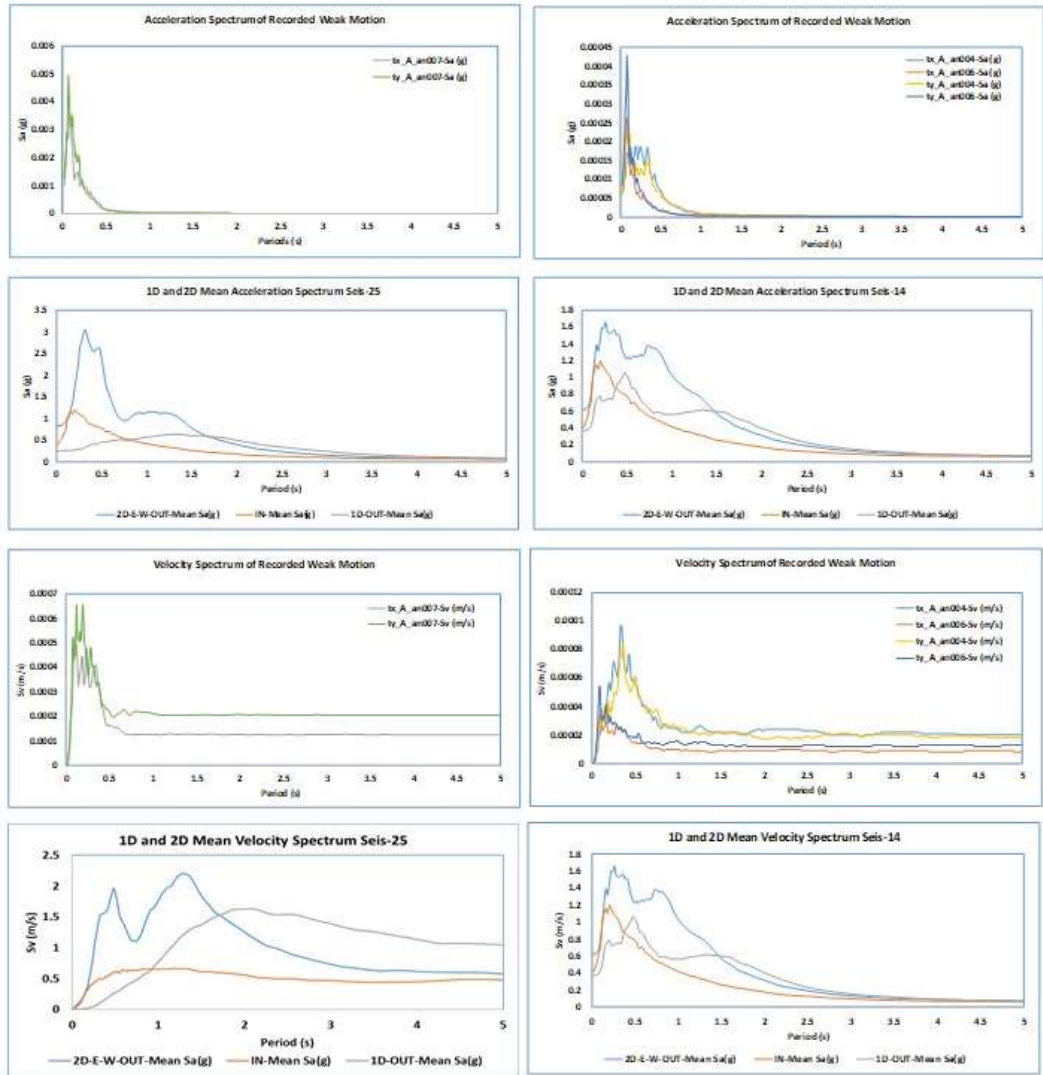


Figure 44. 1D and 2D acceleration site response spectra compared to recorded weak motion and in the soft soil site where 2D and directivity effects were observed in the basin's center.

CHAPTER 7

CONCLUSIONS AND RECOMMENDATIONS

This study has assessed the local site conditions along with the dynamic sediment characteristics in the Gölyaka basin, which tends to possess complex geology because of tectonic deformation caused by near-field faulting. A 3-D basin model was developed to characterize the sediment conditions based on the Vs profiles that have been successfully combined through both active and passive surface wave testing methods that provided a high resolution of the Vs profiles, especially to detect the basin sediment layers. In addition, the provided Vs profiles were correlated with the deep VES results, geology, and available geotechnical boring data. These data allowed to check the validity of the surface seismic testing results and determine the Vs values in the corresponding layers.

Based on the shear wave velocity profiles obtained, the 3-D basin geometry model has been developed, and a shear wave velocity of 1100 m/s was accepted as the bedrock depth limit in the region. Furthermore, the results suggested that the Gölyaka basin was primarily composed of thick clay and sand deposits with some lenses of gravel sediments and with the transition between these layers. The results of this study illustrated that the calculated Vs values with depth implied the prevalence of a low-velocity zone in some pocket areas, especially in the near-field of the fault rupture zone and the saturated lake deposits in the southern boundary. Furthermore, these complexities in the velocity contrast were observed where the sediment layers with lower Vs values were determined in the mid-depth along the basin's center (i.e., at a depth of 50-100 m). The extracted 2-D shear wave velocity profiles illustrated that the thickness of the basin sediment continues down to a depth of approximately 250-350 m with irregular geometry due to over-step faulting near the southern boundary of the basin. As a result, the local site conditions have demonstrated spatial

variations in the near-field area depending on the dimensional basin geometry, material heterogeneity, and topography. As a result, inclined layering and nonlinearity in the V_s profiles have formed. The lateral heterogeneity and incoherence in the V_s measurements were not so dominant in the developed V_s -model but were rather dominant in the near-field of the fault zone, where the low-velocity material is sitting next to the higher velocity material. The surface seismic survey results were complemented with the deep Vertical Electrical Sounding (VES) measurements, the engineering geological and geotechnical data, and the geology to increase the authenticity of the research reported herein.

In the VES results, the lateral variation of basin complexity due to the heterogeneity of the near-fault region was observed. An increase in the thickness of the alluvium in the center of the basin indicates that the alluvial thickness could be much thicker, i.e., almost 450 m. Nevertheless, these results can also be attributed to the transition zones between the deformed material due to the near-field fault activity and thus the tectonic deformation of the rock formations. In addition, the existence of faulting could also be observed throughout the resistivity results that were in good agreement with the geological and topographical observations.

The H/V microtremor measurement verified the estimated basin depth at the Gölyaka region. The correlation between the measured fundamental periods of H/V and estimated V_s profiles presented a good agreement, especially at the basin's center. Inconsistent results have been occasionally observed along the Kocaeli and Duzce fault ruptures in the northern and southern boundaries due to basin edge effects and tectonic deformation of the materials. Additionally, at the western side of the basin, where the bedrock depth is shallow, impedance contrast was observed between these layers, which was also validated by the H/V microtremor results.

A total of 70 computational analyses have been conducted at the ten sites to evaluate the 1D site responses. Additionally, 14 analyses were conducted to determine the two-dimensional soil response along the two sections. The amplification of the surface layers and acceleration response spectra at each site were studied. The results

indicated that the soil responses were stationary at all sites. Hence, the subsequent analyses used the arithmetic mean of the computed amplification and acceleration response spectra.

During the site response analysis, 1D and 2D processed results were compared. Based on the position of the 1D sites concerning the basin and site class, as specified by the TBDY 2018 Turkish code, Four sections have been identified. These sections were divided as follows: dense/weathered rock site at the western of the basin, stiff soil site at the center, soft/weak soil site at the deepest part of the basin, and the boundary at north and south of the basin.

The maximum horizontal acceleration amplitude (MHA) of 2D numerical analysis is higher than that of 1D response analysis of Seis-1 and Seis-3 at very dense/weathered rock sites. This large MHA may be due to shallow bedrock depth's shear wave velocity contrast. MHA was obtained at 0.2 seconds (T) and spectral acceleration (S_a) of 2.5g for 1D and 2D analysis. No evidence of forward directivity or 2D effects was determined due to any response analysis result at the near-fault zone.

By comparing the results of 1D and 2D analysis, it was discovered that the second classified section, which is located in the basin's center, exhibited 2D basin effects in spectral acceleration at a stiff soil site. Furthermore, near-field directivity effects were found at longer periods (1.5s), and this velocity pulse has a longer period due to the nature of directivity. Seis-10 and Seis-14, in particular, are located distant from the 1999 Düzce faults and in the approximate rupture direction of the 1999 Kocaeli and Düzce faults.

The results of 1D and 2D numerical calculations for the third categorized site in soft/weak soils in the deepest part of the region showed 2D basin effects in spectral accelerations in short periods. The 1D results suggested that the acceleration spectrum shifted toward longer periods and the spectral amplitude was moderate in short periods, but the 1D and 2D amplitudes were comparable in longer periods (1s and 2s). Additionally, near-field directivity effects were encountered in longer

periods (1.5s). As a result of the directivity characteristics, this velocity pulse by nature has a longer period, notably for 1D analysis results. A three-dimensional effect can also be noticed for the analysis point of Seis-18 by comparing the acceleration and velocity spectra along the E-W and NW-SE of regions. Considering that Seis-18 is the only point that these two sections share

The two sites are located at the basin's boundary, one at the northern boundary at a very dense site and the other at the southern boundary at a stiff site. When the 1D and 2D response analysis results were compared, they revealed similar acceleration and velocity spectra characteristics. Both 1D and 2D results show a maximum spectral acceleration of 2g over a short period of 0.5 seconds. However, the point Seis-13 at the northern boundary of the basin implies a higher Sa than the point Seis-29 at the southern boundary, which has about 2g Sa. In the 1D analysis results, these two sites show that the Sa values change over longer periods. On the other hand, these sites had higher spectral values in 1D results than 2D results over short periods. This higher Sa may be due to the basin edge effect and nonlinearity of the site's proximity to the fault rupture.

By comparing the site response analyses with the seismic activity recorded at the site, dimensional 2D analysis results and directivity effects were assessed. Accordingly, it was inferred that the recorded weak motion spectral acceleration presented significant similarity with the results of the 1D and 2D analyses. In this case, it was deemed that weak motion was a good indicator of seismic site effects for softer and thicker sediments in the study area.

This research is a pioneer study for a highly seismically active region in the near-fault sites, such as the Gölyaka basin, concerning the evaluation of site response analyses in an account for seismic hazard assessment. For such a large district with growth potential in a near-fault region, while it is highly susceptible to experience a major earthquake, it is vital to have an appropriate well-developed basin model for seismic hazard evaluations, wave propagation, seismic responses for the design in the future, general land use, and urban planning.

In conclusion, it is strongly believed that the model developed in this study is the first novel Vs model developed for the study region in Turkey that mankind can utilize for multiple purposes. The developed Vs basin model can be used to assess seismic hazard. Furthermore, it can be used to evaluate high-resolution surface wave propagations in the study area. Last but not least, the results of the seismic response analysis in this research can be effectively used for future design studies for this area in the case of rapid urbanization located in the near-field domain.

Additional site-specific studies could be performed in this unique basin to more accurately describe the characteristics and potential level of ground shaking in hazard assessments. This study is believed to form an excellent example of why the advanced basin model should address the complexity associated with the characteristics of the near-fault region, which is not yet fully understood concerning the effects of major seismic events.

The research given in this dissertation extends our knowledge of on basin geometry and dimensional seismic site response analyses. The following suggestions, however, represent the research's main restriction and can be addressed in future studies:

- Parametric study of non-linear behavior related to lateral heterogeneity associated with the near-field basin in the seismic response analysis.
- Assessment of the interaction of inclined layer on seismic response.
- Investigation of near-field fling effects in the research area for future design purposes.
- Implementation of a 3D model assessing seismic response studies as well to understand the basin effects further.

REFERENCES

- Aki, K., (1993). "Local site effects on weak and strong ground motion". In: F. Lund (Editor), *New Horizons in Strong Motion: Seismic Studies and Engineering Practice*. Z'ecronophysics, 218: 93-111.
- Akyüz HS, Hartleb R, Barka A, Altunel E, Sunal G, Meyer B, Armijo R (2002) Surface rupture and slip distribution of the 12 November 1999 Düzce earthquake (M 7.1), North Anatolian fault, Bolu, Turkey. *Bull. Seismol. Soc. Am.* 92(6):1-6. <https://doi:10.1785/0120000840>
- Ambraseys NN, Zatopek A (1969) Mudurnu Valley, West Anatolia, Turkey, Earthquake of 22 July 1967. *Bull. Seismol. Soc. Am.* 59:21–89.
- Andrade, J. E., Borja, R. I. (2006) "Quantifying Sensitivity of Local Site Response Models to Statistical Variations in Soil Properties", *Acta Geotechnica*, 1 (1), 3-14.
- Andrus, R.D., Fairbanks, C. D., Zhang, J., Camp, W. M., Casey, T. J., Cleary, T. J., Wright, W. B. 2006. Shear-Wave Velocity and Seismic Response of Near-surface Sediments in Charleston, South Carolina", *Bulletin of the Seismological Society of America*, 96 (5), 1897–1914.
- ASCE 7. 2010. "Minimum Design Loads for Buildings and Other Structures", American Society of Civil Engineers, Reston, VA.
- Augello, A. J., Bray, J. D., Abrahamson, N. A., Seed, R. B. 1998. "Dynamic Properties of Solid Waste Based on Back-Analysis of the OII Landfill", *Journal of Geotechnical Engineering*, 124, 211-222.
- Ayhan ME, Bürgmann R, McClusky S, Lenk O, Aktug B, Herece E, Reilinger RE. (2001) Kinematics of the Mw: 7.2, 12 November 1999, Düzce, Turkey earthquake. *Geophys. Res. Lett.*; 28:367–370

- Aydan, Ö . (2000). GPS ölçümlerine dayanılarak Türkiye'nin yıllık birimdeformasyon ve gerilim hızı dağılımının değerlendirilmesi . *Yerbilimleri* , 21 (22) , 21-31 . Retrieved from <https://dergipark.org.tr/en/pub/yerbilimleri/issue/13618/165011>
- Aydan, Ö, Ulusay, R., Kumsar., H., Tuncay, E. (2000). Site Investigation and Engineering Evaluation of Düzce-Bolu Earthquake of November 12, 1999, *Türkiye Deprem Vakfı (Turkish Earthquake Foundation, TDV)*, 220 p.
- Barani, S., Massa, M., Lovati, S., Ferretti, G. (2013) "Topographic Effects in Probabilistic Seismic Hazard Analysis: The Case of Narni, Central Italy", *WCEE proceedings, lisboa, September*, 10 p.
- Barka A (1996) Slip Distribution along the North Anatolian Fault Associated with the Large Earthquakes of the Period 1939 to 1967, 86:1238–1254.
- Barka A, Akyüz HS, Altunel E, Sunal G, Çakır Z, Dikbas A, Yerli B, Armijo R, Meyer B, De Chabaliér JB, Rockwell T, Dolan JR, Hartleb R, Dawson T, Christofferson S, Tucker A, Fumal T, Langridge R, Stenner H, Lettis W, Bachhuber J, Page W (2002) The surface rupture and slip distribution of the 17 August 1999 İzmit earthquake (M 7.4), North Anatolian fault. *Bull. Seismol. Soc. Am.* 92(1):43-60. <https://doi:10.1785/0120000841>
- Barka AA, Kadinsky-Cade K (1988) Strike-slip fault geometry in Turkey and its influence on earthquake activity. *Tectonics.* 7(6):63-84. <https://doi:10.1029/TC007i003p00663>
- Boaga J, Vaccari F, Panza GF (2010) Shear wave structural models of Venice Plain, Italy, from Time Cross Correlation of seismic noise. *Eng. Geol.* 116:189–195. <https://doi:10.1016/j.enggeo.2010.09.001>
- Bommer, J., Acevedo, A. 2004. "The Use of Real Earthquake Accelerograms as Input to Dynamic Analysis", *Journal of Earthquake Engineering*, 8 (special issue 1), 43-91.

- Boore, D M. 2006. "Determining Subsurface Shear-Wave Velocities: A Review", Third International Symposium on the Effects of Surface Geology on Seismic Motion Grenoble, France, 103.
- Boore, D. M. (1972) "A Note on the Effect of Simple Topography on Seismic SH Waves", Bulletin of the Seismological Society of America, 62 (1), 275-284.
- Borcherdt RD (2002) Empirical evidence for acceleration-dependent amplification factors. Bull. Seismol. Soc. Am. 92: 761–782. doi:10.1785/0120010170
- Borcherdt, R.D., (1970) "Effects of local geology on ground motion near San Francisco Bay". Bull. Seismol. Soc. Am., 60: 29-61.
- Bouckovalas, G. D., Papadimitriou, A. G., Kondis, A., Bakas, G. J. (2006) "Equivalent-Uniform Soil Model for the Seismic Response Analysis of Sites Improved with Inclusions", Proc., 6th European Conf. on Numerical Methods in Geotechnical Engineering, Taylor & Francis, London, 801–807.
- Bradley BA, Cubrinovski M (2011) Near-source strong ground motions observed in the 22 February 2011 Christchurch earthquake. Seismol. Res. Lett. 82:853–865. <https://doi:10.1785/gssrl.82.6.853>
- Brennan, A. J., Thusyanthan, N. I., Madabhushi, S. P. J. 2005. "Evaluation of Shear Modulus and Damping in Dynamic Centrifuge Tests", J Geotech Geoenviron Eng ASCE, 131 (12), 1488 - 1497.
- Bürgmann R, Ayhan ME, Fielding EJ, Wright TJ, McClusky S, Aktug B, Demir C, Lenk O, Türkezer A (2002) Deformation during the 12 November 1999 Düzce, Turkey, earthquake, from GPS and InSAR data. Bull. Seismol. Soc. Am. 92(1):161-171. <https://doi:10.1785/0120000834>
- Cambazoğlu S, Koçkar MK, Akgün H (2016) A generalized seismic source model for the Eastern Marmara Region along the segments of the North Anatolian Fault System. Soil Dyn. Earthq. Eng. 88: 412–426. <https://doi:10.1016/j.soildyn.2016.07.002>

- Çakir Z, Barka AA, Chabalier JB, Armijo R, Meyer B (2003) Kinematics of the November 12, 1999 (Mw=7.2) Düzce earthquake deduced from SAR interferometry. *Turk J Earth Sci*;12:105–18.
- Cavallaro, A., Ferraro, A., Grasso, S., Maugerib, M. 2008. "Site Response Analysis of the Monte Po Hill in the City of Catania", *Seismic Engineering Conference Commemorating the 1908 Messina and Reggio Calabria Earthquake*, CP1020.
- Cavallaro, A., Ferraro, A., Grasso, S., Maugerib, M. 2012. "Topographic Effects on the Monte Po Hill in Catania (Italy)", *Soil Dynamics and Earthquake Engineering* 43, 97–113.
- Chapman M. C., Martin, J. R., Olgun, C. G., Beale J. N. 2006. "Site Response Models for Charleston, South Carolina and Vicinity Developed from Shallow Geotechnical Investigations", *Bulletin of the Seismological Society of America*, 96, 467-489.
- Chouinard, L., Rosset, P., De La Puente, A., Madriz, R., Mitchell, D., Adams, J. 2004. "Seismic Hazard Analysis for Montreal", In *Proceedings of the 13th World Conference on Earthquake Engineering*, Vancouver, Canada, Paper Vol. 7010.
- Cornell C. A. 1968. "Engineering Seismic Risk Analysis", *Bulletin of the Seismological Society of America*, 58 (5),1583-1606.
- Cushing EM, Hollender F, Moiriat D, Guyonnet-Benaize C, Theodoulidis N, Pons-Branchu E, Sépulcre S, Bard PY, Cornou C, Dechamp A, Mariscal A, Roumelioti Z (2020) Building a three dimensional model of the active Plio-Quaternary basin of Argostoli (Cephalonia Island, Greece): An integrated geophysical and geological approach. *Eng. Geol.* 265. <https://doi:10.1016/j.enggeo.2019.105441>
- Darendeli, M. (2001) "Development of a New Family of Normalized Modulus Reduction and Material Damping Curves", Ph.D. Thesis, Dept. of Civil Eng., Univ. of Texas, Austin.

- Dawson, E. M.; Roth, W. H.; Nesarajah, S., Davis, C. A. 2001. "A Practice- Oriented Pore-Pressure Generation Model", published at 2nd International FLAC Symposium, Lyon, France, October, 8 p.
- Dobry R, Borchardt RD, Crouse CB, Idriss IM, Joyner WB, Martin GR, Power MS, Rinne EE, Seed RB (2000) New Site Coefficients and Site Classification System Used in Recent Building Seismic Code Provisions. *Earthq. Spectra* 16: 41–67.
- Dreger DS, Transportation CD, University of California, B.E.E.R.C. (2007) Near-Fault Seismic Ground Motions, UCB/EERC 2007-03. California.
- Eker AM, Akgün H, Koçkar MK (2012) Local site characterization and seismic zonation study by utilizing active and passive surface wave methods: A case study for the northern side of Ankara, Turkey. *Eng. Geol.* 151: 64–81. <https://doi:10.1016/j.enggeo.2012.09.002>
- Eker AM, Koçkar MK, Akgün H (2015) Evaluation of site effect within the tectonic basin in the northern side of Ankara. *Eng. Geol.* 192: 76–91. <https://doi:10.1016/j.enggeo.2015.03.015>
- Emre Ö, Doğan A, Duman TY, Özalp T (2011) 1:250.000ScaleActiveFaultMapSeries of Turkey. General Directorate of Mineral Research and Exploration Ankara-Turkey2011.
- Electrical Power Research Institute (EPRI). 1988. "A Criterion for Determining Exceedance of the Operating Basis Earthquake", Report No. EPRI NP-5930 Palo Alto, California.
- Foti S, Hollender F, Garofalo F, Albarello D, Asten M, Bard PY, Comina C, Cornou C, Cox B, Di Giulio G, Forbriger T, Hayashi K, Lunedei E, Martin A, Mercierat D, Ohrnberger M, Poggi V, Renalier F, Sicilia D, Socco V (2018) Guidelines for the good practice of surface wave analysis: a product of the InterPACIFIC project, *Bulletin of Earthquake Engineering*. <https://doi:10.1007/s10518-017-0206-7>

- Gasparini, D. A., Vanmarcke, E. H. 1976. "SIMQKE: Simulated Earthquake Motions Compatible with Prescribed Response Spectra", Massachusetts Institute of Technology-, Cambridge, Massachusetts.
- Gelagoti, F., Kourkoulis, R., Anastasopoulos, I., Tazoh, T., Gazetas, G. 2010. "Seismic Wave Propagation in a Very Soft Alluvial Valley: Sensitivity to Ground- Motion Details and Soil Nonlinearity, and Generation of a Parasitic Vertical Component", *Bulletin of the Seismological Society of America*, 100 (6), 3035- 3054.
- Geli, L., Bard, P-Y., Jullien, B. 1988. "The Effect of Topography on Earthquake Ground Motion: A Review and New Results", *Bulletin of the Seismological Society of America*, 78 (1), 42-63.
- Gosar A, Stopar R, Rošer J (2008) Comparative test of active and passive multichannel analysis of surface waves (MASW) methods and microtremor HVSr method Primerjalni test aktivne in pasivne večkanalne analize površinskih valov (MASW) ter metode mikrotremorjev (HVSr). *Mater. Geoenvironment* 55: 41–66.
- Gouveia F, Lopes I, Gomes RC (2016) Deeper VS profile from joint analysis of Rayleigh wave data. *Eng. Geol.* 202: 85–98. <https://doi:10.1016/j.enggeo.2016.01.006>
- Gürer, Ö.F., Sangu, E., Özburan, M., (2006). Neotectonics of the SW Marmara region, NW Anatolia, Turkey. *Geol. Mag.* 143, 229. doi:10.1017/S0016756805001469
- Hancock, J., Watson-Lamprey, J., Abrahamson, N., Bommer, J., Markatis, A., McCoy, E., Mendis, R. 2006. "An Improved Method of Matching Response Spectra of Recorded Earthquake Ground Motion Using Wavelets, *J. Earthquake Eng.*, 10, 67–89.
- Hartleb RD, Dolan JF, Akyüz S, Dawson TE, Tucker AZ, Yerli B, et al., (2002) Surface rupture and slip distribution along the Karadere segment of the 17 August 1999 Izmit, Turkey, earthquake. (Special Issue on the 1999 Izmit and Düzce, Turkey, Earthquakes, N.Toksöz [Editor]). *Bull Seism Soc Am*.

- Havenith, H. B., Fäh, D., Polonu, U., Roullé, A. 2007. "S-Wave Velocity Measurements Applied to the Seismic Microzonation of Basel, Upper Rhine Graben", *Geophys. J. Int.*, 170, 346–358.
- Hayashi K (2008) Development of the Surface-wave Methods and Its Application to Site Investigations. Kyoto Univ. Dr. Diss. <https://doi:10.14989/doctor.k13774>
- Herak M (2008) Model HVSR-A Matlab® tool to model horizontal-to-vertical spectral ratio of ambient noise. *Comput. Geosci.* <https://doi:10.1016/j.cageo.2007.07.009>
- Hudson, M., Idriss, I. M., Beikae, M., 1994. "QUAD4M – A Computer Program to Evaluate the Seismic Response of Soil Structures Using Finite Element Procedures and Incorporating a Compliant Base Center for Geotechnical Modeling", Department of Civil and Environmental Engineering, University of California, Davis, CA.
- Ibs-von Seht M, and Wohlenberg J (1999) Microtremor measurements used to map thickness of soft sediments, *Bull. seism. Soc. Am.*, 89(1): 250–259.
- Idriss, I. M., Seed, H. B. 1967. "Response of Earthbanks during Earthquakes", *J. Soil Mech. Found. Div., ASCE*, 93 (SM3), 61-82.
- Joyner WB, Fumal TE, Glassmoyer G (1994) Empirical spectral response ratios for strong motion data from the 1989 Loma Prieta, California, earthquake, in: NCEER-94-SP01, R.S.P. (Ed.), *Proceedings of 1992 NCEER/SEAOC/BSSC Workshop on Site Response during Earthquake and Seismic Code Provisions*. National Center for Earthquake Engineering Research, Buffalo, NY, Los Angeles, California, G.R. Martin (ed.).
- Jibson, R. 1987. "Summary of Research on the Effects Topographic Amplification of Earthquake Shaking of Slope Stability" U.S. Geological Survey, Open-File Report 87-268, Manlo Park, California, USA.

- Koçkar MK (2016) Site characterization of the strong motion stations and evaluation of site effects in the Ankara region during the December 2007 and March 2008 moderate Bala earthquakes. *Environ. Earth Sci.* 75. <https://doi:10.1007/s12665-016-5921-x>
- Koçkar MK, Akgün H (2012) Evaluation of the site effects of the Ankara basin, Turkey. *J. Appl. Geophys.* 83: 120–134. doi:10.1016/j.jappgeo.2012.05.007
- Koçkar MK., Akgün H, Rathje EM (2010) Evaluation of site conditions for the Ankara Basin of Turkey based on seismic site characterization of near-surface geologic materials. *Soil Dyn. Earthq. Eng.* 30: 8–20. <https://doi:10.1016/j.soildyn.2009.05.007>
- KOERI-RETMC (2020) Earthquake Catalog - BOUN KOERI Regional Earthquake-Tsunami Monitoring Center. <http://www.koeri.boun.edu.tr/sismo/2/earthquake-catalog/>
- Kondo H, Awata Y, Emre Ö, Doğan A, Özalp S, Tokay F, Yildirim C, Yoshioka T, Okumura K (2005) Slip distribution, fault geometry, and fault segmentation of the 1944 Bolu-Gerede earthquake rupture, North Anatolian fault, Turkey. *Bull. Seismol. Soc. Am.* 95: 34–49. <https://doi:10.1785/0120040194>
- Kottke, A., Rathje, E. M. 2009. "Technical Manual for Strata", Rep. No. 2008/10, Pacific Earthquake Engineering Research Center, Berkeley, Calif.
- Kramer, S. L. 1996. "Geotechnical Earthquake Engineering", Prentice-Hall, Upper Saddle River.
- Krinitzsky, E. L., Chang, F. K. 1975. "State-of-the-Art for Assessing Earthquake Hazards in the United States Earthquake Intensity and the Selection of Ground Motions for Seismic Design Miscellaneous", Paper S-73-1, Army Engineer Waterways Experiment Station CE Vicksburg Mississippi.
- Kuhlemeyer R.L., Lysmer, J. 1973. "Finite Element Method Accuracy for Wave Propagation Problems", *J. Soil Mech. & Foundations*, Div. ASCE 99 (SM5), 421- 427.

- Lanzo, G. & Silvestri, F., 1999. *Risposta sismica locale: teoria ed esperienze*, Hevelius.
- Lanzo, G., Silvestri, F., Costanzo A., d'Onofrio A., Martelli, L., Pagliaroli, A., Sica, S., Simonelli, A. 2011. "Site Response Studies and Seismic Microzoning in the Middle Aterno Valley (L'Aquila, Central Italy)", *Bull. Earthquake Eng.*, 9, 1417–1442.
- Lanzo, G., Pagliaroli, A. 2012. "Seismic Site Effects at Near-Fault Strong-Motion Stations along the Aterno River Valley during the Mw = 6.3 2009 L'Aquila Earthquake", *Soil Dyn. Earthq. Eng.*, 40, 1 - 14.
- Lettis W, Bachhuber J, Witter R, Brankman C, Randolph CE, Barka A, Page WD, Kaya A (2002) Influence of Releasing Step-Overs on Surface Fault Rupture and Fault Segment Earthquake Segmentation: Examples from the 17 August 1999 I on the North Anatolian Fault, Turkey 19–42.
- Lilhanand, K., Tseng, W. S. 1988. "Development and Application of Realistic Earthquake Time Histories Compatible with Multiple-Damping Design Spectra", *Proceedings of the 9th World Conference on Earthquake Engineering*, Tokyo Japan, II, 819–824.
- Matasovic N., Ordonez G., 2012. "D-MOD2000 – A Computer Program for Seismic Site Response Analysis of Horizontally Layered Soil Deposits, Earthfill Dams and Solid Waste Landfills", Geomotions, LLC; Lacey, Washington, USA.
- Mayne, P. W., Kulhawy, F. H. 1982. "K_o -OCR Relationships in Soil", *Journal of the Geotechnical Engineering Division*, ASCE, 108 (GT6), 851-872.
- McClusky S, Balassanian S, Barka A, Demir C, Ergintav S, Georgiev I, Gurkan O, Hamburger M, Hurst K, Kahle H, Kastens K, Kekelidze G, King R, Kotzev V, Lenk O, Mahmoud S, Mishin A, Nadariya M, Ouzounis A, Paradissis D, Peter Y, Prilepin M, Reilinger R, Sanli I, Seeger H, Tealeb A, Toksöz M.N, Veis G (2000) Global Positioning System constraints on plate kinematics and

- dynamics in the eastern Mediterranean and Caucasus. *J. Geophys. Res. Solid Earth*. <https://doi.org/10.1029/1999jb900351>
- Mori F, Mendicelli A, Moscatelli M, Romagnoli G, Peronace E, Naso G 2020. A new Vs30 map for Italy based on the seismic microzonation dataset. *Eng. Geol.* 275. <https://doi.org/10.1016/j.enggeo.2020.105745>
- MTA 2003. Surface Rupture Associated with the August 17 (1999) İzmit Earthquake. Special Publications Series: 1.
- MTA and Ankara University 1999. Geological Assessment of Alternative Settlement areas for Düzce Province Following 17 August 1999, TÜBİTAK, Earth-Sea-Atmosphere Sciences. and Environment Research Group Report, ANKARA.
- Nakamura Y (1989) A method for dynamic characteristics estimation of subsurface using microtremor on the ground surface. *Q. Rep. Railw. Tech. Res. Inst. (RTRI)* 30 (1): 273–281.
- Ohrnberger M, Scherbaum F, Krüger F, Pelzing R, Reamer SK (2004) How good are shear wave velocity models obtained from inversion of ambient vibrations in the lower Rhine embayment (N.W. Germany) *Boll. di Geofis. Teor. ed Appl.* 45: 215–232.
- Ohrnberger M, Schissele E, Cornou C, Wathelet M, Savvaidis A, Scherbaum F, Jongmans D, Kind F (2004) Microtremor Array Measurements for Site Effect Investigations: Comparison of Analysis Methods for Field Data Crosschecked By Simulated Wavefields. 13th World Conf. Earthq. Eng. Paper no: 0940.
- Okada H, Suto K (2003) The Microtremor Survey Method, *The Microtremor Survey Method*. <https://doi.org/10.1190/1.9781560801740>
- Ordonez, I. M. 2009. "Influence of the Boundary Conditions on the Seismic Response Predictions of a Rockfill Dam by Finite Element Method", *Mater Thesis*, Università degli Studi di Pavia, 67 p.
- Ordonez, G. A. 2000. "SHAKE 2000: A Computer Model for the I-D Analysis of Geotechnical Earthquake Engineering Problems".

- Özalaybey S, Zor E, Ergintav S, Tapirdamaz M.C (2011) Investigation of 3-D basin structures in the İzmit Bay area (Turkey) by single-station microtremor and gravimetric methods. *Geophys. J. Int.* 186: 883–894. <https://doi:10.1111/j.1365-246X.2011.05085.x>
- Özden S, Tatar O, Mesci BL, Koçbulut F, Tutkun SZ, Doğan B, Tüvar O.12 November 1999 Düzce earthquake and its regional meaning. *Geol Bull Turk, Ank* 2000;43(2):61–9 (In Turkish).
- Palyvos N, Pantosti D, Zabci C, D’Addezio G (2007) Paleoseismological Evidence of Recent Earthquakes on the 1967 Mudurnu Valley Earthquake Segment of the North Anatolian Fault Zone. *Bull. Seismol. Soc. Am.* 97: 1646–1661. <https://doi:10.1785/0120060049>
- Park CB., Miller RD, Xia J, Ivanov JM (2007) Multichannel Analysis of Surface Waves (MASW). *Lead. Edge* 26: 60–64.
- Park, C.B., Miller, R.D., Rydén, N., Xia, J., & Ivanov, J. (2005) Combined Use of Active and Passive Surface Waves. *Journal of Environmental and Engineering Geophysics*, 10, 323-334.
- Park CB, Miller RD, Xia J (1999) Multichannel analysis of surface waves. *Geophysics* 64: 800–808. <https://doi:10.1190/1.1444590>
- Park S, Elrick S (1998) Predictions of shear-wave velocities in southern California using surface geology. *Bull. Seismol. Soc. Am.* 88: 677–685.
- Pegah E, Liu H (2016) Application of near-surface seismic refraction tomography and multichannel analysis of surface waves for geotechnical site characterizations: A case study. *Eng. Geol.* 208: 100–113. <https://doi:10.1016/j.enggeo.2016.04.021>
- Phillips, W.S. and Aki, K., (1986). “Site amplification of coda waves from local earthquakes in central California”. *Bull. Seismol. Soc. Am.*, 76: 627-648.

- Piatti C, Foti S, Socco L. V, Boiero D (2013) Building 3D Shear-Wave Velocity Models Using Surface Waves Testing: The Tarcento Basin Case History. *Bull. Seismol. Soc. Am.* 103:1038–1047. <https://doi.org/10.1785/0120120089>
- Pitilakis, K. 2004. "Site Effects", 139–193. *Recent Advances in Earthquake Geotechnical Engineering and Microzonation*. Ed: Ansal, A. Kluwer Academic Publishers, Dordrecht, the Nederland.
- Polat O, Haessler H, Cisternas A, Philip H, Eyidogan H, Aktar M, Frogneux M, Comte D, Gürbüz C (2002) The İzmit (Kocaeli), Turkey earthquake of 17 August 1999: Previous seismicity, aftershocks, and seismotectonics. *Bull. Seismol. Soc. Am.* 92: 361–375. <https://doi.org/10.1785/0120000816>
- Pruska, M. J. 1973. "Effect of Initial Stress on the Stress-Strain Relation", *Proceedings of the 8th International Conference on Soil Mechanics and Foundation Engineering*, Moscow, 4, 26-28.
- Pucci S, Pantosti D, Barchi MR, Palyvos N (2007) A complex seismogenic shear zone: The Düzce segment of North Anatolian Fault (Turkey). *Earth Planet. Sci. Lett.* 262: 185–203. <https://doi.org/10.1016/j.epsl.2007.07.038>
- Bray, J.D. and Rathje, E.M. 1998. "Earthquake-Induced Displacements of Solid-Waste Landfills," *Journal of Geotechnical and Geoenvironmental Engineering*, ASCE, 124(3), pp. 242-253
- Rathje, E. M., Bray, J. D. 2001. "One- and Two-Dimensional Seismic Analysis of Solid-Waste Landfills", *Can. Geotech. J.*, 38, 850–862.
- Rathje, E. M., Kottke, R. K., Trent, W. L. 2010. "Influence of Input Motion and Site Property Variabilities on Seismic Site Response Analysis", *J. Geotech. Geoenviron. Eng.*, 136, 607-619.
- Reilinger R, McClusky S, Vernant P, Lawrence S, Ergintav S, Rahsan C, Kadirov F, Guliev I, Stepanyan R, Nadariya M, Hahubia G, Mahmoud S, Sakr K,

- ArRajehi A, Paradissis D, Al-Aydrus A, Prilepin Mikhail, Guseva T, Evren E, Dmitrotsa A, Filikov S. V, Gomez F, Al-Ghazzi R, Karam G (2006) GPS constraints on contemporary deformation in the Arabia-Africa-Eurasia zone of plate interaction and Implications for active. *J. Geophys. Res.* 111: 1–52.
- Reilinger R, Toksoz N, McClusky S, Barka A (2000) 1999 Izmit, turkey earthquake was no surprise. *GSA Today*. 10 (1).
- Reilinger RE, McClusky SC, Oral MB, King RW, Toksoz, MN, Barka AA, Kinik I, Lenk O, Sanli I (1997) Global Positioning System measurements of present-day crustal movements in the Arabia-Africa-Eurasia plate collision zone. *J. Geophys. Res. Solid Earth*. <https://doi:10.1029/96jb03736>
- Reiter, L. 1990. "Earthquake Hazard Analysis", Columbia University Press, New York, 254 s.
- Rix G.J., Hebelers G.L., Orozco, M.C. (2002) Near surface vs profiling in the New Madrid Seismic Zone using surface wave methods. *Seismological Research Letters*, 73(3), pp. 380-392
- Rodríguez-Marek A, Bray JD, Abrahamson NA (2001) An empirical geotechnical seismic site response procedure. *Earthq. Spectra* 17: 65–87. <https://doi:10.1193/1.1586167>
- Rogers, A.M., Tinsley, J.C. and Borchardt, R.D., (1985) “Predicting relative ground response”. In: J.I. Ziony (Editor), *Evaluating Earthquake Hazards in the Los Angeles Region*. US Geol. Surv. Prof. Pap., 1360: 221-248.
- Rogers, A.M., Borchardt, R.D., Covington, P.A. and Perkins, D.M., (1984) “A comparative ground response study near Los Angeles using recordings of Nevada nuclear tests and the 1971 San Fernando earthquake”. *Bull. Seismol. Soc. Am.*, 74: 1925-1949.
- Seed, H. B., Wong, R. T., Idriss, I. M., Tokimatsu, K. 1986. “Moduli and Damping Factors for Dynamic Analysis of Cohesionless Soils”, *J. of the Geotechnical Engineering Division, ASCE*, 112 (11), 1016-1032.

- Seligson CD (1970) Comments on High-Resolution Frequency-Wavenumber Spectrum Analysis. Proc. IEEE. <https://doi:10.1109/PROC.1970.7825>
- Schnabel, P. B. 1973. "Effects of Local Geology and Distance from Source on Earthquake Ground Motions", Ph.D. Thesis, University of Calif., Berkeley.
- Silva, W., Lee, K. 1987. "WES RASCAL Code for Synthesizing Earthquake Ground Motions, State-of-the-Art for Assessing Earthquake Hazards in the United States", Report 24, Miscellaneous Paper S-73-1, US Army Corps of Engineers, Vicksburg, Mississippi.
- Sitharam, T. G., Anbazhagan, P., 2008, "Seismic Microzonation: Principles, Practices and Experiments", EJGE Bouget08.
- Şimşek O, Dalgıç S (1997) Düzce Ovası killerinin konsolidasyon özellikleri ve jeolojik evrim ile ilişkisi. Geol. Bull. Turkey 40: 29–38.
- Somerville, P. G., Smith, N. F., Graves, R. W., and Abrahamson, N. A. (1997). "Modification of empirical strong ground motion attenuation relations to include the amplitude and duration effects of rupture directivity." Seismol. Res. Lett., 68 (1), 199–222
- Straub C, Kahle HG, Schindler C (1997) GPS and geologic estimates of the tectonic activity in the Marmara Sea region, NW Anatolia. J. Geophys. Res. B Solid Earth. <https://doi:10.1029/97jb02563>
- Takahashi T (2004) International society for the rock mechanics commission on application of geophysics to rock engineering suggesting methods for land geophysics in rock engineering. Int. J. Rock Mech. Min. Sci. 41: 885–914.
- Tucker, B.E. and King, J.L., (1984) "Dependence of sediment- filled valley response on the input amplitude and the valley properties". Bull. Seismol. Soc. Am., 74: 153-165.

- Taymaz T (2000) Seismotectonics of the Marmara Region: Source Characteristics of 1999 Gölcük-Sapanca-Düzce Earthquakes, in: Proceedings of ITU-IAHS, International Conference On The Kocaeli Earthquake 17 August 1999, 2–5 December 1999. Istanbul, pp. 55–78.
- Telford WM, Geldart LP, Sheriff, RE, Keys DA (1976) Applied Geophysics, 1st Editio. ed. Cambridge University Press, New York.
- Tokimatsu K. (1995) Geotechnical Site Characteriza- tion using Surface Waves. Proceedings, First Inter- national Conference on Earthquake Geotechni- cal Engineering, IS-Tokyo '95, Tokyo, Balkema, Rotterdam, pp. 1333-1368
- Uebayashi H, Kawabe H, Kamae K (2012) Reproduction of microseism H/V spectral features using a three-dimensional complex topographical model of the sediment-bedrock interface in the Osaka sedimentary basin. Geophys. J. Int. 189:1060–1074. <https://doi.org/10.1111/j.1365-246X.2012.05408.x>
- Umutlu N, Koketsu K, Milkereit C (2004) The rupture process during the 1999 Düzce, Turkey, earthquake from joint inversion of teleseismic and strong-motion data. Tectonophysics; 391: 315–24.
- Utkucu M, Nalbant SS, McCloskey J, Steacy S, Alptekin Ö (2003) Slip distribution and stress changes associated with the 1999 November 12, Düzce (Turkey) earthquake ($M_w = 7.1$). Geophys. J. Int. <https://doi.org/10.1046/j.1365-246X.2003.01904.x>
- Vucetic, M., Dobry, R. 1991. "Effect of Soil Plasticity on Cyclic Response", J. of the Geotechnical Engineering Division, ASCE, 111 (1), 89-107.
- Wallace, R. M., ROLLINS K.M. 1996. "Amplification of Earthquake Motions in Great Salt Lake Valley due to Deep Basin Shape and Shallow Soil Stratigraphy", Procs. 11th World Conf. on Earthquake Engineering, Acapulco, Mexico, Elsevier, Paper No. 897

- Wang M, Hubbard J, Plesch A, Shaw JH, Wang L (2016) Three-dimensional seismic velocity structure in the Sichuan basin, China. *J. Geophys. Res. Solid Earth* 121:1007–1022. <https://doi:10.1002/2015JB012644>
- Wells, D. L.; Coppersmith, K. J. 1994. "New Empirical Relationships among Magnitude, Rupture Length, Rupture Width, Rupture Area, and Surface Displacement", *Bulletin of the Seismological Society of America*, 84, 974-1002.
- Wills C.J, Gutierrez C.I, Perez F.G, Branum D.M (2015) A next generation Vs30 map for California based on geology and topography. *Bull. Seismol. Soc. Am.* 105:3083–3091. <https://doi:10.1785/0120150105>
- Wills C.J, Petersen M, Bryant W.A, Reichle M, Saucedo G.J, Tan S, Taylor G, Treiman J (2000) A site-conditions map for California based on geology and shear-wave velocity. *Bull. Seismol. Soc. Am.* 90:187–208. <https://doi:10.1785/0120000503>
- Yoon S., Rix G.J. (2004) Combined active-passive surface wave measurements for near surface site characterization. *SAGEEP 2004*, San Antonio, USA, pp. 1556-1564.

APPENDICES

A. Geotechnical Boring Data and Deep Engineering Geological Boring Data

Some of the geotechnical boring and deep boring data are presented herein.

Proje Adı : GÖLYAKA BELEDİYESİ İLAVE MEVZİİ İMAR PROJESİ		SONDAJ LOGU	
Proje Adresi : KUYUDUZU MAHALLESİ-GÖLYAKA-DÜZCE			
Başlangıç Tarihi : 17.02.2008			
Bitiş Tarihi : 17.02.2008			
Sondaj Derinliği : 9,50 M.		Sayfa No : 1	
Yeraltı Su Seviyesi : 2,45 M.		Sondaj No : 2	
Pafta : -	Koordinat	Sondaj Tipi : Rotary	
Ada : -	X	Sondör : S.Albayrak	
Parsel : -	Y	Kontrol Müh : Olcay ÖZFIRAT	

Derinlik	Manevra Boyu	Numune Cinsi	Standart Penetrasyon Deneyi				Litoloji	Açıklamalar
			Darbe Sayısı			Grafik		
			15	30	45			
1								NEBATİ TOPRAK
2	1,50 - 1,95	SPT No	5	5	6	11		az çakıllı kumlu siltli kil CL
3	2,50 - 3,00	UD-1	ALINMADI					
4	3,00 - 3,45	SPT - 1	7	9	10	19		az çakıllı kumlu siltli kil CL
5	4,50 - 4,95	SPT-2	9	11	13	24		az çakıllı kumlu siltli kil CL
6	6,00 - 6,45	SPT - 3	10	14	17	31		az çakıllı kumlu siltli kil CL
7	7,50 - 7,95	SPT - 4	13	17	21	38		az çakıllı kumlu siltli kil CL
8	9,00 - 9,45	SPT - 5	17	21	28	49		az çakıllı kumlu siltli kil CL
9								
10								
11	10,50-10,95	SPT-6						
12								
13	12,00-12,45	SPT-7						KUYU SONU 9,50 M.
14	13,50-13,95							
15	14,50 - 14,95							

Dayanıklılık		Ayrıştırma		İnce Tanerli (Kohenzonuz)		Gri Tanerli (Kohenzonuz)	
Dayanıklı	1. Zayıf	1. Zayıf	N = 0-2 Çok Yumuşak	N = 0-2	Çok Güçsüz		
Orta Dayanıklı	2. Açığışık	2. Açığışık	N = 3-4 Yumuşak	N = 3-4	Güçsüz		
Orta Zayıf	3. O.D. Açığışık	3. O.D. Açığışık	N = 5-8 Orta Katı	N = 5-8	Orta Güçsüz		
Zayıf	4. Çok Açığışık	4. Çok Açığışık	N = 9-15 Katı	N = 9-15	Sarı		
Çok Zayıf	5. Tutarlı Açığışık	5. Tutarlı Açığışık	N = 16-30 Çok Katı	N = 16-30	Çok Güçsüz		
			N = 31-50 Sert	N = 31-50	Güçsüz		

Oranlık		Kaya Kalitesi		Kırıllık	
1-4	P _{0,4} < 4	P _{0,4} < 25	Çok Zayıf	1-1	Seyrek
5-15	4 < P _{0,4} ≤ 15	25 < P _{0,4} ≤ 50	Zayıf	1-2	Orta Seyrek
16-25	16 < P _{0,4} ≤ 25	50 < P _{0,4} ≤ 75	Orta	2-3	Sık
26-35	26 < P _{0,4} ≤ 35	75 < P _{0,4} ≤ 100	Güçlü	3-4	Çok Sık
36-45	36 < P _{0,4} ≤ 45	100 < P _{0,4} ≤ 150	Çok Güçlü	4-5	Yığın

SONDAJ MÜHENDİSİ	İMZA	TARİH
------------------	------	-------

Proje Adı : GÖLYAKA BELEDİYESİ İLAVE MEVZİL İMAR PROJESİ		SONDAJ LOGU	
Proje Adresi : KUYUDUZU MAHALLESİ-GÖLYAKA- DÜZCE			
Başlangıç Tarihi : 18.02.2008			
Bitiş Tarihi : 18.02.2008		Sayfa No : 1	
Sondaj Derinliği : 8.00 M.		Sondaj No : 3	
Yeraltı Su Seviyesi : 3.15 M.		Sondaj Tipi : Rotary	
Pafta : -	Koordinat	Sondör : S.Albayrak	
Ada : -	X	Kontrol Müh : Olca ÖZFIRAT	
Parsel : -	Y		

Derinlik	Manevra Boyu	Numune Cinsi	Standart Penetrasyon Deneyi				Grafik	Litoloji	Açıklamalar
			Darbe Sayısı						
			15	30	45	N _{ort}			
1								NEBATI TOPRAK	
2	1,50 - 1,95	SPT No	5	7	7	14		az çakıllı kumlu siltli kil CL	
3	2,50 - 3,00	UD-1	ALINMADI						
4	3,00 - 3,45	SPT - 1	8	8	10	18		az çakıllı kumlu siltli kil CL	
5	4,50 - 4,95	SPT-2	11	13	17	30		az çakıllı kumlu siltli kil CL	
6	6,00 - 6,45	SPT - 3	16	21	23	44			
7	7,50 - 7,95	SPT - 4	22	29	33	62			
9	9,00 - 9,45	SPT - 5							
10									
11	10,50-10,95	SPT-6							
	12,00-12,45	SPT-7							
14	13,50-13,95								
15	14,50 - 14,95								

Dayanıklılık		Ayrıştırma		İnce Tanerli (Kohenzonuz)		İri Tanerli (Kohenzonuz)	
1) Dayanıklı	1) Taze	1) Taze	N. 0-2 Çok Yumuşak	N. 0-4 Çok Geyrek			
2) Orta Dayanıklı	2) Ayrıştırma	2) Ayrıştırma	N. 3-4 Yumuşak	N. 5-10 Geyrek			
3) Orta Zayıf	3) O.D. Ayrıştırma	3) O.D. Ayrıştırma	N. 5-8 Orta Katı	N. 11-20 Orta Sık			
4) Zayıf	4) Çok Ayrıştırma	4) Çok Ayrıştırma	N. 9-13 Katı	N. 21-30 Sık			
5) Çok Zayıf	5) Tam Ayrıştırma	5) Tam Ayrıştırma	N. 14-30 Çok Katı	N. 31-50 Çok Sık			
			N. > 30 Sert				

Oranlık		Kaya Kalitesi		Kırıllık	
f _{cd} 10-15	Pek Az	f _{cd} 5-10	Pek Az	f _{cd} 10-15	Çok Zayıf
f _{cd} 15-20	Az	f _{cd} 20-25	Az	f _{cd} 20-25	Zayıf
f _{cd} 25-30	Orta	f _{cd} 30-35	Orta	f _{cd} 30-35	Orta
f _{cd} 35-40	Orta	f _{cd} 40-45	Orta	f _{cd} 40-45	Orta
f _{cd} 45-50	Orta	f _{cd} 50-55	Orta	f _{cd} 50-55	Orta
f _{cd} 55-60	Orta	f _{cd} 60-65	Orta	f _{cd} 60-65	Orta
f _{cd} 65-70	Orta	f _{cd} 70-75	Orta	f _{cd} 70-75	Orta
f _{cd} 75-80	Orta	f _{cd} 80-85	Orta	f _{cd} 80-85	Orta
f _{cd} 85-90	Orta	f _{cd} 90-95	Orta	f _{cd} 90-95	Orta
f _{cd} 95-100	Orta	f _{cd} 100-105	Orta	f _{cd} 100-105	Orta
f _{cd} 105-110	Orta	f _{cd} 110-115	Orta	f _{cd} 110-115	Orta
f _{cd} 115-120	Orta	f _{cd} 120-125	Orta	f _{cd} 120-125	Orta
f _{cd} 125-130	Orta	f _{cd} 130-135	Orta	f _{cd} 130-135	Orta
f _{cd} 135-140	Orta	f _{cd} 140-145	Orta	f _{cd} 140-145	Orta
f _{cd} 145-150	Orta	f _{cd} 150-155	Orta	f _{cd} 150-155	Orta
f _{cd} 155-160	Orta	f _{cd} 160-165	Orta	f _{cd} 160-165	Orta
f _{cd} 165-170	Orta	f _{cd} 170-175	Orta	f _{cd} 170-175	Orta
f _{cd} 175-180	Orta	f _{cd} 180-185	Orta	f _{cd} 180-185	Orta
f _{cd} 185-190	Orta	f _{cd} 190-195	Orta	f _{cd} 190-195	Orta
f _{cd} 195-200	Orta	f _{cd} 200-205	Orta	f _{cd} 200-205	Orta
f _{cd} 205-210	Orta	f _{cd} 210-215	Orta	f _{cd} 210-215	Orta
f _{cd} 215-220	Orta	f _{cd} 220-225	Orta	f _{cd} 220-225	Orta
f _{cd} 225-230	Orta	f _{cd} 230-235	Orta	f _{cd} 230-235	Orta
f _{cd} 235-240	Orta	f _{cd} 240-245	Orta	f _{cd} 240-245	Orta
f _{cd} 245-250	Orta	f _{cd} 250-255	Orta	f _{cd} 250-255	Orta
f _{cd} 255-260	Orta	f _{cd} 260-265	Orta	f _{cd} 260-265	Orta
f _{cd} 265-270	Orta	f _{cd} 270-275	Orta	f _{cd} 270-275	Orta
f _{cd} 275-280	Orta	f _{cd} 280-285	Orta	f _{cd} 280-285	Orta
f _{cd} 285-290	Orta	f _{cd} 290-295	Orta	f _{cd} 290-295	Orta
f _{cd} 295-300	Orta	f _{cd} 300-305	Orta	f _{cd} 300-305	Orta
f _{cd} 305-310	Orta	f _{cd} 310-315	Orta	f _{cd} 310-315	Orta
f _{cd} 315-320	Orta	f _{cd} 320-325	Orta	f _{cd} 320-325	Orta
f _{cd} 325-330	Orta	f _{cd} 330-335	Orta	f _{cd} 330-335	Orta
f _{cd} 335-340	Orta	f _{cd} 340-345	Orta	f _{cd} 340-345	Orta
f _{cd} 345-350	Orta	f _{cd} 350-355	Orta	f _{cd} 350-355	Orta
f _{cd} 355-360	Orta	f _{cd} 360-365	Orta	f _{cd} 360-365	Orta
f _{cd} 365-370	Orta	f _{cd} 370-375	Orta	f _{cd} 370-375	Orta
f _{cd} 375-380	Orta	f _{cd} 380-385	Orta	f _{cd} 380-385	Orta
f _{cd} 385-390	Orta	f _{cd} 390-395	Orta	f _{cd} 390-395	Orta
f _{cd} 395-400	Orta	f _{cd} 400-405	Orta	f _{cd} 400-405	Orta
f _{cd} 405-410	Orta	f _{cd} 410-415	Orta	f _{cd} 410-415	Orta
f _{cd} 415-420	Orta	f _{cd} 420-425	Orta	f _{cd} 420-425	Orta
f _{cd} 425-430	Orta	f _{cd} 430-435	Orta	f _{cd} 430-435	Orta
f _{cd} 435-440	Orta	f _{cd} 440-445	Orta	f _{cd} 440-445	Orta
f _{cd} 445-450	Orta	f _{cd} 450-455	Orta	f _{cd} 450-455	Orta
f _{cd} 455-460	Orta	f _{cd} 460-465	Orta	f _{cd} 460-465	Orta
f _{cd} 465-470	Orta	f _{cd} 470-475	Orta	f _{cd} 470-475	Orta
f _{cd} 475-480	Orta	f _{cd} 480-485	Orta	f _{cd} 480-485	Orta
f _{cd} 485-490	Orta	f _{cd} 490-495	Orta	f _{cd} 490-495	Orta
f _{cd} 495-500	Orta	f _{cd} 500-505	Orta	f _{cd} 500-505	Orta
f _{cd} 505-510	Orta	f _{cd} 510-515	Orta	f _{cd} 510-515	Orta
f _{cd} 515-520	Orta	f _{cd} 520-525	Orta	f _{cd} 520-525	Orta
f _{cd} 525-530	Orta	f _{cd} 530-535	Orta	f _{cd} 530-535	Orta
f _{cd} 535-540	Orta	f _{cd} 540-545	Orta	f _{cd} 540-545	Orta
f _{cd} 545-550	Orta	f _{cd} 550-555	Orta	f _{cd} 550-555	Orta
f _{cd} 555-560	Orta	f _{cd} 560-565	Orta	f _{cd} 560-565	Orta
f _{cd} 565-570	Orta	f _{cd} 570-575	Orta	f _{cd} 570-575	Orta
f _{cd} 575-580	Orta	f _{cd} 580-585	Orta	f _{cd} 580-585	Orta
f _{cd} 585-590	Orta	f _{cd} 590-595	Orta	f _{cd} 590-595	Orta
f _{cd} 595-600	Orta	f _{cd} 600-605	Orta	f _{cd} 600-605	Orta
f _{cd} 605-610	Orta	f _{cd} 610-615	Orta	f _{cd} 610-615	Orta
f _{cd} 615-620	Orta	f _{cd} 620-625	Orta	f _{cd} 620-625	Orta
f _{cd} 625-630	Orta	f _{cd} 630-635	Orta	f _{cd} 630-635	Orta
f _{cd} 635-640	Orta	f _{cd} 640-645	Orta	f _{cd} 640-645	Orta
f _{cd} 645-650	Orta	f _{cd} 650-655	Orta	f _{cd} 650-655	Orta
f _{cd} 655-660	Orta	f _{cd} 660-665	Orta	f _{cd} 660-665	Orta
f _{cd} 665-670	Orta	f _{cd} 670-675	Orta	f _{cd} 670-675	Orta
f _{cd} 675-680	Orta	f _{cd} 680-685	Orta	f _{cd} 680-685	Orta
f _{cd} 685-690	Orta	f _{cd} 690-695	Orta	f _{cd} 690-695	Orta
f _{cd} 695-700	Orta	f _{cd} 700-705	Orta	f _{cd} 700-705	Orta
f _{cd} 705-710	Orta	f _{cd} 710-715	Orta	f _{cd} 710-715	Orta
f _{cd} 715-720	Orta	f _{cd} 720-725	Orta	f _{cd} 720-725	Orta
f _{cd} 725-730	Orta	f _{cd} 730-735	Orta	f _{cd} 730-735	Orta
f _{cd} 735-740	Orta	f _{cd} 740-745	Orta	f _{cd} 740-745	Orta
f _{cd} 745-750	Orta	f _{cd} 750-755	Orta	f _{cd} 750-755	Orta
f _{cd} 755-760	Orta	f _{cd} 760-765	Orta	f _{cd} 760-765	Orta
f _{cd} 765-770	Orta	f _{cd} 770-775	Orta	f _{cd} 770-775	Orta
f _{cd} 775-780	Orta	f _{cd} 780-785	Orta	f _{cd} 780-785	Orta
f _{cd} 785-790	Orta	f _{cd} 790-795	Orta	f _{cd} 790-795	Orta
f _{cd} 795-800	Orta	f _{cd} 800-805	Orta	f _{cd} 800-805	Orta
f _{cd} 805-810	Orta	f _{cd} 810-815	Orta	f _{cd} 810-815	Orta
f _{cd} 815-820	Orta	f _{cd} 820-825	Orta	f _{cd} 820-825	Orta
f _{cd} 825-830	Orta	f _{cd} 830-835	Orta	f _{cd} 830-835	Orta
f _{cd} 835-840	Orta	f _{cd} 840-845	Orta	f _{cd} 840-845	Orta
f _{cd} 845-850	Orta	f _{cd} 850-855	Orta	f _{cd} 850-855	Orta
f _{cd} 855-860	Orta	f _{cd} 860-865	Orta	f _{cd} 860-865	Orta
f _{cd} 865-870	Orta	f _{cd} 870-875	Orta	f _{cd} 870-875	Orta
f _{cd} 875-880	Orta	f _{cd} 880-885	Orta	f _{cd} 880-885	Orta
f _{cd} 885-890	Orta	f _{cd} 890-895	Orta	f _{cd} 890-895	Orta
f _{cd} 895-900	Orta	f _{cd} 900-905	Orta	f _{cd} 900-905	Orta
f _{cd} 905-910	Orta	f _{cd} 910-915	Orta	f _{cd} 910-915	Orta
f _{cd} 915-920	Orta	f _{cd} 920-925	Orta	f _{cd} 920-925	Orta
f _{cd} 925-930	Orta	f _{cd} 930-935	Orta	f _{cd} 930-935	Orta
f _{cd} 935-940	Orta	f _{cd} 940-945	Orta	f _{cd} 940-945	Orta
f _{cd} 945-950	Orta	f _{cd} 950-955	Orta	f _{cd} 950-955	Orta
f _{cd} 955-960	Orta	f _{cd} 960-965	Orta	f _{cd} 960-965	Orta
f _{cd} 965-970	Orta	f _{cd} 970-975	Orta	f _{cd} 970-975	Orta
f _{cd} 975-980	Orta	f _{cd} 980-985	Orta	f _{cd} 980-985	Orta
f _{cd} 985-990	Orta	f _{cd} 990-995	Orta	f _{cd} 990-995	Orta
f _{cd} 995-1000	Orta	f _{cd} 1000-1005	Orta	f _{cd} 1000-1005	Orta

SONDAJ MÜHENDİSİ		İMZA	TARİH

		Proje Adı : GÖLYAKA BELEDİYESİ İLAVE MEVZII İMAR PROJESİ				SONDAJ LOGU	
		Proje Adresi : KUYUDUZU MAHALLESİ-GÖLYAKA-DÜZCE					
		Başlangıç Tarihi : 18.02.2008		Bitiş Tarihi : 18.02.2008			
		Sondaj Derinliği : 9.50 M.					
		Yeraltı Su Seviyesi : RASTLANILMADI.					
		Pafta : -		Kordinat		Sondaj No : 4	
		Ada : -		X		Sondaj Tipi : Rotary	
		Parsel : -		Y		Sondör : S.Albayrak	
						Kontrol Müh : Olcay ÖZFIRAT	

Derinlik	Manevra Boyu	Numune Cinsi	Standart Penetrasyon Deneyi				Litoloji	Açıklamalar
			Darbe Sayısı					
			15	30	45	N _{ort}		
1								
2	1,50 - 1,95	SPT No	6	8	8	16		az çakıllı kumlu siltli kil CL
3	2,50 - 3,00	UD-1	ALINDI					
4	3,00 - 3,45	SPT - 1	8	11	13	24		az çakıllı kumlu siltli kil CL
5	4,50 - 4,95	SPT-2	11	17	22	39		
6	6,00 - 6,45	SPT - 3	18	24	27	51		
7								
8	7,50 - 7,95	SPT - 4						
9								
10	9,00 - 9,45	SPT - 5						
11	10,50-10,95	SPT-6						
	12,00-12,45	SPT-7						
14	13,50-13,95							
15	14,50 - 14,95							

Dayanıklılık Dönme Orta Dönme Orta Zayıf Zayıf Çok Zayıf	Ayrışma 1 Taze 2 Ayrışmış 3 Orta Ayrışmış 4 Çok Ayrışmış 5 Tam Ayrışmış	İnce Tanerli (Kohenzonuz) N ₁ 0-2 Çök Yumak N ₂ 3-4 Yumak N ₃ 5-8 Orta Kırıntı N ₄ 9-15 Kırıntı N ₅ 16-50 Çok Kırıntı N ₆ 51-100 Silt	İri Tanerli (Kohenzonuz) N ₁ 0-4 Çök Gevrek N ₂ 5-10 Gevrek N ₃ 11-20 Orta Kırıntı N ₄ 21-40 Kırıntı N ₅ 41-100 Çok Kırıntı
Oranlık N ₁ 0-4 N ₂ 5-10 N ₃ 11-20 N ₄ 21-40 N ₅ 41-100	N ₁ 0-4 N ₂ 5-10 N ₃ 11-20 N ₄ 21-40 N ₅ 41-100	Kaya Kalitesi N ₁ 0-25 Çök Zayıf N ₂ 26-40 Zayıf N ₃ 41-50 Orta N ₄ 51-60 İyi N ₅ 61-100 Çok İyi	Kırıllık N ₁ 0-25 N ₂ 26-40 N ₃ 41-50 N ₄ 51-60 N ₅ 61-100

	SONDAJ MÜHENDİSİ	İMZA	TARİH
--	------------------	------	-------

Proje Adı : GÖLYAKA BELEDİYESİ İLAVE MEVZİLİ İMAR PROJESİ		Proje Adresi : KUYUDUZU MAHALLESİ-GÖLYAKA- DÜZCE	
Başlangıç Tarihi : 19.02.2008		Bitiş Tarihi : 19.02.2008	
Sondaj Derinliği : 8.00 M.		Sayfa No : 1	
Yeraltı Su Seviyesi : RASTLANILMADI		Sondaj No : 5	
Pafta : -		Koordinat	
Ada : -		X	
Parsel : -		Y	
Sondaj Tipi : Rotary		Sondör : S.Albayrak	
Kontrol Müh : Olcay ÖZFIRAT			

Derinlik	Manevra Boyu	Numune Cinsi	Standart Penetrasyon Deneyi				Grafik	Litoloji	Açıklamalar
			Darbe Sayısı						
			15	30	45	N _{ORT}			
1								NEBATİ TOPRAK	
2	1,50 - 1,95	SPT No	5	5	5	10		az çakıllı kumlu siltli kil CL	
3	2,50 - 3,00	UD-1	ALINMADI					az çakıllı kumlu siltli kil CL	
4	3,00 - 3,45	SPT - 1	7	7	9	16		az çakıllı kumlu siltli kil CL	
5	4,50 - 4,95	SPT-2	9	11	14	25		az çakıllı kumlu siltli kil CL	
6	6,00 - 6,45	SPT - 3	11	14	17	31		KUYU SONU 8.00 M.	
7	7,50 - 7,95	SPT - 4	11	17	21	38			
8	9,00 - 9,45	SPT - 5							
9	10,50-10,95	SPT-6							
10	12,00-12,45	SPT-7							
11	13,50-13,95								
12	14,50 - 14,95								
13									
14									
15									

Dayanıklılık		Ayrılma		İmre Tanımlı (Kahenyonlu)		İmre Tanımlı (Kahenyonlu)	
Durumlu	1. Taz	1. Taz	1. Taz	N = 0-2	Çok Yumuşak	N = 0-2	Çok Güçsüz
Orta Durumlu	2. Ayrılma	2. Ayrılma	2. Ayrılma	N = 3-4	Yumuşak	N = 3-4	Güçsüz
Orta Zayıf	3. O.D. Ayrılma	3. O.D. Ayrılma	3. O.D. Ayrılma	N = 5-8	Orta Katı	N = 5-8	Orta Güçsüz
Zayıf	4. Çok Ayrılma	4. Çok Ayrılma	4. Çok Ayrılma	N = 9-13	Katı	N = 9-13	Güçsüz
Çok Zayıf	5. Tam Ayrılma	5. Tam Ayrılma	5. Tam Ayrılma	N = 14-30	Çok Katı	N = 14-30	Güçsüz
				N = 30-50	Sert	N = 30-50	Güçsüz

Oranlık		Kaya Kalitesi		Kırıllık	
Pek Az	1-5%	Pek Az	1-5%	1-5%	Sevrek
Az	6-20%	Az	6-20%	6-20%	Orta Sevrek
Orta	21-40%	Orta	21-40%	21-40%	Güçsüz
Çok	41-60%	Çok	41-60%	41-60%	Güçsüz
Çok Çok	61-100%	Çok Çok	61-100%	61-100%	Güçsüz

SONDAJ MÜHENDİSİ	İMZA	TARİH

Proje Adı : GÖLYAKA BELEDİYESİ İLAVE MEVZİİ İMAR PROJESİ		SONDAJ LOGU	
Proje Adresi : KUYUDUZU MAHALLESİ-GÖLYAKA- DÜZCE			
Başlangıç Tarihi : 19.02.2008			
Bitiş Tarihi : 19.02.2008			
Sondaj Derinliği : 9.50 M.		Sayfa No : 1	
Yeraltı Su Seviyesi : RASTLANILMADI		Sondaj No : 6	
Pafta : -	Koordinat	Sondaj Tipi : Rotary	
Ada : -	X	Sondör : S.Albayrak	
Parsel : -	Y	Kontrol Müh : Olcay ÖZFIRAT	

Derinlik	Manevra Boyu	Numune Cinsi	Standart Penetrasyon Deneyi				Grafik	Litoloji	Açıklamalar
			Darbe Sayısı						
			15	30	45	N _{ort}			
1									NEBATİ TOPRAK
2	1,50 - 1,95	SPT No	6	8	9	17			az çakıllı kumlu siltli kil CL
3	2,50 - 3,00	UD-1	ALINMADI						
4	3,00 - 3,45	SPT - 1	11	14	17	31			az çakıllı kumlu siltli kil CL
5	4,50 - 4,95	SPT-2	14	21	27	48			az çakıllı kumlu siltli kil CL
6	6,00 - 6,45	SPT - 3	18	26	31	57			az çakıllı kumlu siltli kil CL
7									
8	7,50 - 7,95	SPT - 4	21	28	34	62			az çakıllı kumlu siltli kil CL
9	9,00 - 9,45	SPT - 5	27	33	37	70			az çakıllı kumlu siltli kil CL
10									
11	10,50-10,95	SPT-6							
12	12,00-12,45	SPT-7							
13									
14	13,50-13,95								
15	14,50 - 14,95								

Dayanıklılık		Ayrıştırma		İnce Taneli (Kühnyonoz)		İri Taneli (Kühnyonoz)	
1	Dayanıklı	1	Taş	N : 0-2	Çok Yumuşak	N : 0-4	Çok Zayıf
2	Orta Dayanıklı	2	Ayrıştırma	N : 3-4	Yumuşak	N : 5-10	Zayıf
3	Orta Zayıf	3	Orta Dayanıklı	N : 5-8	Orta Katı	N : 11-20	Orta Sağ
4	Zayıf	4	Çok Ayrıştırma	N : 9-13	Katı	N : 21-30	Sa
5	Çok Zayıf	5	Taş Ayrıştırma	N : 14-30	Çok Katı	N : 31-50	Çok Sağ

Oranlık		Kaya Kalitesi		Kırıllık	
f _{cd} 105	Pek Az	f _{cd} 4-7	Pek Az	f _{cd} 10-25	Çok Zayıf
f _{cd} 4-15	Az	f _{cd} 5-20	Az	f _{cd} 25-50	Zayıf
f _{cd} 15-25	Çok	f _{cd} 20-50	Çok	f _{cd} 50-75	Orta
f _{cd} 25	Yük	f _{cd} 75-100	Çok	f _{cd} 75-100	İyi
		f _{cd} 100-150	Çok	f _{cd} 100-150	Çok İyi

SONDAJ MÜHENDİSİ		İMZA	TARİH

Proje Adı : GÖLYAKA BELEDİYESİ İLAVE MEVZİİ İMAR PROJESİ		SONDAJ LOGU	
Proje Adresi : KUYUDUZU MAHALLESİ-GÖLYAKA-DÜZCE			
Başlangıç Tarihi : 20.02.2008			
Bitiş Tarihi : 20.02.2008			
Sondaj Derinliği : 9.50 M.		Sayfa No : 1	
Yeraltı Su Seviyesi : RASTLANILMADI		Sondaj No : 7	
Pafta : -	Koordinat	Sondaj Tipi : Rotary	
Ada : -	X	Sondör : S.Albayrak	
Parsel : -	Y	Kontrol Müh : Olcay ÖZFIRAT	

Derinlik	Manevra Boyu	Numune Cinsi	Standart Penetrasyon Deneyi				Litoloji	Açıklamalar		
			Darbe Sayısı			Grafik				
			15	30	45				N ₆₀	
1								NEBATI TOPRAK		
2	1,50 - 1,95	SPT No	7	7	9	16		az çakıllı kumlu siltli kil CL		
3	2,50 - 3,00	UD-1	ALINMADI					az çakıllı kumlu siltli kil CL		
4	3,00 - 3,45	SPT - 1	11	11	14	25		az çakıllı kumlu siltli kil CL		
5	4,50 - 4,95	SPT-2	13	17	21	38		az çakıllı kumlu siltli kil CL		
6	6,00 - 6,45	SPT - 3	17	23	27	50		az çakıllı kumlu siltli kil CL		
7	7,50 - 7,95	SPT - 4	21	28	34	62		az çakıllı kumlu siltli kil CL		
8	9,00 - 9,45	SPT - 5	24	31	37	68		az çakıllı kumlu siltli kil CL		
9	10,50-10,95	SPT-6						KUYU SONU 9.50 M.		
10										
11	12,00-12,45	SPT-7								
12										
13	13,50-13,95									
14	14,50 - 14,95									
Dayanıklılık			Ayrışma			İnce Tanlı (Kökenyonsuz)		İri Tanlı (Kökenyonsuz)		
1	Dacamlı		1	Taze		N ₁₀ = 2		Cok Yumuşak	N ₁₀ = 4	Cok Gerek
2	Orta Dacamlı		2	Ayrışma		N ₁₀ = 4	Yumuşak	N ₁₀ = 4	Gerek	
3	Orta Zayıf		3	1/10 Ayrışma		N ₁₀ = 8	Orta Sık	N ₁₀ = 8	Orta Sık	
4	Zayıf		4	Cok Ayrışma		N ₁₀ = 15	Kıvrık	N ₁₀ = 15	Sık	
5	Cok Zayıf		5	Tam Ayrışma		N ₁₀ = 30	Cok Kıvrık	N ₁₀ = 30	Cok Sık	
Oranlık			Kaya Kalitesi			Kırıllık		Kırıllık		
N ₁₀ < 4	Pek Az	% 4 -	Pek Az			N ₁₀ < 25	Cok Zayıf	N ₁₀ < 25	Seyrek	
N ₁₀ 4-15	Az	% 4-20	Az			N ₁₀ 25-50	Zayıf	N ₁₀ 25-50	Orta Seyrek	
N ₁₀ 15-25	Cok	% 20-30	Cok			N ₁₀ 50-75	Orta	N ₁₀ 50-75	Sık	
N ₁₀ > 25	Ve	% 30-80	Ve			N ₁₀ > 75	Sık	N ₁₀ > 75	Cok Sık	
						SONDAJ MÜHENDİSİ		İMZA		
								TARİH		

Proje Adı : GÖLYAKA BELEDİYESİ İLAVE MEVZII İMAR PROJESİ		SONDAJ LOGU	
Proje Adresi : KUYUDUZU MAHALLESİ-GÖLYAKA-DÜZCE			
Başlangıç Tarihi : 20.02.2008			
Bitiş Tarihi : 20.02.2008			
Sondaj Derinliği : 8,00 M.		Sayfa No : 1	
Yeraltı Su Seviyesi : RASTLANILMADI.		Sondaj No : 8	
Pafta : -	Koordinat	Sondaj Tipi	Rotary
Ada : -	X	Sondör	S.Albayrak
Parsel : -	Y	Kontrol Müh	Olca ÖZFIRAT

Derinlik	Manevra Boyu	Numune Cinsi	Standart Penetrasyon Deneyi				Grafik	Litoloji	Açıklamalar
			Darbe Sayısı						
			15	30	45	Non			
1								NEBATI TOPRAK	
2	1,50 - 1,95	SPT No	6	7	7	14		az çakıllı kumlu siltli kil CL	
3	2,50 - 3,00	UD-1	ALINMADI						
4	3,00 - 3,45	SPT - 1	8	11	13	24		az çakıllı kumlu siltli kil CL	
5	4,50 - 4,95	SPT-2	11	14	17	31			
6	6,00 - 6,45	SPT - 3	17	21	24	45		az çakıllı kumlu siltli kil CL	
7									
8	7,50 - 7,95	SPT - 4	19	24	31	55			
9									
10	9,00 - 9,45	SPT - 5							
11	10,50-10,95	SPT-6							
12									
13	12,00-12,45	SPT-7						KUYU SONU 8.00 M.	
14	13,50-13,95								
15	14,50 - 14,95								

Dayanıklılık		Ayrılma		İnce Taneli (Kohesiyonlu)		İri Taneli (Kohesiyonsuz)	
Dayanıklılık	1. Tane	2. Ayrılma	3. O.D. Ayrılma	4. Çok Ayrılma	5. Tam Ayrılma	6. Çok Çökük	7. Çökük
Orta Dayanıklılık	2. Ayrılma	3. O.D. Ayrılma	4. Çok Ayrılma	5. Tam Ayrılma	6. Çok Çökük	7. Çökük	8. Çökük
Orta Zayıf	3. O.D. Ayrılma	4. Çok Ayrılma	5. Tam Ayrılma	6. Çok Çökük	7. Çökük	8. Çökük	9. Çökük
Zayıf	4. Çok Ayrılma	5. Tam Ayrılma	6. Çok Çökük	7. Çökük	8. Çökük	9. Çökük	10. Çökük
Çok Zayıf	5. Tam Ayrılma	6. Çok Çökük	7. Çökük	8. Çökük	9. Çökük	10. Çökük	11. Çökük

Oranlık		Kaya Kalitesi		Kırıllık	
Pek Az	% 5-10	Pek Az	% 10-25	Pek Az	% 1-5
Az	% 10-20	Az	% 25-50	Az	% 5-10
Orta	% 20-50	Orta	% 50-75	Orta	% 10-20
Çok	% 50-100	Çok	% 75-100	Çok	% 20-50

SONDAJ MÜHENDİSİ	İMZA	TARİH
------------------	------	-------

Kayseri'den: 01.12.15 Samsat Şube Baş Müh.

Kayseri'den: 01.12.15 Samsat Şube Baş Müh.

Key No :
Ref No :

Kayseri'den: 01.12.15 Samsat Şube Baş Müh.

Aktier	Verkauf (100)	100

D- Kıyma başı kırması

APPROVED	DATE	BY

A hand-drawn map of the E-Kaya area. It shows a river labeled 'Kaya' flowing from the top left towards the bottom right. Another river or path is labeled 'Kaya' and flows from the top right towards the bottom left. The area is divided into several sections by these lines. Labels include 'Kaya' (twice), 'Kaya' (once), and 'Kaya' (once). There are also some numbers and other markings.

[illegible]*T. Kunze* (ed.)

	1st floor	2nd floor	3rd floor	4th floor
Sit 5 (m)	-	-	-	-
On 3 (m)	-	-	-	-
Ventim floor	-	-	-	-
wooded (board)	-	-	-	-
Sit 5 (m)	-	-	-	-
On 3 (m)	-	-	-	-
Ventim floor	-	-	-	-

69.00-268.50

5. Yürütme	Arşiv No:	
	Ticari Tanıtı:	
	<u>III Formasyon Tanıtı</u>	

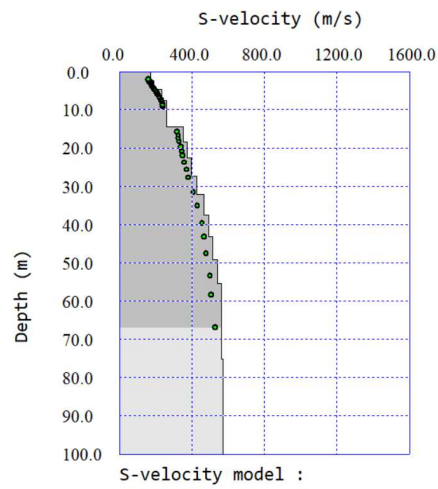
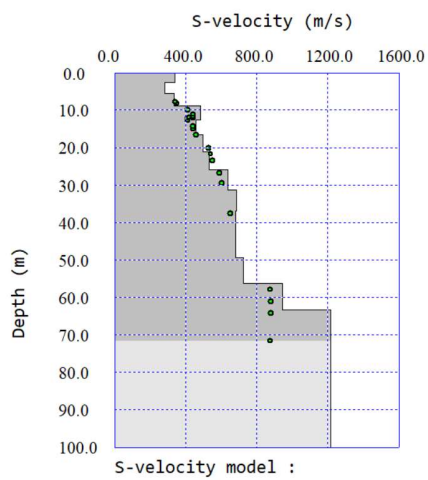
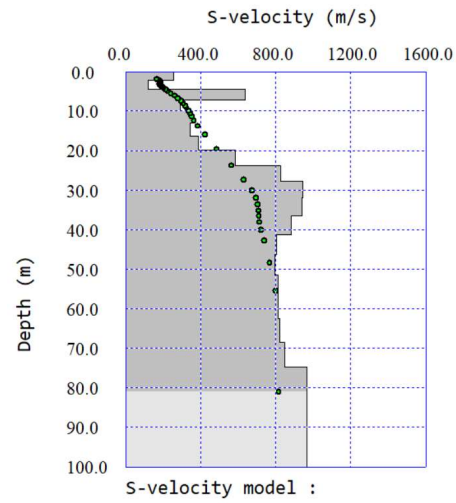
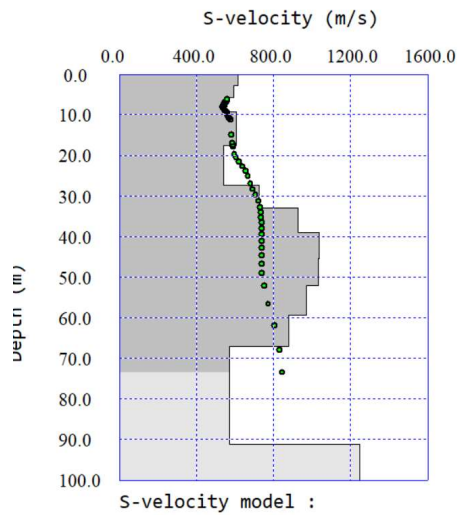
125-130 m. Kuzeydoğu, güneydoğu, güneybatı ve batı
5-7 m. Sığa.
7-10 m. Kilit: Kumsal, kaya, gri renkli.
10-15 m. Kumsal, kilit: Kaya, gri renkli, çam,
gökkuşak, pürüzlü, kumara, çam, kilit,
kaya, kilit, kumsal, kumsal.
20-30 m. Kilit: Kaya, gri renkli, plastik,
kaya, kilit.
30-40 m. Sığa.
40-45 m. Kumsal, kilit: Kaya, gri, çam,
kumsal, pürüzlü, kumara, çam, kilit.
60-65 m. Kilit: Kaya, gri renkli, plastik,
kaya, kilit.
65-125 m. Kumsal, kilit: Kaya, gri kumsal ve çam,
ve kilit 5-20 m. Kumsal, kilit, kumsal.
125-135 m. Kumsal, çam, ve kilit, pürüzlü,
kumsal, kilit, kumara, kumara, kumara, kumara.
135-150 m. Kilit, kumsal, kumara.
150-160, 50 m. Kumsal ve çam, kilit, pürüzlü,
kumsal, kumara, kumara, kumara, kumara.

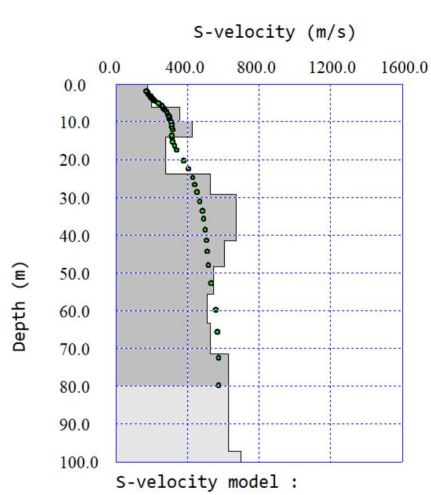
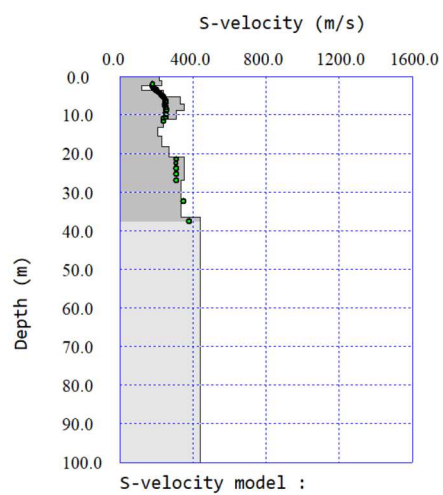
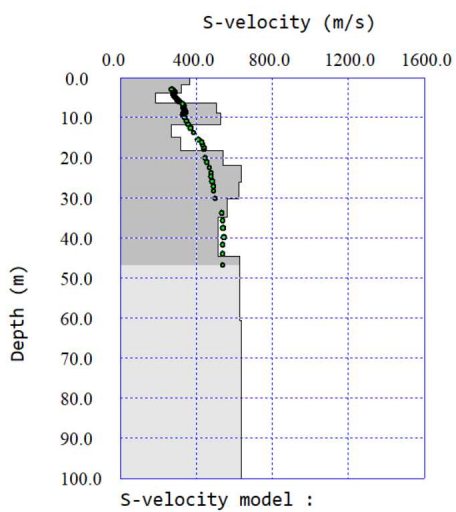
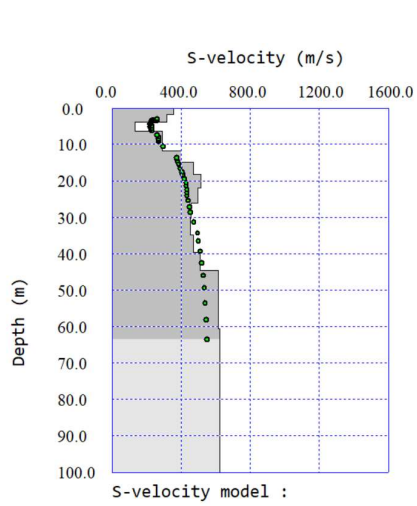
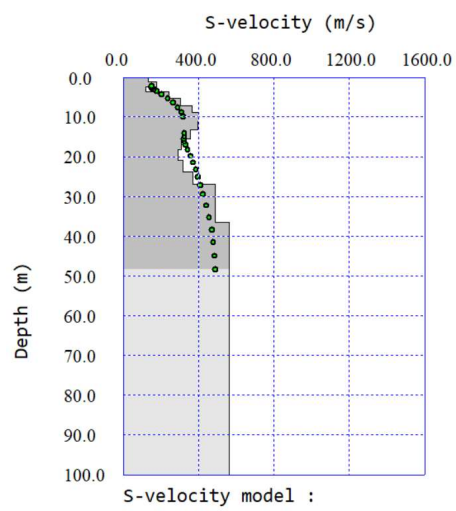
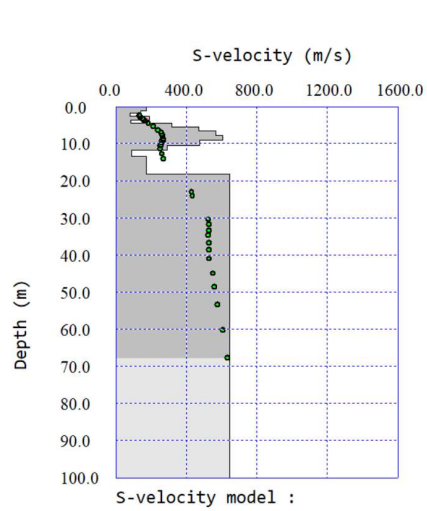
127

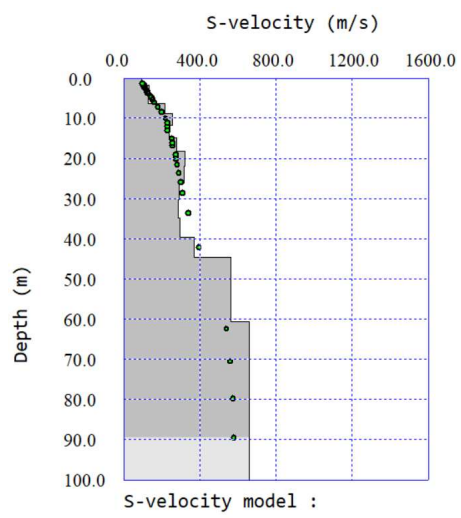
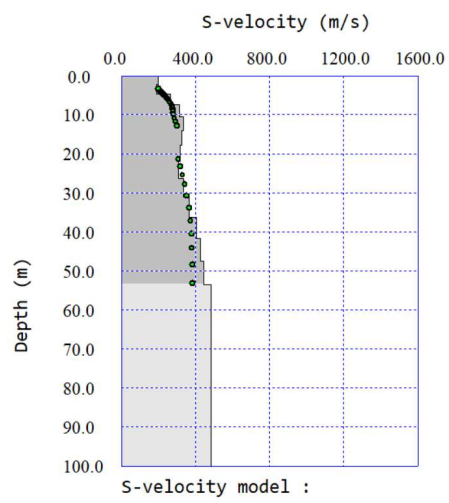
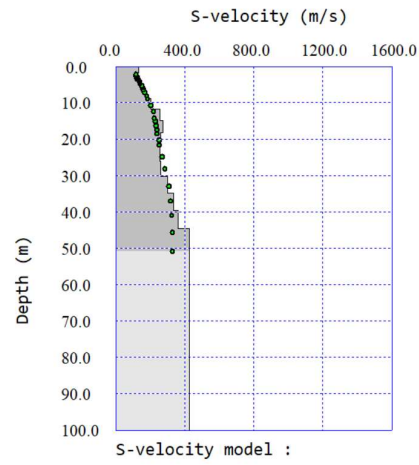
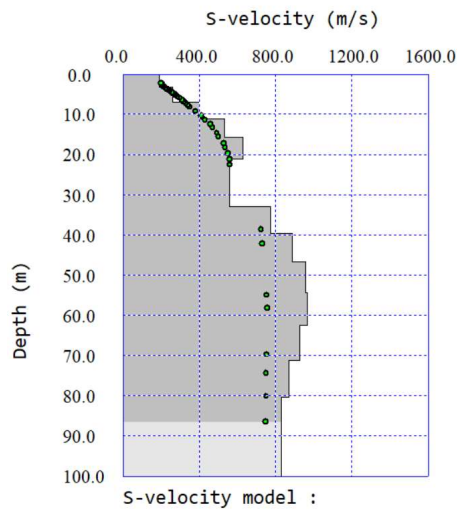
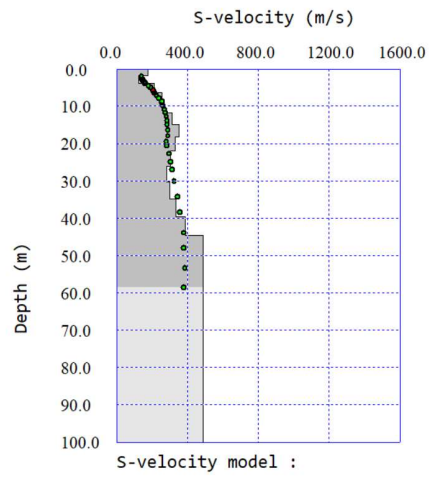
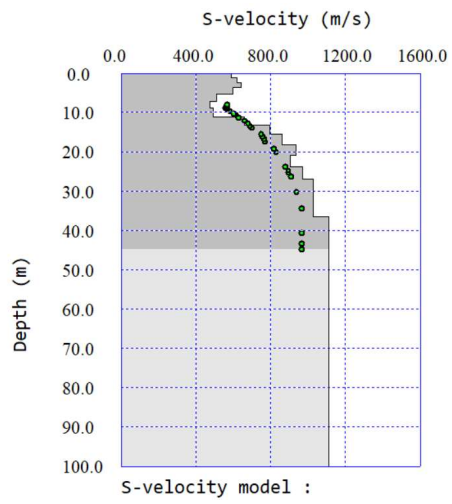
ÖZYAPICI MÜHENDİSLİK		Proje Adı: AKSU HES PROJESİ		SONDAJ LOGU					
Proje Adresi: AKSU KÖYÜ GÖLYAKA - DÜZCE		Başlangıç Tarihi: 08.03.2011		Sayfa No: 1					
Bitiş Tarihi: 08.03.2011		Sondaj No: SK-1		Sondaj Tipi: Rotary					
Sondaj Derinliği: 20,0m		Veraltı Su Seviyesi: -3,00m		Son koor. (y): 583991					
Pafta: *		Ada: *		Sondör: RIDVAN YAPICI					
Parsel: 213-214		Kontrol Müh: KAYHAN YILDIRIM							
Derinlik	Manevra Boyu metre	Numune Cinsi	Standart Penetrasyon Deneyi				Grafik	Litoloji	Açıklamalar
			Darbe Sayısı						
			15	30	45	N ₆₀			
1,50	1,00-1,50	UD							Nebati Toprak
1,50	1,50-1,95	SPT-1	8	11	11	22			AZ KUMLU SİLTİLİ SARI KİL (CH)
3,00	3,00-3,45	SPT-2	4	4	5	9			AZ KUMLU SİLTİLİ GRİ KİL (CH)
4,50	4,50-4,95	SPT-3	6	7	8	15			ÇOK AZ ÇAKILLI AZ KUMLU SİLTİLİ SARI KİL (CH)
6,00	6,00-6,45	SPT-4	13	14	18	32			KUMLU SİLTİLİ GRİ KİL (CL)
7,50	7,50-7,95	SPT-5	11	13	15	28			AZ KUMLU SİLTİLİ SARI KİL (CL)
9,00	9,00-9,45	SPT-6	14	18	19	37			KUMLU SİLTİLİ GRİ KİL (CL)
10,50	10,50-10,95	SPT-7	10	11	11	22			AZ KUMLU SİLTİLİ SARI KİL (CL)
12,00	12,00-12,45	SPT-8	13	14	17	31			KUMLU SİLTİLİ GRİ KİL (CL)
13,50	13,50-13,95	SPT-9	14	18	20	38			AZ KUMLU SİLTİLİ SARI KİL (CL)
15,00									KUMLU SİLTİLİ GRİ KİL (CL)
16,50	16,50-16,95	SPT-10	10	11	16	27			
18,00									
19,50	19,50-19,95	SPT-11	16	18	26	44			
21,00									
Dayanıklılık		Ayrılma		İnce Taneli (Kobenzonlu)		İri Taneli (Kobenzonlu)			
1 Dayanıklı		1 Taze		N: 0-2 Çok Yumuşak		N: 0-4 Çok Gevsek			
2 Orta Dayanıklı		2 Ayrılma		N: 3-4 Yumuşak		N: 5-10 Gevsek			
3 Orta Zayıf		3 O.D. Ayrılma		N: 5-8 Orta Katı		N: 11-30 Orta Sıkı			
4 Zayıf		4 Çok Ayrılma		N: 9-13 Katı		N: 31-50 Sıkı			
5 Çok Zayıf		5 Tam Ayrılma		N: 14-30 Çok Katı		N: >50 Çok Sıkı			
Granül		% 5 > Pek Az		% 0-25 Çok Zayıf		% 0-4 Çok Gevsek			
% 5-15 Az		% 5-20 Az		% 25-50 Zayıf		N: 5-10 Gevsek			
% 15-25 Çok		% 20-50 Çok		% 50-75 Orta		N: 11-30 Orta Sıkı			
% 53 > Ve				% 75-90 İyi		N: 31-50 Sıkı			
				% 90-100 Çok İyi		N: >50 Çok Sıkı			
ÖZYAPICI MÜH.		SONDAJ MÜHENDİSİ		KAYHAN YILDIRIM		İMZA			
İNŞAAT-TARIM ÜRN.-NAKLİYE-TURİZM-TEKSTİL		KAYHAN YILDIRIM		JEOLOJİ MÜHENDİSİ					
SAN. VE TİC. LTD.ŞTİ		ODA SİCİL NO:7898							

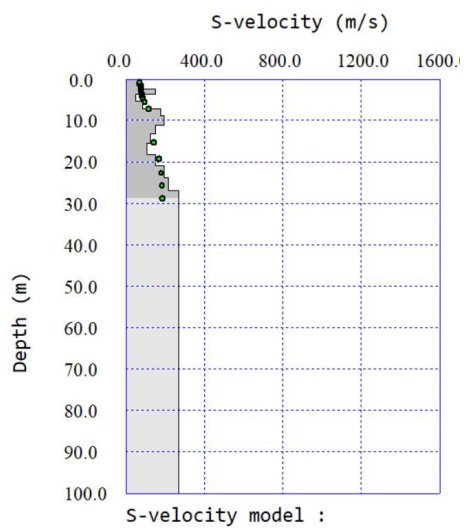
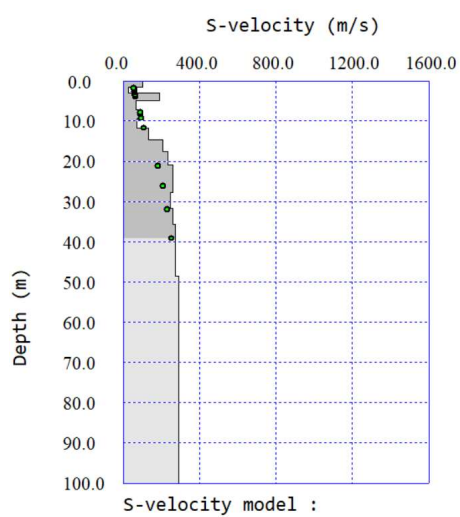
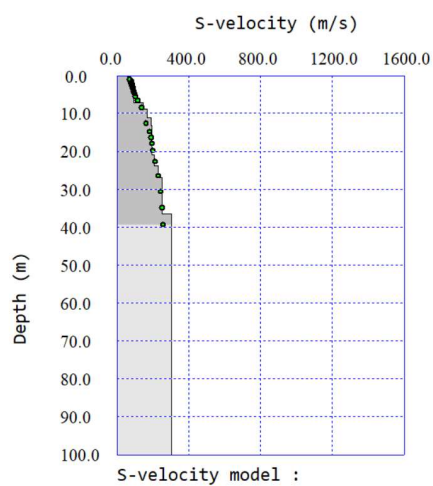
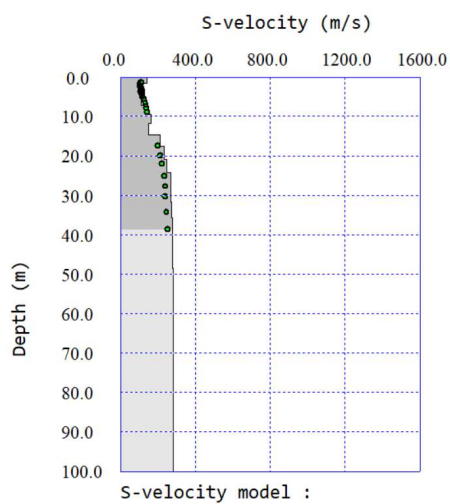
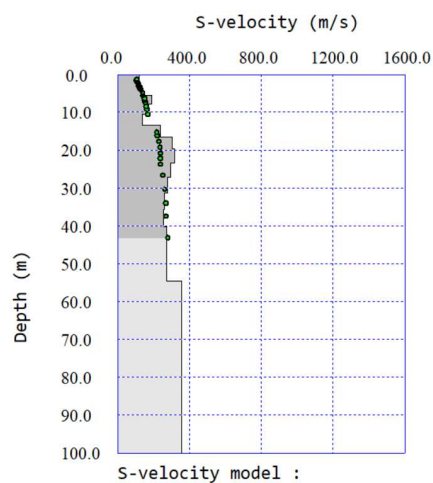
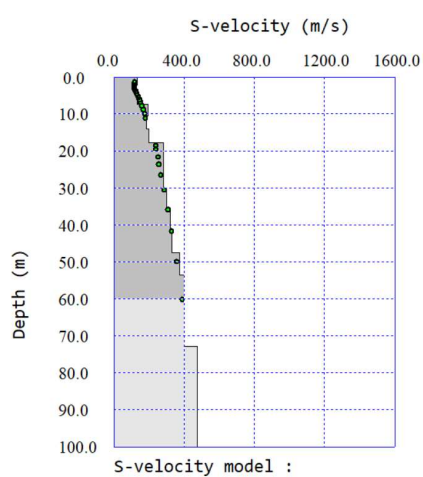
B. Surface Wave Method Analysis Results (MASW and MAM)

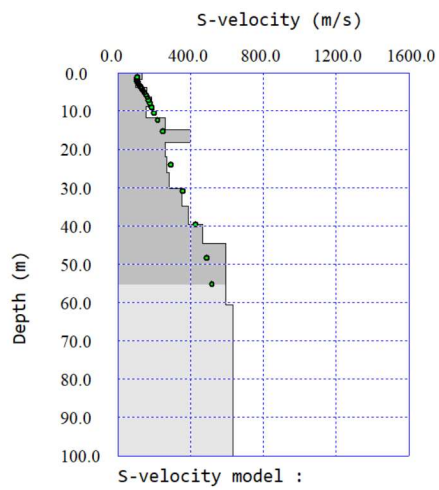
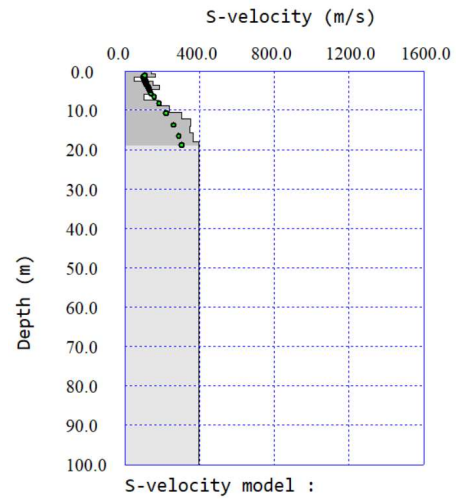
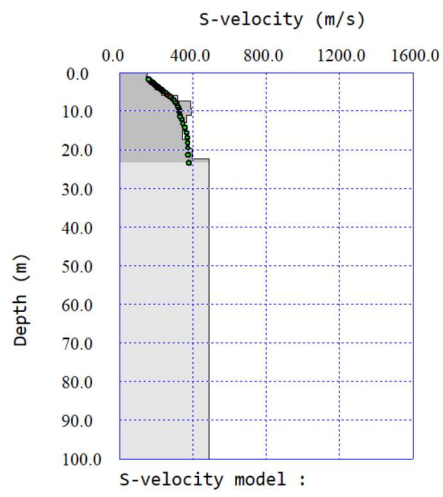
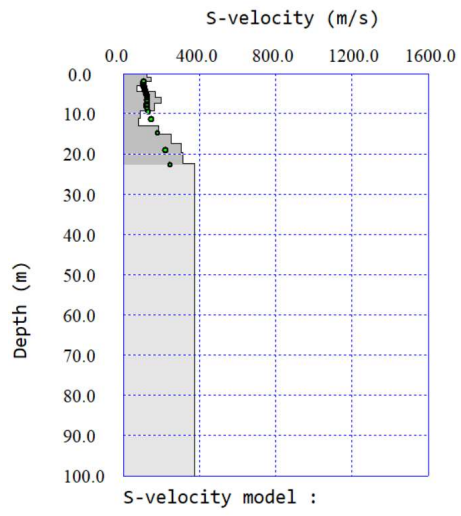
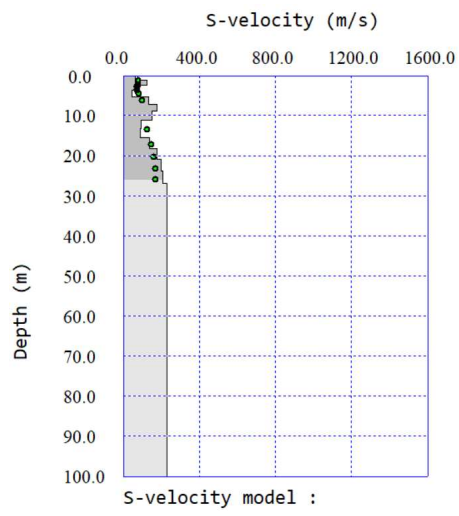
All of the processed and analyzed MASW and MAM data.





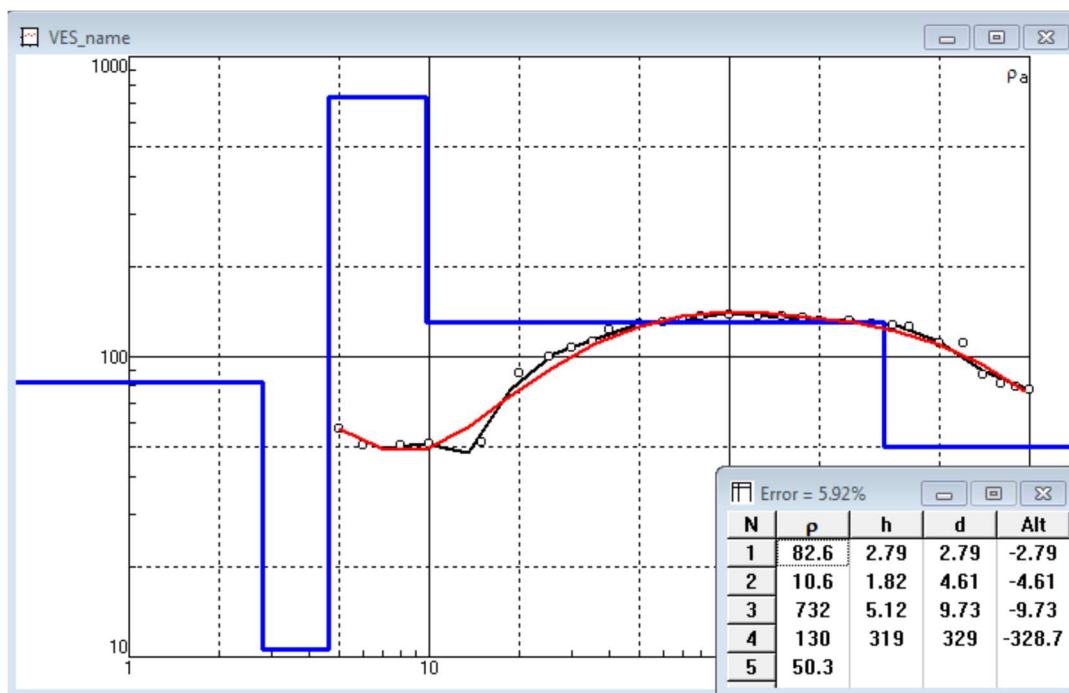
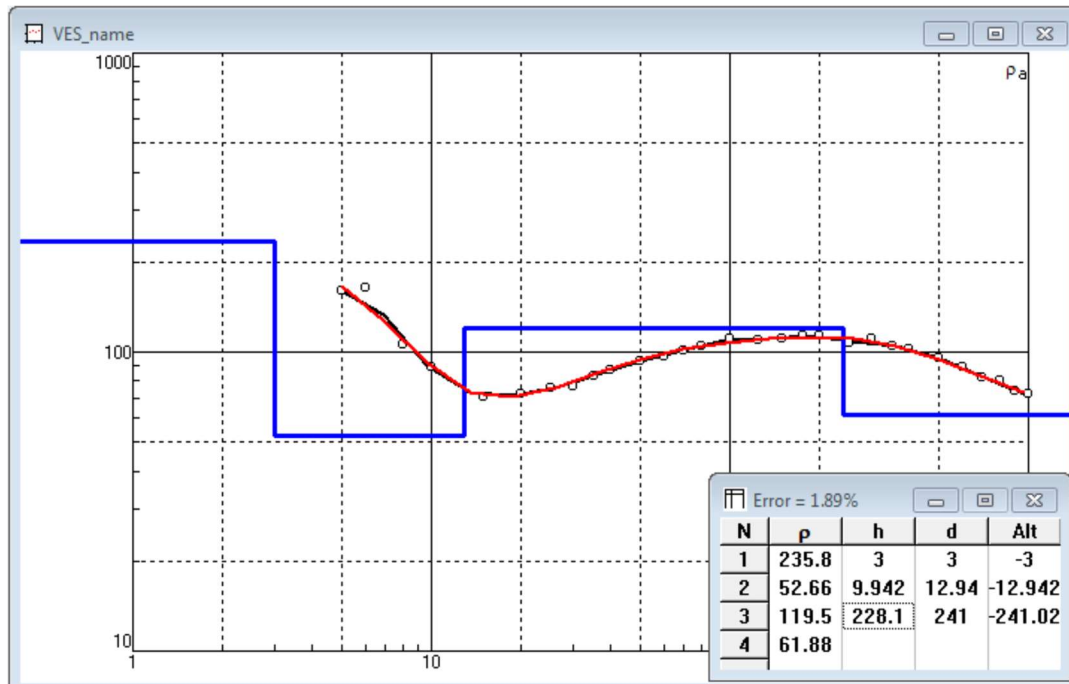


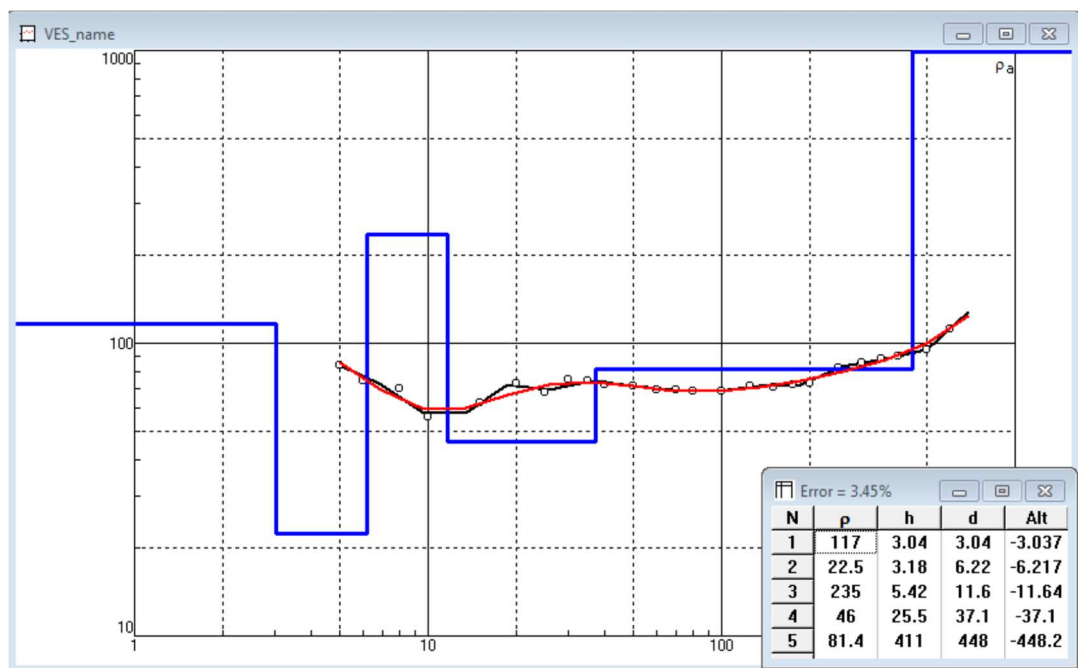
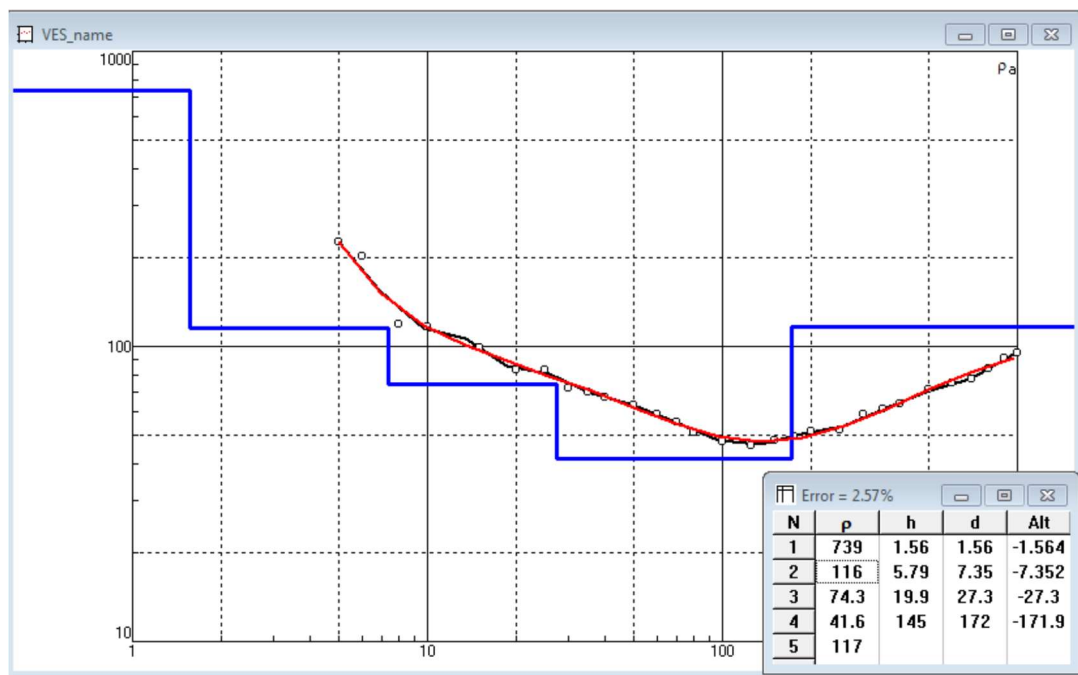


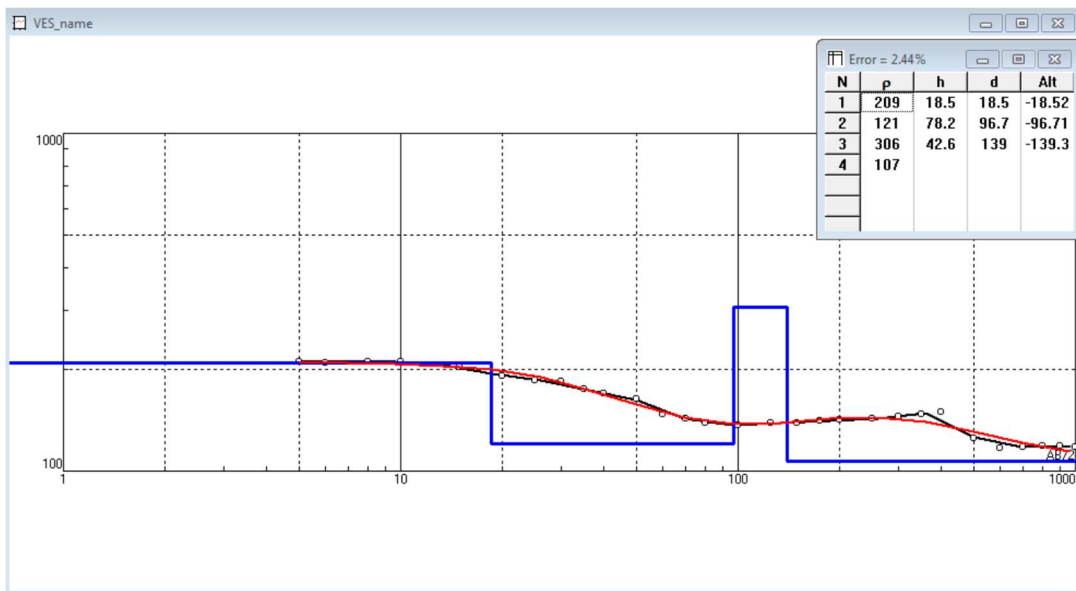
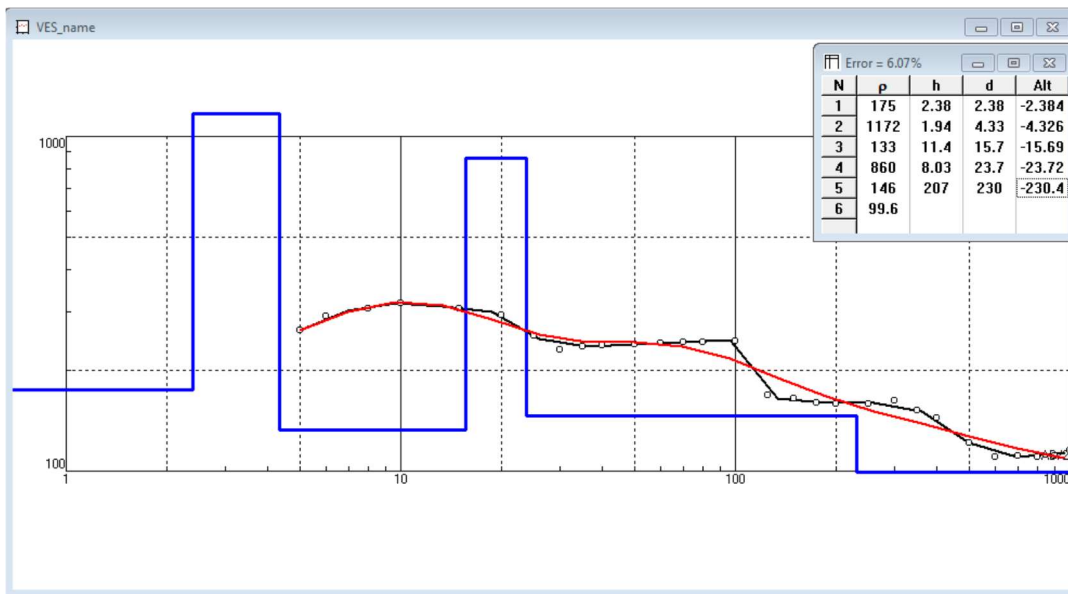


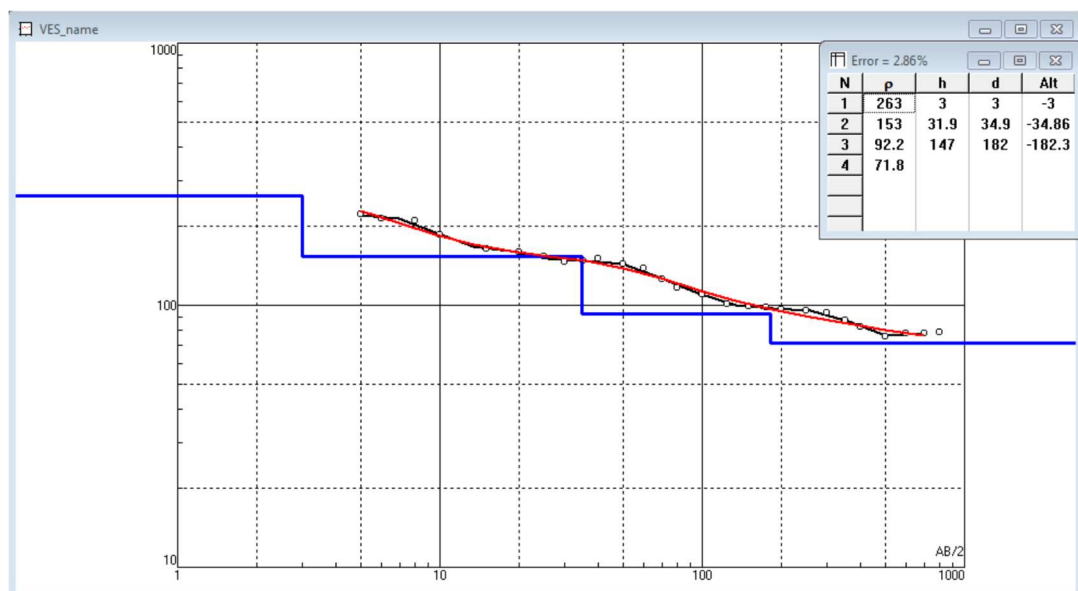
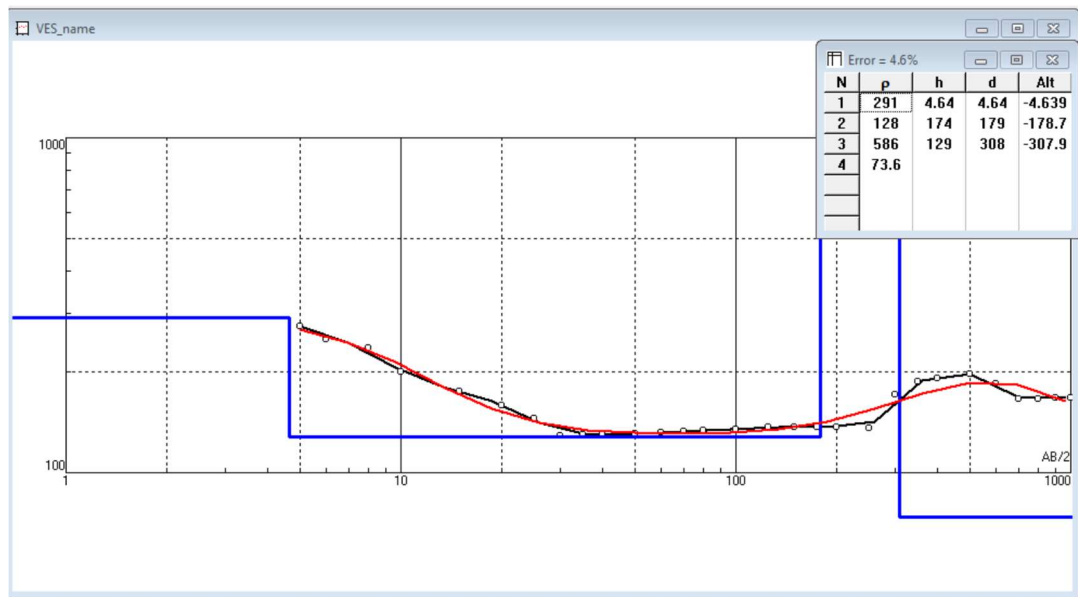
C. Vertical Electrical Sounding (VES) Results

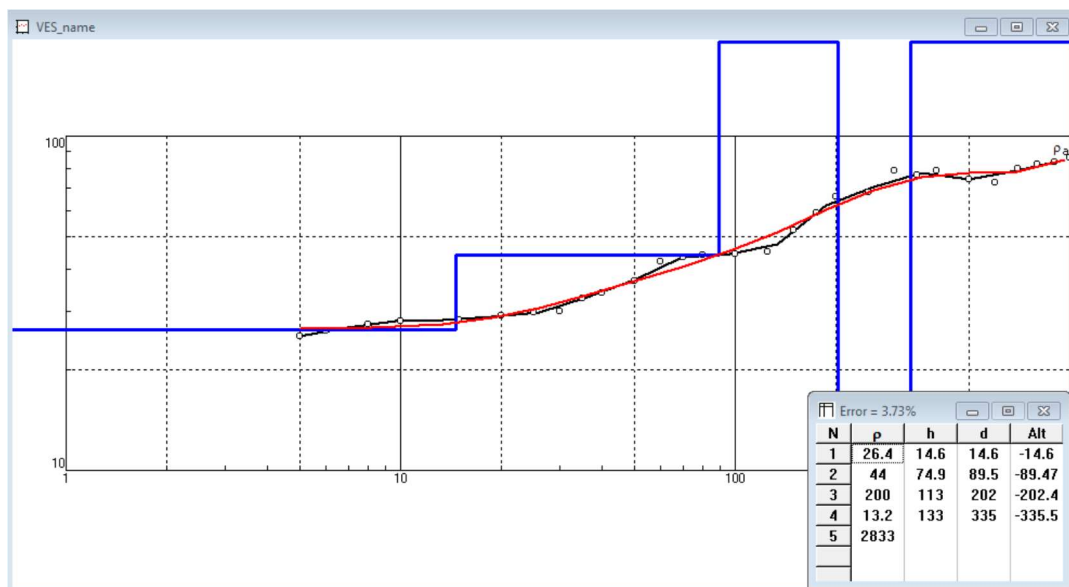
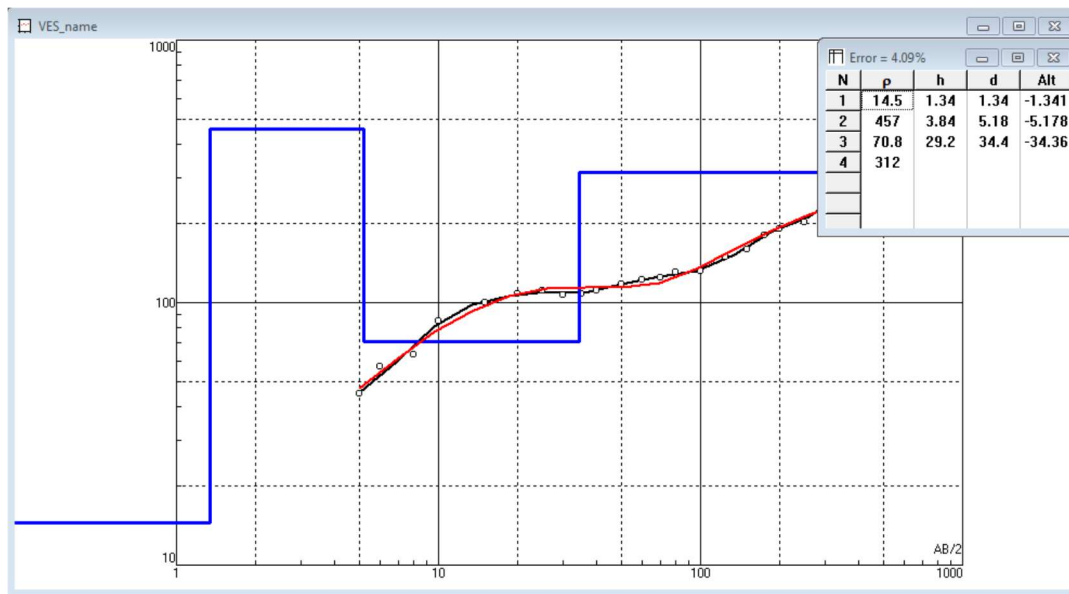
All processed vertical electrical sounding (VES) data

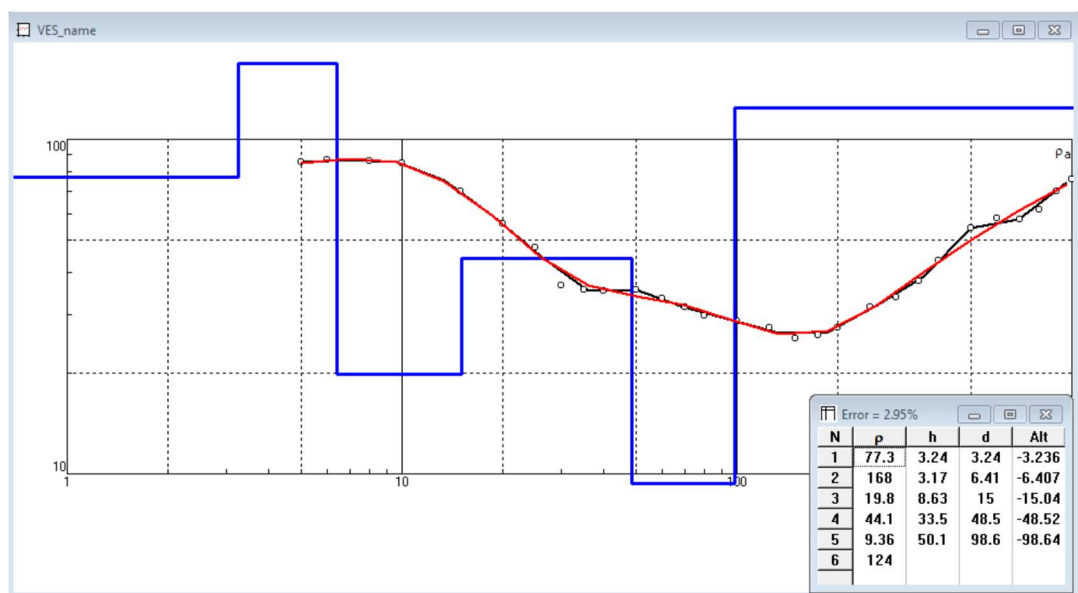
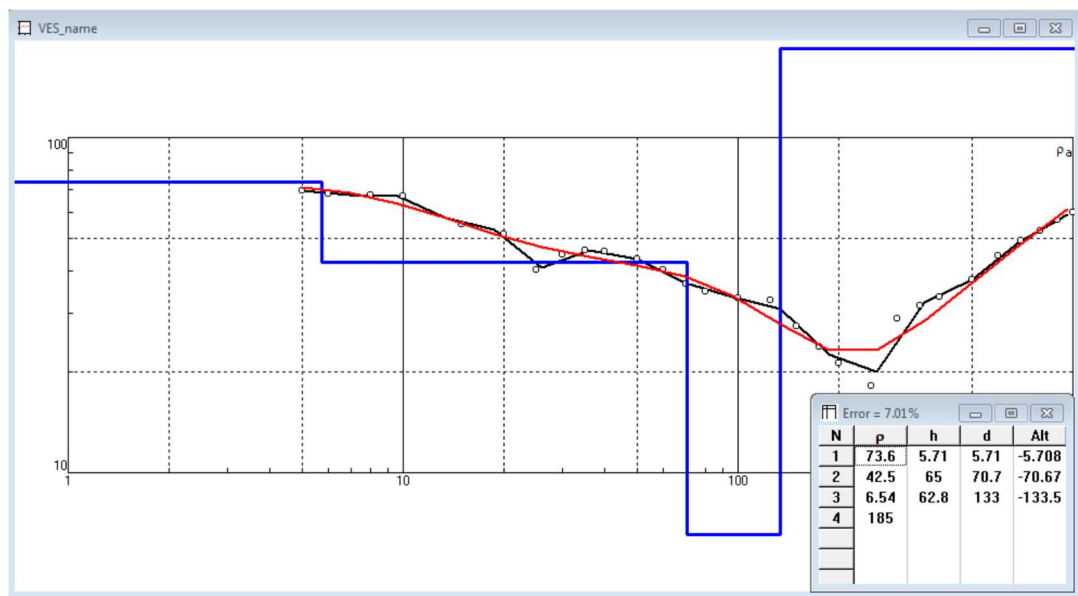


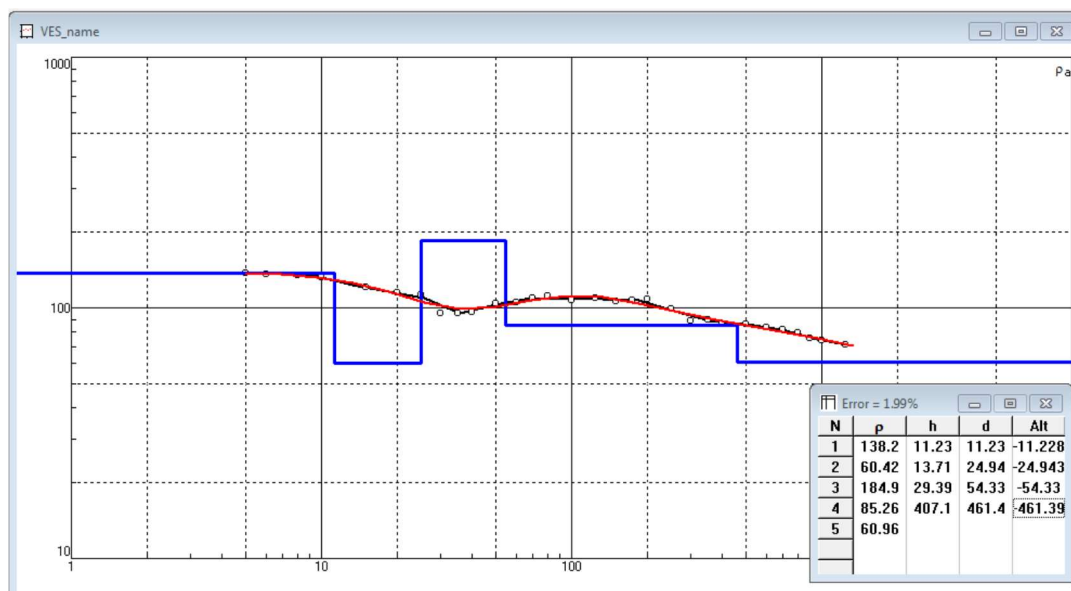
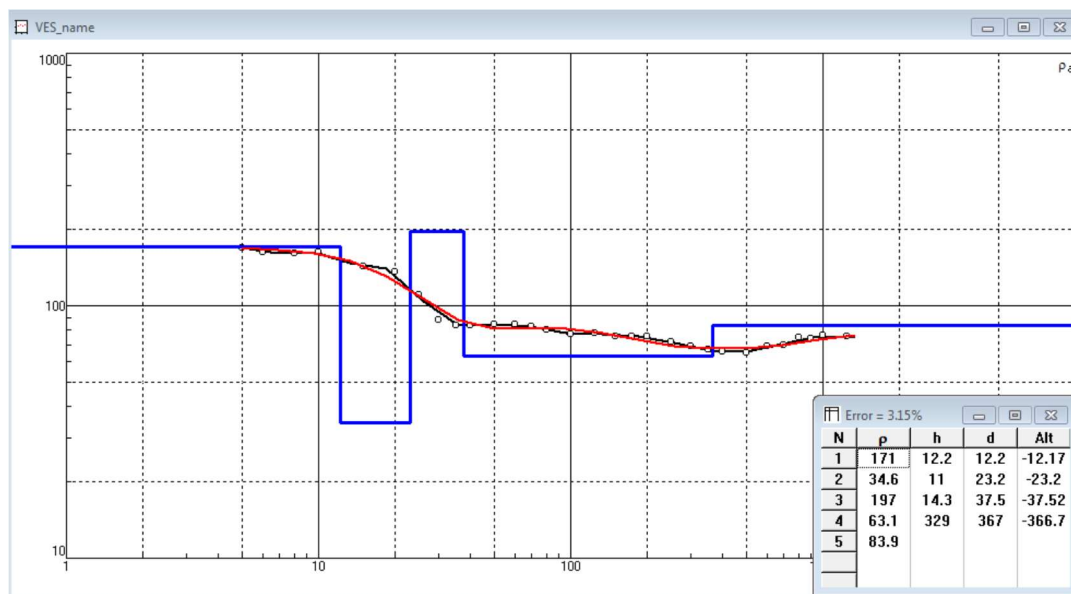






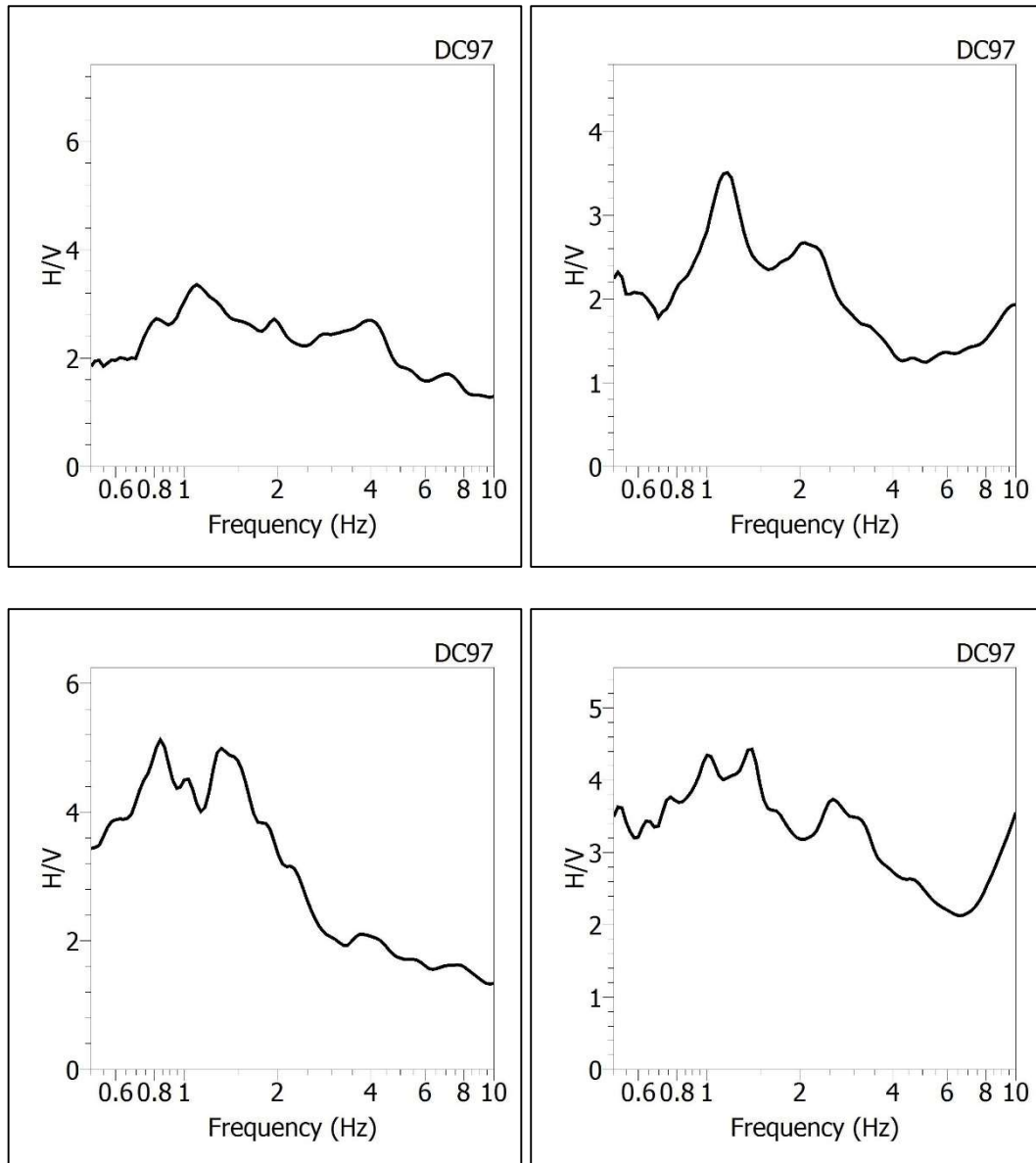


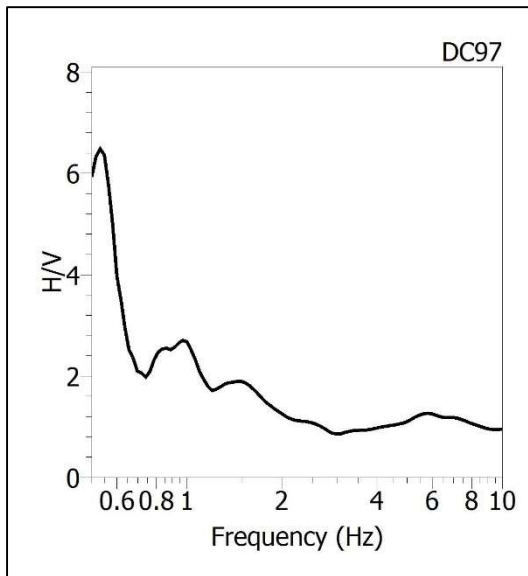
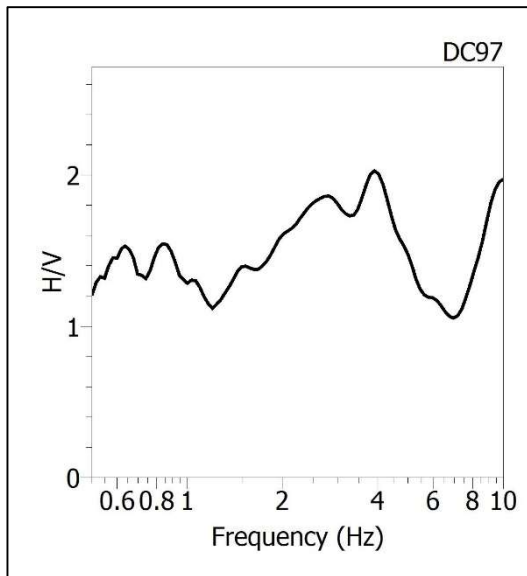
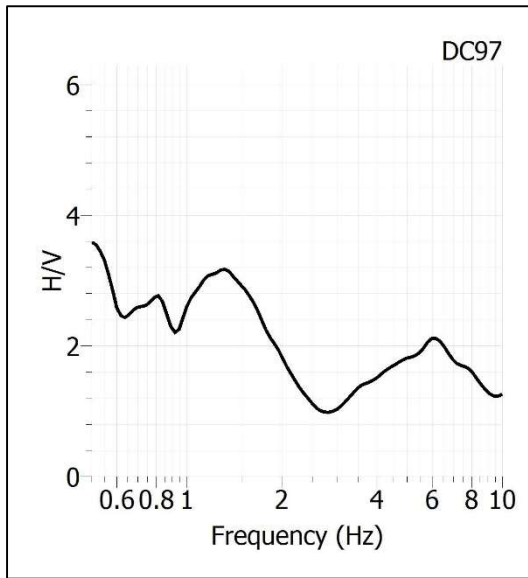
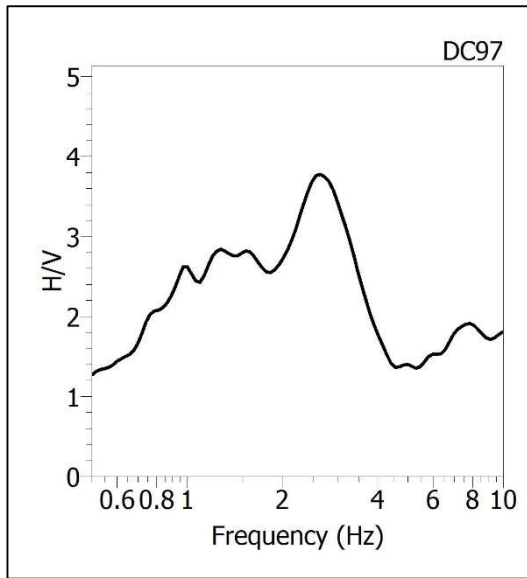


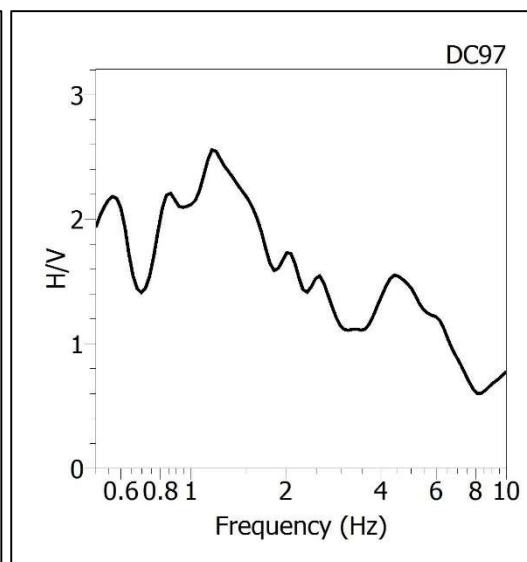
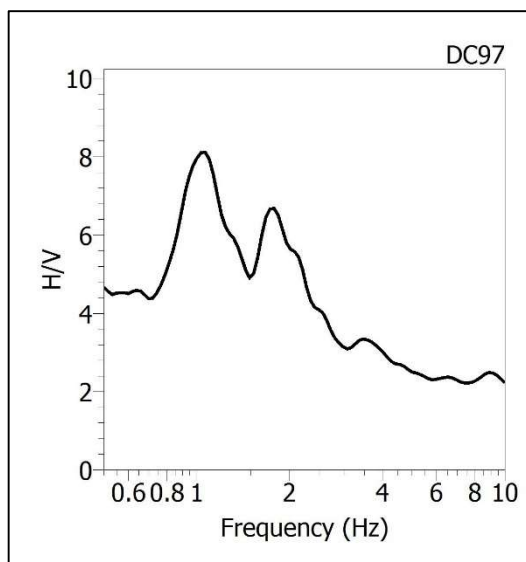
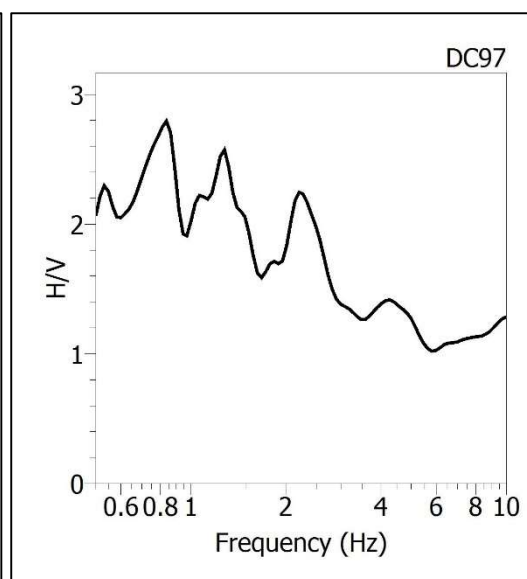
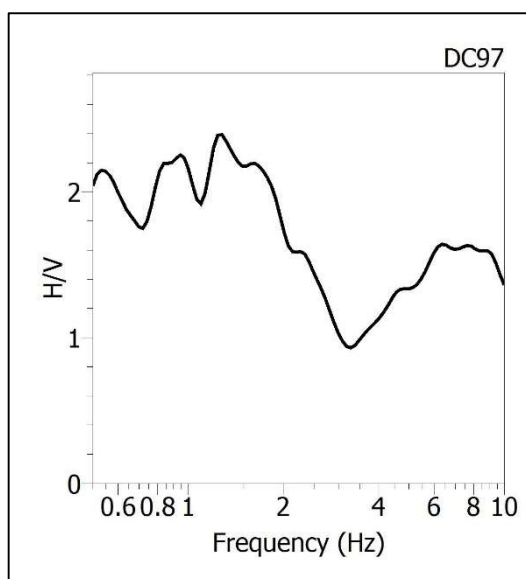


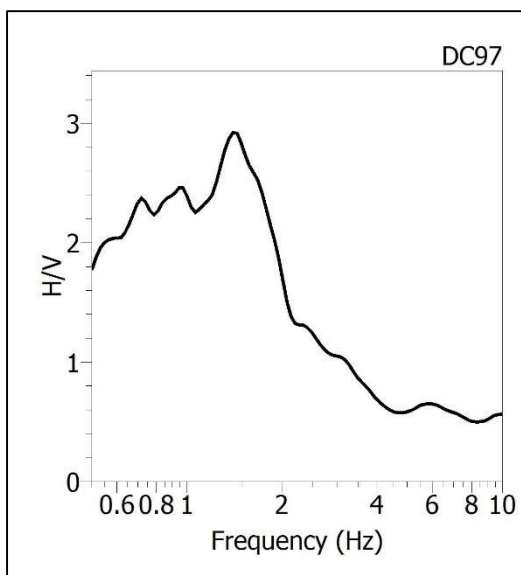
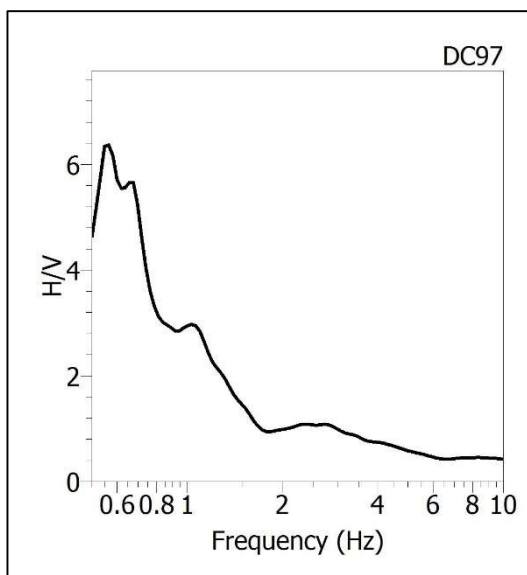
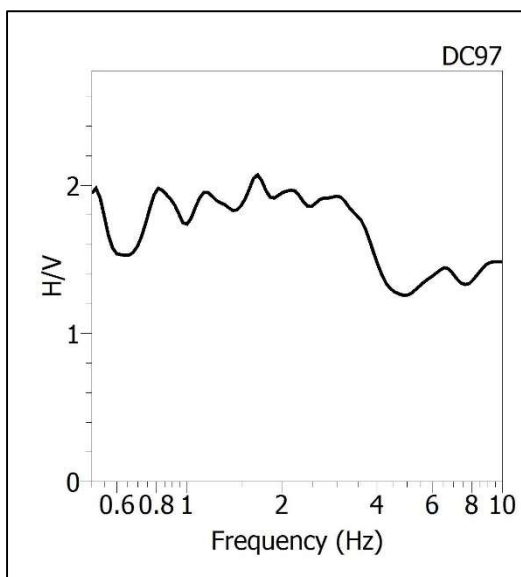
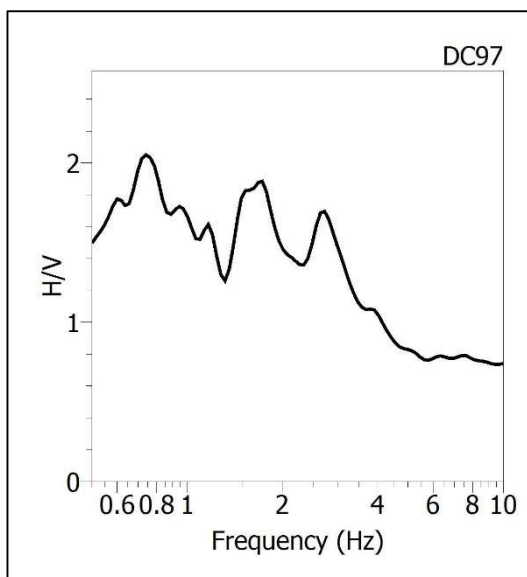
D. H/V Spectral ratio Results

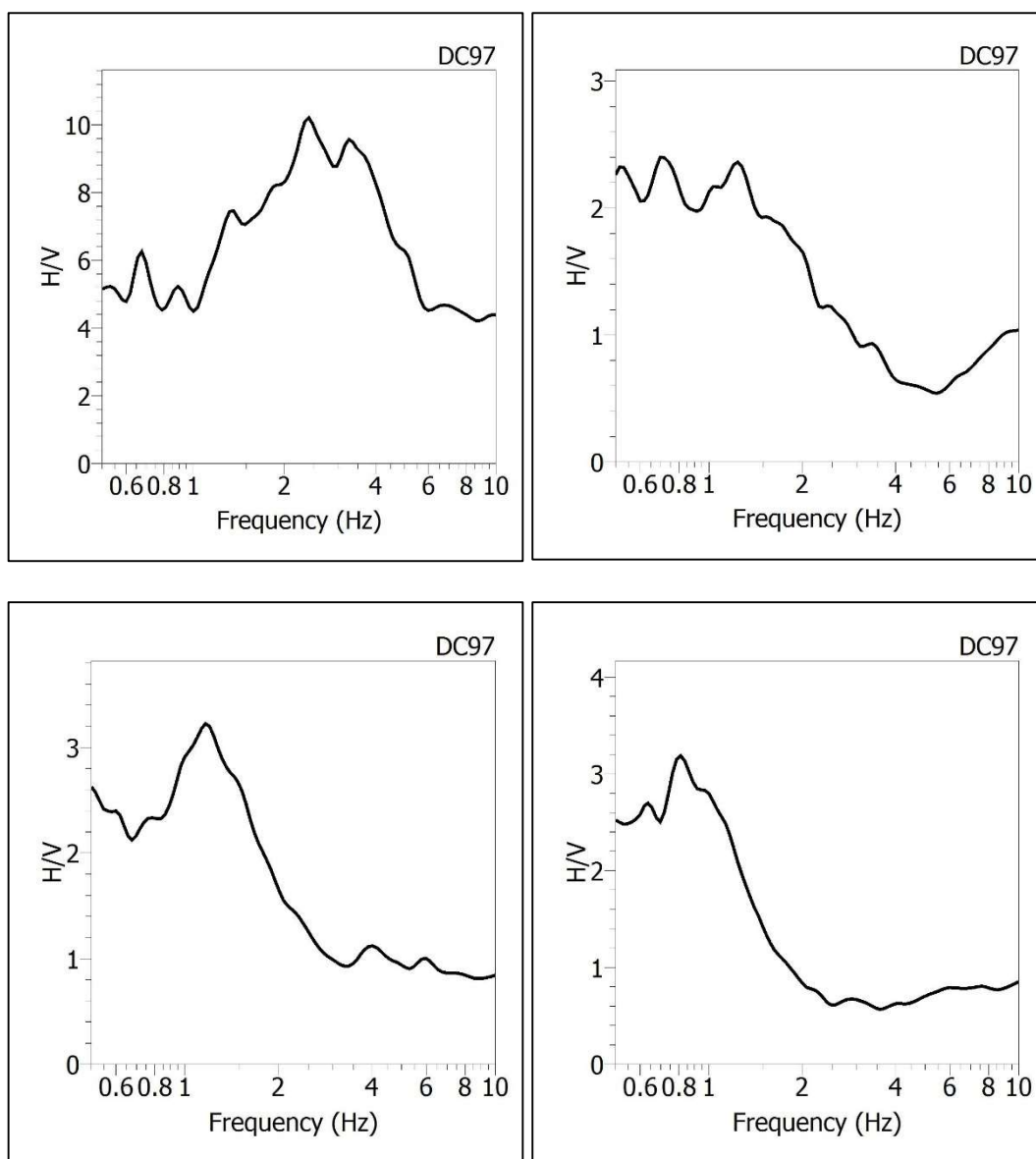
All of the processed H/V spectral ratio curves acquired from the measuring points

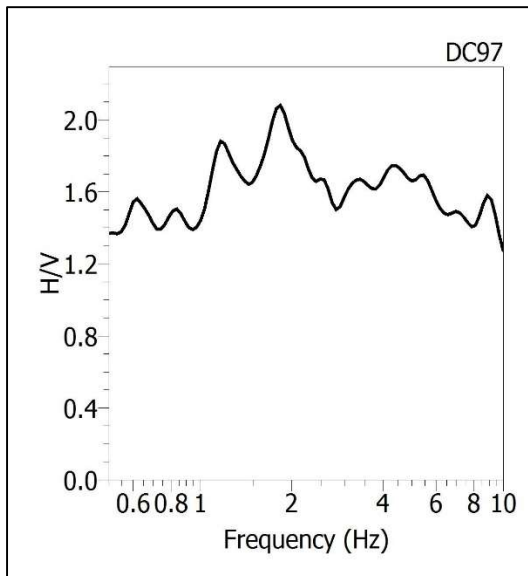
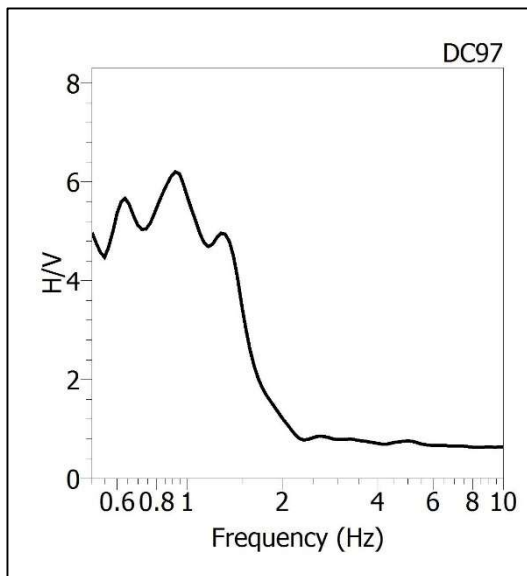
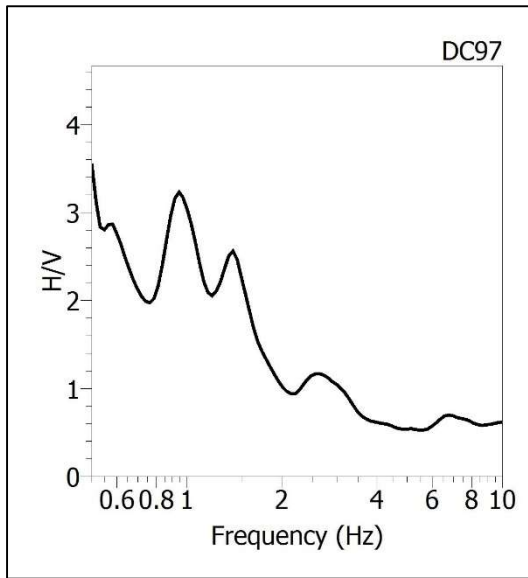
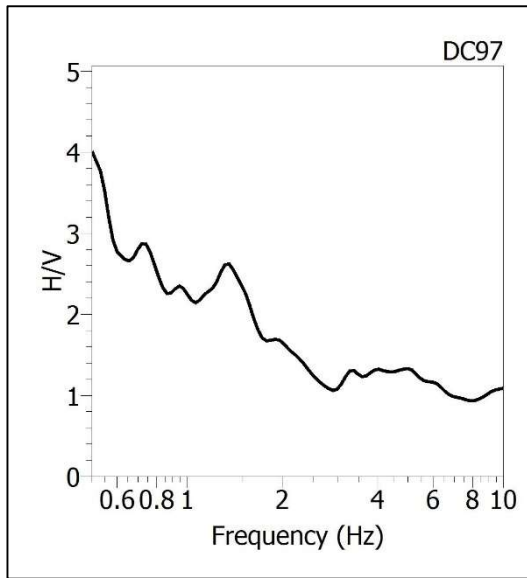


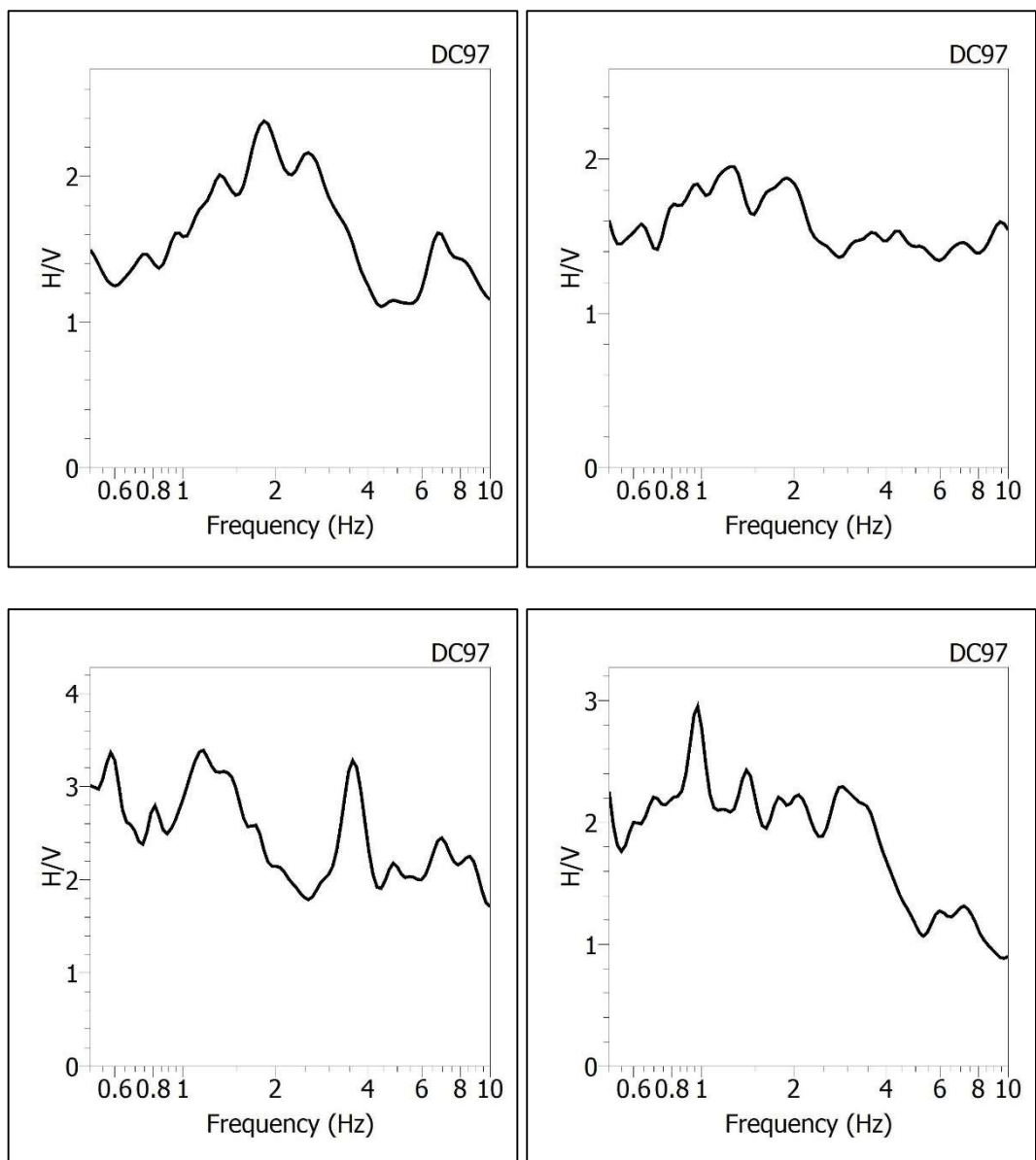


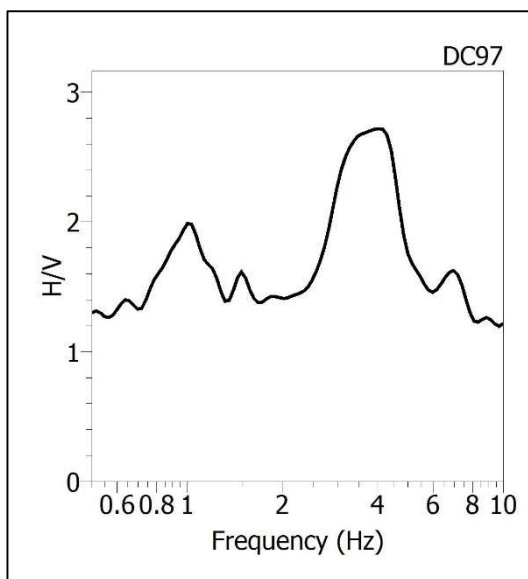












CURRICULUM VITAE

PERSONAL INFORMATION

Surname, Name: Yousefi Babil, Karim

Nationality: Iranian

Date and Place of Birth: 22 February 1983, Tabriz

Marital Status: Married

Phone: +90 531 961 90 17

Fax: -

email: yousefibabil.karim@metu.edu.tr

EDUCATION

Degree	Institution	Year of Graduation
MS	U of Isfahan Engineering Geology, Iran	2007
BS	U of Tabriz Geology, Iran	2005
High School	Shariati High School, Osku, Iran	2001

WORK EXPERIENCE

Year	Place	Enrollment
2018-Present	Akademi Proje Mühendislik	Control Chief
2013-2018	ATAC Mühendislik	Research Assistant

FOREIGN LANGUAGES

Advanced English, Azeri Bilingual, Bilingual Persian, Turkish Fluent

PUBLICATIONS

1. Kelam, A.A., Karimzadeh, S., Yousefibabil, K., Akgün, H., Askan, A., Erberik, M. A., Koçkar, M.K., Pekcan, O., Ciftci, H., An evaluation of seismic hazard and potential damage in Gaziantep, Turkey using site specific models for sources, velocity structure and building stock, Soil Dynamics and Earthquake Engineering, (154), <https://doi.org/10.1016/j.soildyn.2021.107129> (2022).

2. Yousefi-Bavil, K., Koçkar, M. K., Akgün, H., Near Field Directivity Effects in 2D Site Response Analysis, 6th International Conference on Earthquake Engineering and Seismology (6.ICEES), 13-15 Oct., BTU, Gebze, Turkey (2021)
3. Yousefi-Bavil, K., Koçkar, M.K., Akgün, H., Alüvyon havzaların yakın alan sismik saha tepki analizi: Gölyaka, Düzce ile ilgili bir vaka çalışması, 73rd Geological Congress of Turkey with international participation, 6-10 April, Turkey (2020) (In Turkish)
4. Babil, A. Y., & Babil, K. Y.. SCPAT: a MATLAB-based toolbox for analysing swath characteristic profiles. *Arabian Journal of Geosciences*, 12(9), 1-14 (2019).
5. Akgün, H., Türkmenoğlu, A. G., Kelam, A. A., Yousefi-Bavil, K., Öner, G., & Koçkar, M. K.. Assessment of the effect of mineralogy on the geotechnical parameters of clayey soils: a case study for the Orta County, Çankırı, Turkey. *Applied Clay Science*, 164, 44-53 (2018).
6. Yousefi-Bavil, K., Koçkar, M. K., Akgün, H., Development of A 3-D Topographical Basin Structure Based On Seismic and Geotechnical Data: Case Study At A High Seismicity Area of Gölyaka, Düzce, Turkey, 16th European Conference on Earthquake Engineering (16ECEE), 18-21 June, Thessalonik, Greece (2018).
7. Yousefi-Bavil, K., Kerem Koçkar, M., & Akgün, H.. 3-D basin geometry model to determine the site effects based on geophysical and geotechnical data: Case study at near-field and high seismicity area of Gölyaka, Düzce, Turkey. In EGU General Assembly Conference Abstracts (p. 14633) (2018, April).
8. Yousefi-Bavil, K., Koçkar, M. K., Akgün, H., Near Field Sesimic Site Response Analysis of Alluvial Basin: A Case study For The Gölyaka, Düzce, Turkey, 4th International Conference on Earthquake Engineering and Seismology (4UDMSK), 11-13 October, Anadolu University, Eskişehir (2017).
9. Yousefi-Bavil, K., Akgün, H., Eker, A.M., Cambazoğlu, S. and Koçkar, M.K., "Integration of Surface Wave Seismic Survey Testing Results and Segmented Seismic Source Model of NAFS for PSHA of the Gölyaka-Düzce Tectonic Basin, Turkey", 6ICEGE (6th International Conference on Earthquake Geotechnical Engineering), 1-4 November, Paper No 402, Christchurch, New Zealand, 8 p (2015).
10. Yousefi-Bavil, Eker, A.M., Cambazoğlu, S., Koçkar, M.K., Akgün, H. "Yüzey Dalgasi Etüt sonuçlarının Entegrasyonu ile Gölyaka-Düzce Tektonik Baseninin Olasılıksal Sismik Tehlike Değerlendirmesi", 3.TDMSK (3. Türkiye Deprem Mühendisliği ve Sismoloji Konferansı), 14-16 Ekim, No: 224, DEU, Izmir, Turkey, 8 p (2015).
11. Asghari-Kaljahi, E., Yousefi-Bavil, K., & Babazadeh, M.. A study of ground natural temperature along Tabriz metro line 2, Iran. In *Engineering Geology for Society and Territory-Volume 6* (pp. 295-298). Springer, Cham. (2015)

Sport, Finance, Book, Computer Technologies, Movies